The motion of thin–cored vortex filaments: the equations of motion and their solution for some special cases

Thesis by
Michael F. Lough

In partial fulfillment of the requirements
for the degree of
Doctor of Philosophy

California Institute of Technology
Pasadena, California

1995

(Submitted August 24, 1994)

Acknowledgements

For the completion of this thesis, the product of five years in the Applied Mathematics Department at Caltech, I owe a great many thanks to those who have helped me along the way. Principally, my advisor Professor Philip Saffman deserves most of the credit as he offered me invaluable guidance and also gave me the freedom to persue aspects of the problem solving technique from my own viewpoint. I also thank Professor Derek Moore, who offered some keen perspectives on formulating and solving some of the problems considered in this thesis. My family also deserve my gratitude for their unfailing support, and to my mother Mary, sister Annemarie, and brothers Matthew and Declan, I extend my deepest thanks. It saddens me greatly that my father died before I had the chance of sharing most of my academic successes with him, but I'm sure he has had a lofty vantage point from which he has observed and continues to observe my progress.

I have also benefited from an abundance of very good friends who have influenced me greatly and made my last year a very "Lucky" one. Special thanks to Barry for helping me view life from a more tolerant point of view, to Suni for always being willing to do something fun, to Kayvan for relinquishing Burgers and to John for preserving my liver! Generally, I have tried to interact with people in such a way as to be a positive influence on their lives, but I concede that it has not always turned out this way, and I extend my apologies to those I have influenced negatively.

I dedicate this thesis to all those who have lent me a helping hand in this voyage called Life.

Abstract

This thesis looks at the motion of vortex filaments, which are regions in a fluid flow where the vorticity field, equal to the curl of the velocity field, is negligible outside a cylindrical type tube — the filament. The vortex filament is said to be thin–cored if the radius of the tube is much smaller than any axial length scale along the filament. This thin core assumption allows the motion of the filament to be described by the motion of the centerline of the tube, when it is coupled to the internal core dynamics via an asymptotic matching procedure. Our studies of the motion and dynamics of such structures can be grouped into three topics: (1) analyses of equations of motion for thin–cored vortex filaments, (2) an analysis of the linear stability of a vortex ring moving along the axis of a pipe and (3) the construction of finite amplitude wave solutions for the shape of the centerline of planar vortex filament.

Our main thrust in the first topic is to show that the "new" equations derived by Klein and Majda (1991) are merely a reformulation of some of the more well known equations for vortex filament motion; in particular we show that their equations can be obtained by a linearization of the well known cut–off equation. The cut–off equation has been used by a number of authors (e.g., Crow (1970), Widnall and Sullivan (1973), etc.) to analyse problems in vortex motion, and a systematic justification for the equation was provided by Moore and Saffman (1972), who showed the equation was asymptotically correct.

With regard to the second topic, questions of stability naturally arise when one considers coherent structures, such as vortex rings. The stability of a vortex ring in an unbounded fluid was first examined by Thomson (1883) who found that the ring was stable to infinitesimal perturbations (the vortex ring being a model for the so–called indestructible atom). Widnall and Sullivan (1973) reconsidered the stability problem, but retained terms of higher order in the small parameter (i.e., the ratio of core radius to ring radius). Their results indicated a spurious instability where the

only unstable perturbations were those with wavelengths that were comparable with the core radius (a situation for which the cut–off equation is inapplicable). For the case where the ring moves inside a cylindrical pipe, along its axis, only the effect of the wall on the speed of the ring had been computed to date (Raja Gopal (1963) and Brasseur (1979)). From the theoretical point of view, the effect of the wall on the stability of the ring has, until now, been unknown. We show that the wall induces an instability on the vortex ring characterized by a tendancy for the ring to tilt out of its original plane.

The so–called local induction equation, for vortex filament motion, corresponds to the zero core radius limit of the cut–off equation. Hasimoto (1972) showed that there was a direct relationship between the local induction equation and the cubic Schrödinger equation, a completely integrable equation. He also computed the corresponding soliton solution of the equation. Kida (1981) computed a general solution of the equation having periodic shape parameters. Both of these solutions are finite amplitude wave solutions for vortex filaments whose motion is governed by the local induction equation. Unfortunately, the local induction equation is known to admit some solutions that are unphysical, a fact which lends credence to the belief that the general solutions are also unphysical. Accordingly, it is important to see whether equations containing more physics also admit finite amplitude wave solutions. Kelvin (1880) obtained a solution of the linearized problem for periodic waves of infinitesimal amplitude that lay in a rotating plane. (In fact, Kelvin's solutions described infinitesimal filament waves having a general three–dimensional structure.) We numerically compute such plane wave solutions to the full nonlinear equations and continue the solution to finite amplitude.

Contents

CHAPTER 1

VORTEX DYNAMICS FOR THIN–CORED VORTEX FILAMENTS

1.1 Introduction

There are many reasons for examining problems in vortex dynamics. From our point of view the principal reason is that regions of intense vorticity in an otherwise calm flow are quite often compact and remain so for a long period of time. This has implications for the remainder of the fluid, since the fluid velocity can be thought of as being induced completely by the vorticity field. For such a point of view we adopt a liberal interpretation of what is meant by the vorticity field in that we assume that any boundaries in the fluid, which induce the irrotational part of the velocity field, can be replaced as boundaries of new fluid regions containing so–called image vorticity (see section 2.4 of *Vortex Dynamics* by Saffman (1992)). Consequently, a complete description of the evolution of the vorticity field leads to a complete description of the evolution of the entire flow field.

To be specific, it is well known that a vorticity field $\boldsymbol{\omega}(\mathbf{x},t)$ occupying a region $\mathcal{D}$ in an otherwise unbounded fluid induces a velocity field $\mathbf{u}(\mathbf{x},t)$ given by a Biot–Savart integral

$$\mathbf{u}(\mathbf{x},t)=\frac{1}{4\pi}\int_{\mathcal{D}}\boldsymbol{\omega}(\mathbf{x}',t)\times\frac{(\mathbf{x}-\mathbf{x}')}{|\mathbf{x}-\mathbf{x}'|^3}d\mathbf{x}'. \tag{1.1.1}$$

Using (1.1.1) allows us to compute the entire flow field. However, the evolution of the vorticity field is itself highly non–trivial. Fortunately, the type of problems we are concerned with are problems where the vorticity is concentrated inside some tubular region, which may be either closed or infinitely long. If the diameter of the tube is small compared with some length scale along the tube, then it proves convenient to assume that the vorticity is concentrated on the centerline of the tube and is directed along the tangent to the centerline. Such an idealized construct is called a

thin–cored vortex filament and the centerline of the tube is simply referred to as the vortex filament. The thin–cored vortex filament approximation assumes that the gross motion of the vortex tube is adequately described by the motion of the centerline.

Suppose the situation being considered is as indicated in figure 1.1.1, where the vortex tube has core radius a, strength Γ and centerline $\mathbf{X}(s,t)$ (s is arclength along the centerline). An intrinsic orthonormal triad $\{\mathbf{s}, \mathbf{n}, \mathbf{b}\}$ is associated with any space curve, where the unit vectors are the tangent, principal normal and binormal, respectively. These vectors, which are functions of arclength and possibly time, satisfy a set of vector differential equations called the Frenet–Serret formulae

$$\begin{aligned} \mathbf{s} &= \frac{\partial \mathbf{X}}{\partial s} \\ \frac{\partial \mathbf{s}}{\partial s} &= \kappa \mathbf{n} \\ \frac{\partial \mathbf{n}}{\partial s} &= \tau \mathbf{b} - \kappa \mathbf{s} \\ \frac{\partial \mathbf{b}}{\partial s} &= -\tau \mathbf{n} \end{aligned} \tag{1.1.2}$$

The radius of curvature, ρ, indicated in figure 1.1.1, is the inverse of the curvature, κ, appearing in (1.1.2). The torsion, τ, which appears in (1.1.2), is a measure of the rate at which the orthonormal triad $\{\mathbf{s}, \mathbf{n}, \mathbf{b}\}$ twists about the curve as one moves in the direction of increasing arclength.

The thin–cored vortex filament approximation replaces the vorticity field $\boldsymbol{\omega}(\mathbf{x},t)$ by

$$\boldsymbol{\omega}(\mathbf{x},t) = \Gamma \delta(n)\delta(b)\mathbf{s}, \tag{1.1.3}$$

where, as required, the vorticity is concentrated on the centerline, has strength Γ and is directed along the tangent to the centerline. Consequently, the velocity at a point $\mathbf{x}$ in the fluid, according to (1.1.1) and (1.1.3), reduces to

$$\mathbf{u}(\mathbf{x},t) = \frac{\Gamma}{4\pi} \oint \mathbf{s}' \times \frac{(\mathbf{x} - \mathbf{X}(s',t))}{|\mathbf{x} - \mathbf{X}(s',t)|^3} ds'. \tag{1.1.4}$$

Now the problem becomes apparent, if we replace $\mathbf{x}$ by a point $\mathbf{X}(s,t)$, on the filament, then the integral diverges logarithmically. (To be exact, if we attempt to carry this

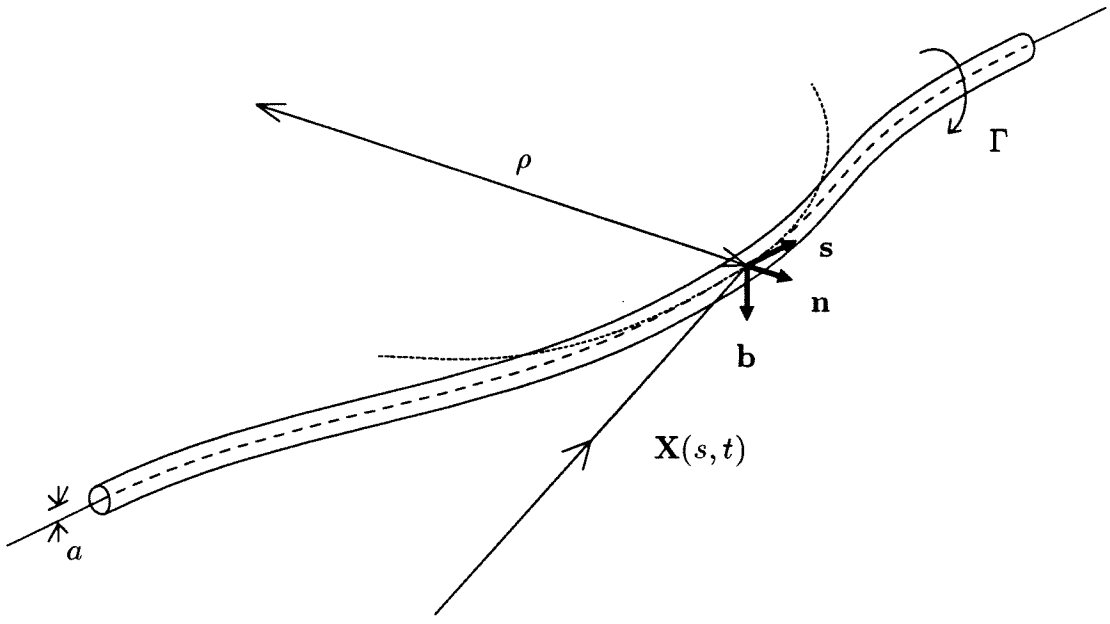

Figure 1.1.1 A vortex filament with core radius a and strength Γ centered on a time dependent space curve $\mathbf{X}(s,t)$. The orientation of the unit vectors $\mathbf{s}$, $\mathbf{n}$ and $\mathbf{b}$ are indicated for an arbitrary point on the curve. We also indicate the radius of curvature, ρ, and part of the osculating circle at $\mathbf{X}(s,t)$.

out in a limiting process then we also have encounter a singularity that behaves like $1/|\mathbf{x}-\mathbf{X}(s,t)|$ and this is clearly shown in appendix B.) Consequently, (1.1.4) cannot be used to describe the self–induced velocity of the filament. The way around this problem is to use (1.1.4) in an asymptotic matching procedure, and we outline several such procedures in the next few sections.

1.2 A general description of the matching procedures for vortex filaments

At the end of section 1.1, we remarked how a regular expression for the self induced velocity can be obtained by using (1.1.4) in an asymptotic matching procedure. The asymptotic matching procedure is based on a perturbation series of the flow field in terms of some small dimensionless parameter, ϵ. The assumption of a thin–cored vortex tube leads to a natural definition for ϵ. For thin–cored vortex filaments we identify two length scales: a short length scale, a, corresponding to a *measure* for

the core radius and a much longer length scale, R, which (typically) corresponds to a *measure* for the radius of curvature, ρ. By taking the ratio of these quantities, we obtain a small dimensionless parameter, $\epsilon = a/R$.

A note about the vorticity field is in order at this point, because there are three possible assumptions that can be made. The first assumption is that the flow is inviscid and there is a well defined core boundary outside of which the vorticity is identically zero. The second possible assumption that can be made is also for an inviscid flow, but this time the core boundary is only vaguely defined, and outside the core there is a weak vorticity field which decays exponentially fast to zero the farther we move away from the core. The final possible assumption that can be made is that the fluid flow is viscous and, correspondingly, the vorticity field decays smoothly to zero outside the core. The second two assumptions mean that a well defined core boundary does not exist and, consequently, the determination of a core boundary does not figure in the matching procedure. Moore and Saffman (1972) use the first assumption, Fukumoto and Miyazaki (1991), the second assumption and Callegari and Ting (1978) adopt the third assumption.

In all of the matching procedures, an inner region is identified in the neighborhood of the core, where the flow field is assumed to be described by the Euler equations (or the Navier–Stokes equations in the case of viscous flows). The next step requires the introduction of a quasi–cylindrical coordinate system, where the axial coordinate, s, is the arclength along the filament curve and the polar coordinates, (r, θ), are the polar coordinates in a plane perpendicular to the tangent to the filament curve. By a suitable scaling of the variables and the introduction of the perturbation series in ϵ, a system of hierarchical equations can be derived from the Euler or Navier–Stokes equations. The solution to these equations provide a perturbation solution to the flow field in the inner region. The full details of this procedure are presented in appendix A.

The outer region is taken to be far from the core, where the flow field is assumed to be governed by the Biot–Savart integral (1.1.4). The field point $\mathbf{x}$ appearing in

(1.1.4) has the representation

$$\mathbf{x} = \mathbf{X}(s,t) + r(\mathbf{e_x}\cos\theta + \mathbf{e_y}\sin\theta) \tag{1.2.1}$$

in terms of the quasi–cylindrical polar coordinate system. To carry out the matching, we require a representation for the Biot–Savart integral in the limit where $r \to 0$. This is a singular limit for the integral so the dominant terms will be the singular terms. A common procedure for obtaining these terms (the procedure adopted by Callegari and Ting and by Fukumoto and Miyazaki) is to expand the filament curve in a Taylor series in arclength, about the singular point. This is then used to obtain an approximation for the integrand which is integrated over some finite length, $2L$, centered on the singular point. This length is assumed to scale like R so that when $r = O(a)$ any contributions essentially come from an infinite section of the filament. If the filament is closed, then L can be chosen as half the length of the filament; however, if the filament is open then L is essentially arbitrary. (We will see that so long as L scales like R, then the equations of motion can be written in a way that is independent of L!) A second procedure for isolating the singular terms (adopted by Moore and Saffman) is to subtract from the integrand in (1.1.4) a second integrand having the same singular behavior. The singular behavior of the integrand is essentially characterized by the radius of curvature. Consequently, any curve passing through the singular point, possessing the same intrinsic orthonormal triad and having the same radius of curvature, will exhibit the same singular behavior when used in the Biot–Savart integrand. Any pair of such curves are said to be osculating (kissing) at the singular point. We note that the Taylor series expansion of the filament curve, described above, osculates with the filament curve. Moore and Saffman chose to use the osculating circle to isolate the singular terms in the Biot–Savart integral. Moreover, they chose to carry out the matching procedure in a non–standard fashion by first expressing the equations of motion in conservation form. The advantage of this formulation is that it requires a less detailed knowledge of the flow to achieve a certain degree of accuracy. The equation of motion obtained by Moore and Saffman

takes the form

$$\frac{\partial \mathbf{X}(s,t)}{\partial t} = \frac{\Gamma}{4\pi\rho}\left[\ln\left(\frac{8\rho}{a}\right) + A - \epsilon\frac{16\pi^2}{\Gamma^2}\int_0^\infty \xi w^{(0)}(\xi) w_0^{(1)}(\xi) d\xi\right]\mathbf{b} - \frac{4\pi}{\Gamma}\left[\int_0^\infty \xi w^{(0)}(\xi) d\xi\right]\mathbf{s}\wedge\frac{\partial}{\partial s}\left(\frac{\partial \mathbf{X}(s,t)}{\partial t}\right) - \frac{2\pi}{\Gamma}\left[\int_0^\infty \xi^2 v^{(0)}(\xi) w^{(0)}(\xi) d\xi\right]\mathbf{s}\wedge\frac{\partial}{\partial s}\left(\frac{\mathbf{b}}{\rho}\right) + \mathbf{Q}_{MS}, \qquad (1.2.2)$$

where $\mathbf{Q}_{MS}$ is a desingularized Biot–Savart integral obtained, as described above, by subtracting from the integrand the integrand corresponding to the osculating circular filament. The functions $v^{(0)}(\xi)$ and $w^{(0)}(\xi)$ are the leading order components of the azimuthal and axial velocities, respectively, in the vortex core (expressed as functions of the radial distance from the centerline). The function $w_0^{(1)}(\xi)$ is the axisymmetric component of the first order correction to the axial velocity in the core. The parameter A is given by

$$A = \frac{4\pi^2}{\Gamma^2}\int_0^a \xi\left[v^{(0)}(\xi)\right]^2 d\xi - \frac{1}{2} - \frac{8\pi^2}{\Gamma^2}\int_0^a \xi\left[w^{(0)}(\xi)\right]^2 d\xi \qquad (1.2.3)$$

which is $-1/4$ for a filament with uniform vorticity in the core and containing no axial flow.

Callegari and Ting (1978) carry out the matching procedure for a viscous flow by matching the first two terms of a perturbation expansion of the flow field. Their expression for the velocity of the filament is

$$\frac{\partial \mathbf{X}(s,t)}{\partial t} = \frac{\Gamma}{4\pi\rho}\left[\ln\left(\frac{2L}{a}\right) + A_\infty\right]\mathbf{b} + \mathbf{Q}_{CT} \qquad (1.2.4)$$

where

$$A_\infty = \lim_{r\to\infty}\left(\frac{4\pi^2}{\Gamma^2}\int_0^r \xi\left[v^{(0)}(\xi)\right]^2 d\xi - \ln\left(\frac{r}{a}\right)\right) - \frac{1}{2} - \frac{8\pi^2}{\Gamma^2}\int_0^\infty \xi\left[w^{(0)}(\xi)\right]^2 d\xi \qquad (1.2.5)$$

is the natural extension of (1.2.3) to smooth velocity profiles. The quantity $\mathbf{Q}_{CT}$ is a desingularization of the Biot–Savart integral where the difference between the

integrand and its approximation using the Taylor series is integrated over the length of the filament. In this case the filament is assumed to be closed so that

$$2L = \oint ds'. \tag{1.2.6}$$

When the filament is infinitely long, equation (1.2.4) is no longer applicable since the integral in (1.2.6) is infinite, so the length L must then be chosen in some other way. As long as L scales like R, the derivation of (1.2.4) ensures that $\mathbf{Q}_{CT}$ contains the term $-\Gamma \ln(2L)/4\pi R$ so that (1.2.4) is, in fact, independent of L.

Fukumoto and Miyazaki (1991) perform the matching for the case of an inviscid core with a smooth vorticity profile. They match the first two terms and part of the third term in the perturbation expansion of the flow field. In the third term of the perturbation expansion, the components of the flow proportional to $\sin 2\phi$ and $\cos 2\phi$ are not matched. (This angle ϕ is given by $\phi = \theta - \phi_0(s)$ where $d\phi_0/ds = \tau$, the torsion, see appendix A.) The equation they obtain for the velocity of the filament is

$$\begin{aligned}\frac{\partial \mathbf{X}(s,t)}{\partial t} = \frac{\Gamma}{4\pi\rho}\left[\ln\left(\frac{2L}{a}\right) + A_\infty - \epsilon\frac{16\pi^2}{\Gamma^2}\int_0^\infty \xi w^{(0)}(\xi) w_0^{(1)}(\xi) d\xi\right]\mathbf{b} \\ - \frac{4\pi}{\Gamma}\left[\int_0^\infty \xi w^{(0)}(\xi) d\xi\right]\mathbf{s}\wedge\frac{\partial}{\partial s}\left(\frac{\partial \mathbf{X}(s,t)}{\partial t}\right) \\ - \frac{2\pi}{\Gamma}\left[\int_0^\infty \xi^2 v^{(0)}(\xi) w^{(0)}(\xi) d\xi\right]\mathbf{s}\wedge\frac{\partial}{\partial s}\left(\frac{\mathbf{b}}{\rho}\right) + \mathbf{Q}_{FM}\end{aligned} \tag{1.2.7}$$

where $\mathbf{Q}_{FM}$ is the desingularized Biot Savart integral. As with the Callegari and Ting analysis, the derivation of (1.2.7) assumes that L scales like R. In the next section we will see that matching the components proportional to $\cos\phi$ and $\sin\phi$ does not admit a prescription for L. Also, matching these terms does not directly affect the velocity of the filament. Finally, we note that both the Moore–Saffman equation and the Fukumoto–Miyazaki equation contain higher order corrections (dependent on the axial velocity) that are absent from the Callegari–Ting equation.

1.3 Completion of Fukumoto and Miyazaki's matching procedure

In this section we match the velocity components from the third term of the perturbation expansion of the velocity field left unmatched by Fukumoto and Miyazaki.

Fukumoto and Miyazaki showed that the first three terms in the perturbation expansion of the external velocity, relative to the velocity of the filament, are given by

$$\begin{aligned}\mathbf{v} = &\frac{\Gamma}{2\pi r}\mathbf{e}_\theta + \frac{\Gamma}{4\pi\rho}\left\{\left[\ln\left(\frac{2L}{r}\right) - 1\right]\sin(\phi)\mathbf{e}_r + \left[\ln\left(\frac{2L}{r}\right)\right]\cos(\phi)\mathbf{e}_\theta\right\} \\ &+ \frac{3\Gamma r}{8\pi\rho^2}\left\{\left[\ln\left(\frac{2L}{r}\right) - \frac{4}{3}\right]\sin(2\phi)\mathbf{e}_r + \left[\ln\left(\frac{2L}{r}\right) - \frac{5}{6}\right]\cos(2\phi)\mathbf{e}_\theta + \frac{1}{18}\mathbf{e}_\theta\right\} \\ &+ \mathbf{Q} - \frac{\partial \mathbf{X}}{\partial t} + O\left(\frac{\Gamma r^2}{4\pi\rho^3}\right). \end{aligned} \tag{1.3.1}$$

The derivation of (1.3.1) is presented in appendix B. The quantity refered to by $\mathbf{Q}$ is what remains of the Biot–Savart integral.

Suppose, at this point, that the filament is a vortex ring of radius ρ, strength Γ, and has core radius a. Equation (1.3.1) gives an expression for the velocity of the velocity field outside the core of the ring. This velocity can also be computed using a stream function formulation leading to an expression for the stream function in terms of complete elliptic integrals (see section 10.1 of *Vortex Dynamics* by Saffman (1992)). Employing this approach implies that the velocity field is given by

$$\begin{aligned}\mathbf{v}_\circ = &\frac{\Gamma}{2\pi r}\mathbf{e}_\theta + \frac{\Gamma}{4\pi\rho}\left\{\left[\ln\left(\frac{8\rho}{r}\right) - 1\right]\sin(\phi)\mathbf{e}_r + \left[\ln\left(\frac{8\rho}{r}\right)\right]\cos(\phi)\mathbf{e}_\theta\right\} \\ &+ \frac{3\Gamma r}{8\pi\rho^2}\left\{\left[\ln\left(\frac{8\rho}{r}\right) - \frac{4}{3}\right]\sin(2\phi)\mathbf{e}_r + \left[\ln\left(\frac{8\rho}{r}\right) - \frac{5}{6}\right]\cos(2\phi)\mathbf{e}_\theta\right\} \\ &- \frac{\partial \mathbf{X}_\circ}{\partial t} + O\left(\frac{\Gamma r^2}{4\pi\rho^3}\right) \end{aligned} \tag{1.3.2}$$

where the subscript $\circ$ is used to signify that this expression is specifically for a vortex ring. Equations (1.3.1) and (1.3.2) purportedly describe the same flow field, but they have differences. First, we see that there is no $\mathbf{Q}$ term in (1.3.2) signifying that all contributions have been computed to the order indicated. Secondly, we note that there is no axisymmetric part in the third term of (1.3.2), while there is such a part in the corresponding term of (1.3.1). If L satisfies (1.2.6), i.e., $L = \pi\rho$, and we take $\mathbf{Q}$ to be what remains of the Biot–Savart integral after a length of $2L$ has been removed from the range of integration, then it follows that $\mathbf{Q} = \mathbf{0}$. Unfortunately, the $\ln(2L/r)$ terms appearing in (1.3.1) become $\ln(2\pi\rho/r)$ and not $\ln(8\rho/r)$ (which

is what we require to recover (1.3.2)). This means that when L is given by (1.2.6), then $\mathbf{Q}$ corresponds to the integral, over the length of the filament, of the difference between the Biot–Savart integrand and its approximation, obtained using the Taylor series expansion of the filament curve.

On the other hand, if L does not satisfy (1.2.6), then we must have $L < \pi\rho$. The velocity field $\mathbf{v}_\circ$, given by (1.3.2), can be rewritten as

$$\begin{aligned}\mathbf{v}_\circ = {} & \frac{\Gamma}{2\pi r}\mathbf{e}_\theta + \frac{\Gamma}{4\pi\rho}\left\{\left[\ln\left(\frac{8\rho}{\lambda r}\right) - 1\right]\sin(\phi)\mathbf{e}_r + \left[\ln\left(\frac{8\rho}{\lambda r}\right)\right]\cos(\phi)\mathbf{e}_\theta\right\} \\ & + \frac{3\Gamma r}{8\pi\rho^2}\left\{\left[\ln\left(\frac{8\rho}{\lambda r}\right) - \frac{4}{3}\right]\sin(2\phi)\mathbf{e}_r + \left[\ln\left(\frac{8\rho}{\lambda r}\right) - \frac{5}{6}\right]\cos(2\phi)\mathbf{e}_\theta + \mu\mathbf{e}_\theta\right\} \\ & + \mathbf{Q}_\circ - \frac{\partial \mathbf{X}_\circ}{\partial t} + O\left(\frac{\Gamma r^2}{4\pi\rho^3}\right) \end{aligned} \tag{1.3.3}$$

where

$$\lambda = \csc\left(\frac{L}{2\rho}\right) + \cot\left(\frac{L}{2\rho}\right) \tag{1.3.4}$$

$$\mu = -\frac{1}{4}\csc\left(\frac{L}{2\rho}\right)\cot\left(\frac{L}{2\rho}\right) \tag{1.3.5}$$

and $\mathbf{Q}_\circ$ is what remains of the Biot–Savart integral after a length of $2L$, centered on the singular point, has been removed from the range of integration (i.e., the same as the $\mathbf{Q}$ of (1.3.1)). For (1.3.1) and (1.3.3) to be the same, we require $8\rho/\lambda = 2L$, i.e., we take L to satisfy

$$\frac{L}{\rho}\left(1 + \cos\left(\frac{L}{2\rho}\right)\right) = 4\sin\left(\frac{L}{2\rho}\right). \tag{1.3.6}$$

The only solution to (1.3.6) for $L < \pi\rho$ is

$$L = 0. \tag{1.3.7}$$

However, this violates the assumption that L scales like $R = \rho$. Consequently, we conclude that if L scales like ρ, then the desingularized Biot–Savart integral, $\mathbf{Q}$, corresponds to the integral, over the length of the filament, of the difference between the Biot–Savart integrand and $\mathcal{H}(1 - |s - s'|/L)$ times its approximation using the Taylor series approximation (where $\mathcal{H}$ is the Heaviside step function).

Now we turn our attention to the inner flow region where the radial coordinate is scaled by the core radius a, i.e., we introduce $r' = r/a$. As we mentioned in section 1.2, a complete description of the equations in the inner region is provided in appendix A. However, for the sake of continuity we repeat some of the important equations here. The velocity field in the inner region is written as

$$\mathbf{v} = \frac{\Gamma}{2\pi a}\Big\{v^{(0)}\mathbf{e}_\theta + w^{(0)}\mathbf{s} + \epsilon\left(u^{(1)}\mathbf{e}_r + v^{(1)}\mathbf{e}_\theta + w^{(1)}\mathbf{s}\right) + \epsilon^2\left(u^{(2)}\mathbf{e}_r + v^{(2)}\mathbf{e}_\theta + w^{(2)}\mathbf{s}\right) + O(\epsilon^3)\Big\}. \tag{1.3.8}$$

We are interested in the third term in this perturbation expansion. The radial and azimuthal velocity components have the following Fourier decomposition

$$u^{(2)} = u_0^{(2)} + u_{c1}^{(2)}\cos(\phi) + u_{s1}^{(2)}\sin(\phi) + u_{s2}^{(2)}\sin(2\phi) \tag{1.3.9}$$

$$v^{(2)} = v_0^{(2)} + v_{c1}^{(2)}\cos(\phi) + v_{s1}^{(2)}\sin(\phi) + v_{c2}^{(2)}\cos(2\phi). \tag{1.3.10}$$

The terms $u_{s2}^{(2)}$ and $v_{c2}^{(2)}$ were not matched by Fukumoto and Miyazaki, yet equation (1.3.1) describes their asymptotic behavior. The Euler equations predict that $v_{c2}^{(2)}$ satisfies

$$v_{c2}^{(2)} = \frac{1}{2}\frac{\partial}{\partial r'}\left(r' u_{s2}^{(2)}\right) - \frac{1}{4}\frac{\partial}{\partial r'}\left(r'^2 u_{s1}^{(1)}\right) + \frac{1}{2}r' v_{c1}^{(1)} \tag{1.3.11}$$

and that $u_{s2}^{(2)}$ satisfies

$$\frac{\partial^2 u_{s2}^{(2)}}{\partial r'^2} + \frac{3}{r'}\frac{\partial u_{s2}^{(2)}}{\partial r'} - \frac{1}{v^{(0)}}\left(\frac{\partial^2 v^{(0)}}{\partial r'^2} + \frac{1}{r'}\frac{\partial v^{(0)}}{\partial r'} + \frac{2v^{(0)}}{r'^2}\right)u_{s2}^{(2)} = F\left[v^{(0)}(r'), w^{(0)}(r')\right] \tag{1.3.12}$$

where the right–hand side is a complicated functional of the leading order core velocities (see appendix A). The differential operator given by the left–hand side of (1.3.12) has regular singular points at $r' = 0$ and $r' = \infty$ with ordinary points for $0 < r' < \infty$. Using the asymptotic form of $v^{(0)}$ (which $\sim 1/r'$,) as $r' \to \infty$, we find one solution $u_\infty^i(r) \sim r$ and the other solution $u_\infty^r(r') \sim 1/r'^3$ as $r' \to \infty$. Alternatively, there is one solution $u_0^r(r')$ which vanishes at the origin and a second solution $u_0^i(r')$ which is

singular at the origin. Consequently, the solution to (1.3.12) can be written as

$$u_{s2}^{(2)}(r) = \gamma_{s_2}^{(2)} u_0^r(r) + u_\infty^r(r) \int_0^r \frac{d\xi}{\xi^3 [u_\infty^r(\xi)]^2} \int_0^\xi \eta^3 u_\infty^r(\eta) F\left[v^{(0)}(\eta), w^{(0)}(\eta)\right] d\eta, \quad (1.3.13)$$

which vanishes at the origin. Now it is clear we must have b and c (not both zero,) such that $u_0^r(r') = b u_\infty^i(r') + c u_\infty^r(r')$. The constants b and c are not free, but depend on the form of the leading order azimuthal velocity $v^{(0)}$ through the differential equation (1.3.12). According to (1.3.1) we have the following asymptotic form for the velocity component $u_{s2}^{(2)}$

$$\begin{aligned} u_{s2}^{(2)} &\sim \frac{3}{8}\frac{r}{a}\left[\ln\left(\frac{2L}{r}\right) - \frac{4}{3}\right] \\ &= -\frac{3}{8} r' \ln(r') + \frac{3}{8} r' \left[\ln\left(\frac{2L}{a}\right) - \frac{4}{3}\right] + \frac{r'}{2}\left(\mathbf{Q}_{s_1}^{(1)} \cdot \mathbf{n} + \mathbf{Q}_{c_1}^{(1)} \cdot \mathbf{b}\right) \end{aligned} \quad (1.3.14)$$

where the last terms come from the desingularized Biot–Savart integral. Now the asymptotic form of (1.3.13) is

$$u_{s2}^{(2)} \sim -\frac{3}{8} r' \ln(r') + r' \left\{ \gamma_{s_2}^{(2)} b + \frac{1}{4}\mathcal{A} + \frac{3\kappa'^2}{32} \right\} \quad (1.3.15)$$

where $\kappa' = R\kappa$ and

$$\mathcal{A} = \lim_{\zeta \to \infty} \left\{ \int_0^\zeta \eta^3 u_\infty^r(\eta) F\left[v^{(0)}(\eta), w^{(0)}(\eta)\right] d\eta - \frac{3}{2}\ln(\zeta) \right\}. \quad (1.3.16)$$

Comparing (1.3.14) and (1.3.15) we find

$$\gamma_{s_2}^{(2)} b = \frac{3}{8}\left[\ln\left(\frac{2L}{a}\right) - \frac{4}{3}\right] - \frac{3}{32} - \frac{1}{4}\mathcal{A} + \frac{1}{2}\left(\mathbf{Q}_{s_1}^{(1)} \cdot \mathbf{n} + \mathbf{Q}_{c_1}^{(1)} \cdot \mathbf{b}\right). \quad (1.3.17)$$

The contributions from the desingularized Biot–Savart integral provide terms that remove the dependence of L from the right–hand side of (1.3.17). Clearly, the matching has provided no further information on L.

1.4 Other equations of motion used in the literature

There are three other equations of motion that are used quite frequently in the literature. These are associated with the local induction approximation, the cut–off

approximation and the Rosenhead approximation. Since we use these equations at various points throughout this work, we provide a brief description of them here.

The equation associated with the local induction approximation is the subject of a very large body of work, the most of the three equations. In the local induction approximation, the equation of motion of the filament is taken to be given by

$$\frac{\partial \mathbf{X}}{\partial t} = \frac{\Gamma}{4\pi\rho} \ln\left(\frac{\rho}{a}\right) \mathbf{b}, \tag{1.4.1}$$

i.e., it is the limit of the equations presented in section 1.2, when $a/\rho \to 0$. Usually, it is assumed further that $\ln(\rho/a)$ varies slowly enough that it can be treated as a constant over the length of the filament and consequently it is absorbed, along with $\Gamma/4\pi$, into the time to yield the following nonlinear equation

$$\frac{\partial \mathbf{X}}{\partial t_*} = \frac{\partial \mathbf{X}}{\partial s} \times \frac{\partial^2 \mathbf{X}}{\partial s^2} \tag{1.4.2}$$

where t_* is the scaled time and the right–hand side follows from the Frenet–Serret formulae. Hasimoto (1972) showed that if one considered the complex scalar function $\psi(s, t_*)$ given by

$$\psi(s, t_*) = \kappa(s, t_*) \exp\left(i \int_0^s \tau(s', t_*) ds'\right), \tag{1.4.3}$$

then the local induction equation (1.4.2) is equivalent to the cubic Schrödinger equation

$$i\frac{\partial \psi}{\partial t_*} + \frac{\partial^2 \psi}{\partial s^2} + \frac{1}{2}\left(|\psi|^2 + A(t_*)\right)\psi = 0 \tag{1.4.4}$$

where $A(t_*)$ is an arbitrary function of t_*. This new formulation of the equation of motion is very advantageous, since it is well known that the cubic Schrödinger equation is completely integrable, possessing soliton solutions as well as the more general cnoidal wave type solutions (see section 17.8 of *Linear and Nonlinear Waves* by Whitham (1974)). The equation of the filament for the former case was found by Hasimoto by integrating the Frenet–Serret formulae. The equation of the filament for the latter case is very hard to obtain by integrating the Frenet–Serret formulae, but Kida (1981) obtained the equation directly from (1.4.2). Since Hasimoto's work,

there has been a profusion of papers which examine various aspects of the local induction equation from the viewpoint of nonlinear wave theory. Unfortunately, the local induction equation has some serious drawbacks since it admits unphysical filament shapes as solutions (i.e., filaments which intersect themselves). Also, from the point of view of dynamics, the equation does not account for self–induced stretching of vortex filaments.

The second approximation, the cut–off approximation, has been unjustly cast as second rate by many workers in vortex dynamics over the last couple of decades. It appeared in its first incarnation when it was proposed by Crow (1970) that the Biot–Savart line integral could be desingularized by removing a small interval of length $2a\delta$, centered on the singular point, from the range of integration, yielding

$$\frac{\partial \mathbf{X}(s,t)}{\partial t} = \frac{\Gamma}{4\pi} \int_{[\delta]} \mathbf{s}_* \times \frac{(\mathbf{X}(s,t) - \mathbf{X}(s_*,t))}{|\mathbf{X}(s,t) - \mathbf{X}(s_*,t)|^3} ds_*. \tag{1.4.5}$$

The subscript $[\delta]$, on the integral in (1.4.5), indicates that the length $2a\delta$ is omitted from the range of integration. Crow computed the values of δ which admitted the correct speed for a vortex ring and the correct frequency of rotation for a displacement wave on a columnar vortex. Both values of δ were identical, although Crow admits that due to an arithmetical error he originally believed that there was a small discrepancy. Moore and Saffman showed that the cut–off equation was asymptotically equivalent to their equation when $w_0^{(1)} = 0$ and the cut–off length is given by

$$\begin{aligned} \ln(2\delta) &= -A_\infty \\ &= -\lim_{r\to\infty} \left(\frac{4\pi^2}{\Gamma^2} \int_0^r \xi \left[v^{(0)}(\xi) \right]^2 d\xi - \ln\left(\frac{r}{a}\right) \right) \\ &\quad + \frac{1}{2} + \frac{8\pi^2}{\Gamma^2} \int_0^\infty \xi \left[w^{(0)}(\xi) \right]^2 d\xi. \end{aligned} \tag{1.4.6}$$

Essentially, this is the same prescription for δ obtained by Crow. However, Moore and Saffman's equations are valid for arbitrary shaped filaments, so (1.4.5–6) is also valid for arbitrary shaped filaments. It is this last fact that has been a source of contention, since some fluid mechanicians remain under the impression that the use of the cut–off equation for a filament of arbitrary shape is ad–hoc. This impression

is not correct, since Moore and Saffman justified the equation to be asymptotically valid for filaments of arbitrary shape.

The last approximation we consider, the Rosenhead approximation, is fundamentally different from the other two types of approximation, since the corresponding equation of motion cannot be considered as a formal or asymptotic limit of the equations in section 1.2. In the Rosenhead approximation the kernel of the Biot–Savart integral is desingularized, so that the equation of motion is written as

$$\frac{\partial \mathbf{X}(s,t)}{\partial t} = \frac{\Gamma}{4\pi}\int_{[\delta]} \mathbf{s}_* \times \frac{(\mathbf{X}(s,t)-\mathbf{X}(s_*,t))}{(|\mathbf{X}(s,t)-\mathbf{X}(s_*,t)|^2+\mu^2)^{3/2}} ds_* \tag{1.4.7}$$

where

$$\mu = a\exp(\delta - 1)\,. \tag{1.4.8}$$

Such a method of desingularization is usually classed as belonging to a group of methods called "blob" type methods (Leonard (1980)). The expression (1.4.8) for μ is obtained by forcing (1.4.7) to be equivalent to (1.4.5). When Rosenhead (1930) originally proposed (1.4.7) as an equation describing vortex filament motion, he simply stated that μ scaled like a. In fact, Thomson (1883) used this expression with $\mu = a$ and obtained the expression $(\Gamma/4\pi\rho)[\ln(8\rho/a) - 1]$ for the speed of a vortex ring, the correct speed having $-1/4$ in place of the -1.

To summarize, we have seen that equation (1.4.2) is completely local and integrable, and accordingly has been analyzed from a number of different points of view. However, we have noted that the equation is generally accepted as providing a poor model of vortex filament motion. Equation (1.4.5), on the other hand, contains much more physics — the effect of the flow in the core is taken into account and vortex filament stretching is permitted. This has lead to the equation being used in a number of analytic investigations into questions concerning the stability of vortex filaments. In chapter 3 we use the cut–off equation to consider the stability of a vortex ring confined to move inside a cylindrical pipe and along its axis. Unfortunately, the cut–off equation is inconvenient to use in numerical algorithms, since the segment cut–off from the range of integration usually interferes with the numerical grid. The Rosen-

head approximation is better suited for numerical algorithms. In chapter 4 we obtain steady periodic planar filaments that are solutions of the Rosenhead equation.

CHAPTER 2

ON THE DYNAMICS OF ULTRA–THIN VORTEX FILAMENTS

2.1 Introduction

In this chapter we consider a special case for the motion of thin–cored vortex filaments. As described in chapter 1, a vortex filament is assumed to be a concentration of vorticity in a cylindrical type tube centered on some time dependent space curve $\mathbf{X}(q,t)$, where q marks position along the curve. The core radius of the filament is denoted by a and is assumed to be small compared with some length scale associated with the filament; typically, the length scale chosen for comparison is the radius of curvature ρ. The strength of the filament is denoted by Γ. We saw that the Biot–Savart integral, while correctly giving the velocities at points away from the core, gives a divergent answer when used to describe the velocity of a point on a non–rectilinear filament (see also *An introduction to fluid dynamics* by Batchelor (1967),) and that the actual velocity of the filament depends on the internal core structure. This is manifested by the Kelvin (1867) formula

$$U = \frac{\Gamma}{4\pi\rho}\left[\ln\left(\frac{8\rho}{a}\right) - \frac{1}{4}\right] \tag{2.1.1}$$

for the speed of an inviscid uniform thin–cored vortex ring. Subsequent to Kelvin's work, studies of vortex filament dynamics employed ad–hoc desingularizations in the Biot–Savart integral (e.g., the works of Thomson (1883), Rosenhead (1930) and Crow (1970) consider various desingularization procedures, some of which are described in section 1.6). The desingularization procedure proposed by Crow was to remove some specified interval, about the singular point, from the range of integration. As we saw in section 1.4, for a filament centered on the curve $\mathbf{X}$ with arclength $\hat{s}$, this procedure gives the following cut–off integral for the equation of motion

$$\frac{\partial \mathbf{X}(\hat{s},t)}{\partial t} = \frac{\Gamma}{4\pi}\int_{[\delta]} \hat{\mathbf{s}}_* \times \frac{(\mathbf{X}(\hat{s}) - \mathbf{X}(\hat{s}_*))}{|\mathbf{X}(\hat{s}) - \mathbf{X}(\hat{s}_*)|^3} d\hat{s}_*, \tag{2.1.2}$$

where $[\delta]$ indicates that a length $2a\delta$, centered on the point with arclength coordinate $\hat{s}$, is removed from the range of integration. The cut–off length was usually chosen to yield the correct velocity for a vortex ring with the same core structure. This approach is called the cut–off approximation. Moore and Saffman (1972) re–examined the general problem and obtained an asymptotically valid approximation for the velocity of an arbitrary thin–cored vortex filament, by using a force balance argument in an asymptotic matching procedure. They then showed that this expression, for the velocity, was asymptotically equivalent to a cut–off integral with a specific cut–off length and thus removed the ad–hoc nature of the procedure. The prescription for the cut–off length was, in fact, identical to that in the cut–off approximation, but to emphasize that the procedure has been made rational we shall refer to the formulation proposed by Moore and Saffman as the cut–off equation. The Moore and Saffman analysis only explicitly deals with the case of inviscid flow with the vorticity in the core having compact support, but the viscous or infinite support corrections to the cut–off length are obviously the same as those prescribed by Saffman (1970) for the velocity of a viscous vortex ring, so that the formula (3.5) in the Moore and Saffman paper becomes the general formula

$$\ln(2\delta) = -\ln(a) - \lim_{r\to\infty}\left(\frac{4\pi^2}{\Gamma^2}\int_0^r \zeta v^2 d\zeta - \ln(r)\right) + \frac{1}{2} + \frac{8\pi^2}{\Gamma^2}\int_0^\infty \zeta w^2 d\zeta, \quad (2.1.3)$$

where v and w are the azimuthal and axial velocity, in the core, as functions of distance, ζ, from the center line. The equations (2.1.2–3) can easily be shown (see section 2.4) to be a transformation of equations (6.1–5) in the paper by Callegari and Ting (1978) with $a = \rho\sqrt{\nu/\Gamma}$, where ν is the kinematic viscosity.

Recently, a new equation of motion has been proposed by Klein and Majda (1991a,b) for a vortex filament centered on the following space curve

$$\tilde{\mathbf{X}}(\tilde{s},\tilde{t}) = \tilde{s}\mathbf{s}_0 + \epsilon^2\tilde{\mathbf{X}}^{(2)}\left(\frac{\tilde{s}}{\epsilon}, \frac{\bar{t}}{g(\epsilon)}\right), \quad (2.1.4)$$

where the tilde symbol is used (and will be used subsequently) to indicate non–dimensional variables. Lengths are made non–dimensional with respect to a reference radius of curvature ρ_0, velocities are made non–dimensional with respect to the reference speed $\Gamma/4\pi\rho_0$ and time is made non–dimensional with respect to the reference

time $4\pi\rho_0^2/\Gamma$. Scaling in this way leads to a non-dimensional radius of curvature $\tilde{\rho} = O(1)$. The type of filament described by (2.1.4) is a perturbation of a straight line vortex, where the unit vector $\mathbf{s}_0$ is parallel to the straight line and $\tilde{s}$ measures distance along the straight line. The type of situation being considered is shown in figure 2.1.1, where we depict the filament curve as being enclosed in a tube, representing the vortex core. The amplitude of the perturbation of the curve from the straight line is given by D, which is $O(\epsilon^2\rho)$. The wavelength of the perturbation is Λ, which is $O(\epsilon\rho)$. The perturbation parameter ϵ is assumed to be small and is related to the dimensionless core radius, $\tilde{a}$, through the following relation

$$\epsilon^2 \left[\ln\left(\frac{2\epsilon}{\tilde{a}}\right) + C \right] = 1, \tag{2.1.5}$$

where C is an $O(1)$ quantity, which depends on the core structure as

$$C = \ln(\tilde{a}) + \lim_{\tilde{r}\to\infty} \left(\frac{1}{4}\int_0^{\tilde{r}} \tilde{\zeta}\tilde{v}^2 d\tilde{\zeta} - \ln(\tilde{r}) \right) - \frac{1}{2} - \frac{1}{2}\int_0^{\infty} \tilde{\zeta}\tilde{w}^2 d\tilde{\zeta}, \tag{2.1.6}$$

where $\tilde{v}$ and $\tilde{w}$ are dimensionless azimuthal and axial velocities in the core, scaled on the core radius a instead of ρ_0. Note that $\tilde{a}$ is $O(\epsilon\exp(-1/\epsilon^2))$, so that such filaments can justifiably be called ultra-thin. (In appendix C we show that for the trailing vortex of an aircraft, assuming Λ scales on the wingspan of the aircraft, the ultra-thin requirement means that for $\epsilon \leq 0.2$ the core radius is less than the mean free path in air, at standard atmospheric conditions.) The scaled time appearing in (2.1.4) is related to the time $\tilde{t}$ by

$$\bar{t} = \left[\ln\left(\frac{2\epsilon}{\tilde{a}}\right) + C \right] \tilde{t}. \tag{2.1.7}$$

Finally the function $g(\epsilon)$ is taken to be ϵ^2.

As we mentioned above, the Klein and Majda regime, which requires the scaling specified by (2.1.5), is a special limit of the more general case of thin-cored vortex filament motion, where it is assumed that the ratio $a/\rho \ll 1$. It is special because it assumes that an intermediate length scale is present in the filament geometry. This intermediate length scale is the wavelength Λ of the perturbation, which is assumed to be much larger than the core radius and much smaller than the radius

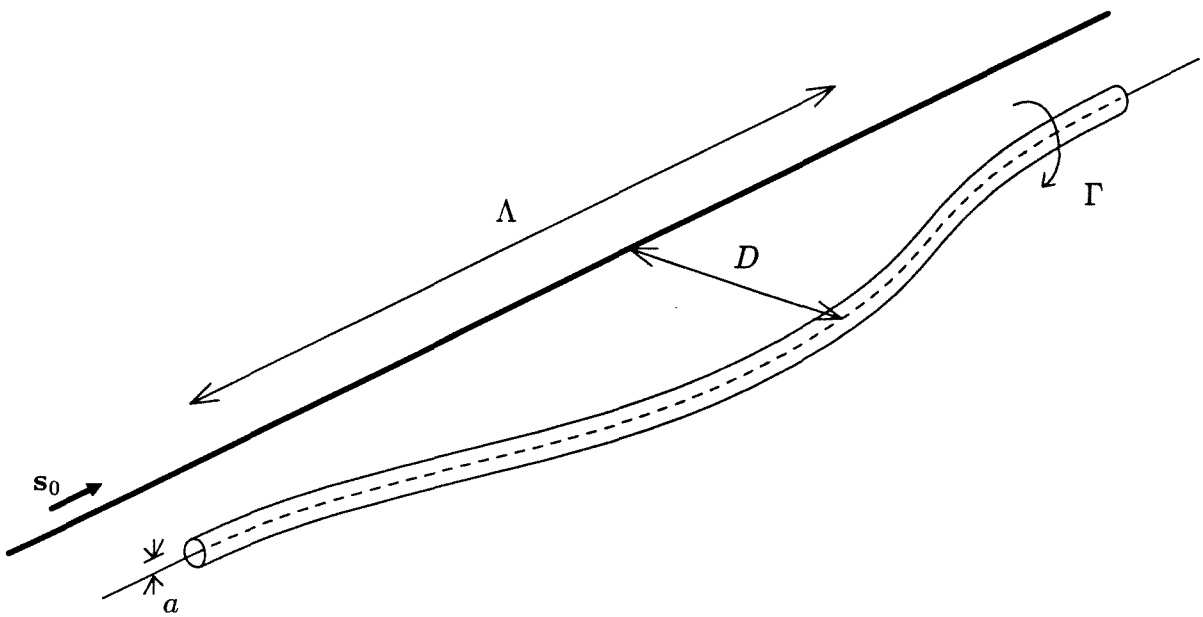

Figure 2.1.1 The filament and associated dimensional parameters. The radius of curvature, ρ, of the filament is $O(\Lambda^2/D)$. Λ and D are related to ϵ by $\Lambda/\rho = O(\epsilon)$, $D/\rho = O(\epsilon^2)$.

of curvature. From the numerical work of Chorin (1982) and Siggia (1985), Klein and Majda suspected that filaments exhibiting this ordering of scales could develop hairpin and kink type structures through stretching brought about by the filaments self-induction. Inspired by this Klein and Majda considered the filament, described above, and followed the procedure used by Callegari and Ting, where the flow inside a viscous vortex core is matched to an external irrotational flow described by the Biot–Savart integral, to obtain the following asymptotic equation of motion

$$\frac{\partial \tilde{\mathbf{X}}}{\partial \bar{t}} = \tilde{\kappa}\hat{\mathbf{b}} + \epsilon^2 \mathcal{I}\left[\tilde{\mathbf{X}}^{(2)}\right] \times \mathbf{s}_0, \tag{2.1.8}$$

where $\mathcal{I}$ is a linear integral operator given by

$$\mathcal{I}[\mathbf{Y}] = \int_{-\infty}^{\infty} \left(\mathbf{Y}(\sigma + h) - \mathbf{Y}(h) - h\mathbf{Y}_\sigma(\sigma + h) + \frac{h^2}{2}\mathcal{H}(1 - |h|)\mathbf{Y}_{\sigma\sigma}(\sigma) \right) \frac{dh}{|h|^3}, \tag{2.1.9}$$

with $\mathcal{H}$ denoting the Heaviside step function. At this point we remark that we shall use the caret symbol to denote that the variables we are working with are those associated with the perturbed filament. Consequently, $\hat{s}$ is the arclength associated

with the perturbed filament curve, while s is the arclength along the straight line or unperturbed filament curve. By a clever application of the Hasimoto (1972) transform, Klein and Majda showed that (2.1.8) was equivalent to a nonlinear Schrödinger equation which takes the form

$$-\imath\frac{\partial\tilde{\psi}}{\partial\tau} = \frac{\partial^2\tilde{\psi}}{\partial\hat{\sigma}^2} + \epsilon^2\left(\frac{1}{2}\left|\tilde{\psi}\right|^2\tilde{\psi} - \mathcal{I}[\tilde{\psi}]\right), \tag{2.1.10}$$

where the filament function $\tilde{\psi}$ depends on the curvature, $\tilde{\kappa}$, and torsion, $\tilde{T}$, in the following way,

$$\tilde{\psi} = \tilde{\kappa}\exp\left(\imath\int_0^{\tilde{s}}\tilde{T}d\tilde{s}\right), \tag{2.1.11}$$

and the time scale τ is $\bar{t}/g(\epsilon)$. The novel equation (2.1.10) shows explicitly how the integral operator competes with the cubic nonlinearity (i.e., how the stretching competes with the local induction part of the motion). Owing to the nature of the terms contained in (2.1.10), the equation is called *the filament equation with self stretching*, by Klein and Majda.

In (2.1.2) and (2.1.8), we have two apparently different equations claiming to describe the same phenomena, and it is important to know if they are actually the same, or if in fact they contain different physics. For this purpose, in section 2.2, we consider the problem of the rotation rate of a helical filament of large pitch, i.e., one for which $D \ll \Lambda$. Moore and Saffman applied their equations and obtained an expression for the rotation rate. This expression, obtained assuming $a \ll \rho$, agreed with the results obtained for helical filaments that were infinitesimal perturbations of a columnar vortex (i.e., filaments for which $D \ll a$). As a particular example of the latter problem, we have the study of Kelvin (1880), who considered the situation where the vorticity in the core was uniform and there was no axial flow in the core. We go on to describe the work of Klein and Majda (1991b) who considered the motion and stability of a helical filament in their regime. The expression obtained from the Klein and Majda equation, for the rotation rate of a filament having uniform vorticity and no axial flow in the core, differs from the Kelvin expression. It is shown, however, that we can attribute this difference to the transcendentally small core required in

the Klein and Majda geometry, which violates the $D \ll a$ criterion necessary for overlap with the Kelvin analysis. After a careful reconsideration of the problem, taking account of the transcendentally small core, we show that the cut–off equation predicts the same rotation rate as the equation of Klein and Majda. In section 2.3 we establish the exact relationship between (2.1.8) and the cut–off equation, and we show that using the same filament, as used by Klein and Majda, in the cut–off equation leads to (2.1.8), when $\ln(2\delta) = -C$, which is obvious from (2.1.3) and (2.1.6). Thus *the filament equation with self stretching* is equivalent to a special case of the cut–off equation.

It is now useful, in order to facilitate the comparison of (2.1.2) and (2.1.8), to put the equations of Klein and Majda into dimensional form. The relevant dimensional quantities, according to the scalings used by Klein and Majda, are

$$\mathbf{X} = \tilde{\mathbf{X}}\rho_0, \quad a = \tilde{a}\rho_0, \quad \Lambda = \epsilon\rho_0, \quad t = \tilde{t}\frac{4\pi\rho_0^2}{\Gamma}. \tag{2.1.12}$$

The quantity Λ is the wavelength of the perturbation. We note that Λ is defined by (2.1.5) if a is given and the characteristic radius of curvature ρ_0 is specified. With these scalings the equation of the perturbed filament, which was given by (2.1.4), becomes

$$\mathbf{X}(s,t) = s\mathbf{s}_0 + \epsilon^2\mathbf{X}^{(2)}\left(\frac{s}{\Lambda}, \frac{\Gamma}{4\pi\epsilon^4\rho_0^2}t\right). \tag{2.1.13}$$

The asymptotic equation (2.1.8) describing the motion of a point on the filament transforms to the dimensional equation

$$\frac{\partial \mathbf{X}}{\partial t} = \frac{\Gamma}{4\pi}\left[\ln\left(\frac{2\epsilon\rho_0}{a}\right) + C\right]\kappa\hat{\mathbf{b}} + \frac{\Gamma}{4\pi\rho_0^2}\mathcal{I}\left[\mathbf{X}^{(2)}\right] \times \mathbf{s}_0, \tag{2.1.14}$$

where in terms of dimensional quantities, C, given by (2.1.6), transforms to

$$C = \ln(a) + \lim_{r\to\infty}\left(\frac{4\pi^2}{\Gamma^2}\int_0^r \zeta v^2 d\zeta - \ln(r)\right) - \frac{1}{2} - \frac{8\pi^2}{\Gamma^2}\int_0^\infty \zeta w^2 d\zeta, \tag{2.1.15}$$

which is $-\ln(2\delta)$.

2.2 The rotation rate of a helical filament of large pitch

Moore and Saffman (1972) considered the general case of the motion of a curved, thin cored vortex filament containing axial flow. (The work of Adebiyi (1981), who rigorously examined the existence and motion of helical filaments of small cross–section by reformulating the problem in terms of an integral equation, ought to be mentioned at this point. He independently confirmed that the equation of motion for a helical filament was correctly given by the Moore–Saffman equations with the error being the same as that given in the Moore–Saffman paper.) As mentioned in section 2.1, they showed that their equations could be reformulated as the cut–off equation, i.e., equations (2.1.2–3). They applied the cut–off equation to the motion of a filament which takes the shape of a helix of large pitch and is given by

$$\mathbf{X} = D\left(\mathbf{i}\cos\theta + \mathbf{j}\sin\theta - \mathbf{k}\left(\frac{\theta - \Omega t}{\gamma}\right)\right), \tag{2.2.1}$$

where the pitch of the helix is $1/\gamma$ and the radius of the cylinder, whose surface contains the helix, is given by D. The radius of curvature is $\rho = D + D/\gamma^2$. Also, Ω (to be found) is the rotation rate of the helical filament. For small γ (i.e., large pitch), the rotation rate was found to be

$$\Omega_{MS} = \frac{\Gamma\gamma^2}{4\pi D^2}\left[\ln\left(\frac{2D}{\gamma a}\right) + \frac{1}{2} - E - \ln 2\delta\right] + O(\gamma^4 \ln\left(\frac{D}{\gamma a}\right)) \tag{2.2.2}$$

where δ satisfies (2.1.3) and $E = 0.5772\ldots$ is Euler's number.

Klein and Majda (1991b) applied their filament equation (2.1.8) to a number of specific problems. Their studies culminate with some numerical experiments that indicated that some solutions to their equations developed kink or hairpin type structures in finite time. (It is worth noting that Moore (1972), Dhanak (1981), and Dhanak and de Bernardinis (1981) carried out computations, using the Rosenhead desingularization procedure, which showed no kinking or hairpins for the evolution of some types of vortex filaments.) However, of interest to us is their study on the motion and stability of a helical filament, and we now compare the results of the cut–off equation with the Klein–Majda equation. Klein and Majda considered the following filament function

$$\tilde{\psi}_H(\sigma,\tau) = \tilde{A}\exp\left(\imath\left(\tilde{\xi}\sigma - \tilde{\Omega}_{KM}\tau\right)\right), \tag{2.2.3}$$

which represents a helix with constant curvature $\tilde{A}$ and constant torsion $\tilde{\xi}/\epsilon$. Substitution of (2.2.18) into the filament equation (2.1.10) yields the following for the rotation rate

$$\tilde{\Omega}_{KM} = \tilde{\xi}^2 \left[1 + \epsilon^2 \left(\frac{1}{2} - E - \ln(|\tilde{\xi}|)\right)\right] - \frac{1}{2}\epsilon^2 \tilde{A}^2, \tag{2.2.4}$$

which is made dimensional by multiplying by $\Gamma/4\pi\epsilon^4\rho_0^2$. The relationship between the variables in (2.2.3–4) and those in (2.2.1) is easily established. Consider the following equation for the helical filament, which at time $t = 0$ takes the form

$$\mathbf{X} = \epsilon^2 D_0 \left[\mathbf{i}\cos(\sigma) + \mathbf{j}\sin(\sigma)\right] - \mathbf{k}s, \tag{2.2.5}$$

where $D_0 = O(\rho_0)$ and σ is given by s/Λ. Now we recall that ρ_0 is assumed to be a scaling factor so that the true radius of curvature, ρ, satisfies $\rho/\rho_0 = O(1)$. We will be more specific at this point and take $\rho_0 = D_0$. The filament given by (2.2.5) is of the Klein and Majda type (i.e., it is in the same form as (2.1.13)) and is a helix of large pitch. The non–dimensional curvature and torsion of the filament are given by

$$\tilde{A} = 1 - \epsilon^2 \tag{2.2.6}$$

$$\frac{\tilde{\xi}}{\epsilon} = -\frac{1}{\epsilon}\left(1 - \epsilon^2\right) \tag{2.2.7}$$

which along with (2.2.5) yields the following for the dimensional rotation rate

$$\Omega_{KM} = \frac{\Gamma}{4\pi\epsilon^2 D_0^2}\left[\ln\left(\frac{2\epsilon D_0}{a}\right) - \frac{1}{4} - E + O(\epsilon^2)\right]. \tag{2.2.8}$$

Now for the situation being considered (i.e., uniform vorticity and no axial flow in the core) the rotation rate of the filament given by (2.2.2) reduces to

$$\Omega_K = \frac{\Gamma\gamma^2}{4\pi D^2}\left[\ln\left(\frac{2D}{\gamma a}\right) + \frac{1}{4} - E\right]. \tag{2.2.9}$$

This is the classical Kelvin result, obtained by Kelvin through the consideration of infinitesimal perturbations to a columnar vortex (i.e., perturbations for which $D \ll a$). Comparison of (2.2.1) and (2.2.5) establishes the relationship between the various

parameters; simply take $D = \epsilon^2 D_0$ and $\gamma = \epsilon$. Consequently, (2.2.9) can be rewritten as

$$\Omega = \frac{\Gamma}{4\pi\epsilon^2 D_0^2}\left[\ln\left(\frac{2\epsilon D_0}{a}\right) + \frac{1}{4} - E\right]. \tag{2.2.10}$$

Clearly, (2.2.10) differs from (2.2.8) by $\Gamma/8\pi\epsilon^2 D_0^2$.

This apparent paradox seems to indicate that the Klein and Majda equations are somehow including some physical effect absent from the previous theories. However, as we alluded to earlier, this is not the case. To see this we return to the filament (2.2.1) and reconsider the application of the cut–off equation. To have an overlap between the thin filament theory and the Kelvin analysis requires $\gamma \ll 1$ and consequently the Moore and Saffman calculation retained only the leading order terms in γ. Retaining higher order terms in γ, we obtain the following equation for the rotation rate

$$\Omega = \frac{\Gamma\gamma^2}{4\pi D^2}\left[\ln\left(\frac{2D}{\gamma a}\right) + \frac{1}{4} - E - \frac{1}{2}\gamma^2\left(\ln\left(\frac{2D}{\gamma a}\right) - 4\ln 2 - \frac{1}{2} + E\right)\right] + O(\gamma^6 \ln\left(\frac{D}{\gamma a}\right)). \tag{2.2.11}$$

(The calculation of (2.2.11) from (2.1.2) and (2.2.1) is an involved and difficult calculation, and the details are presented in appendix D.) In terms of the variables D_0 and ϵ, this is written as

$$\Omega = \frac{\Gamma}{4\pi\epsilon^2 D_0^2}\left[\ln\left(\frac{2\epsilon D_0}{a}\right) + \frac{1}{4} - E - \frac{1}{2}\left(1 + \epsilon^2\left(E - \frac{1}{4} - 4\ln 2\right)\right)\right], \tag{2.2.12}$$

which agrees with the Klein–Majda result. In transforming (2.2.11) to (2.2.12) we clearly see that the difference between (2.2.8) and (2.2.10) is due to the fact that we have a situation where $\ln(D/a\gamma) \sim 1/\gamma^2$ (the ultra–thin condition) and consequently the error terms of (2.2.2), which were ignored in obtaining (2.2.9) (from which we obtain (2.2.10)) are significant!

In summary we have that the rotation rate of a helical filament of large pitch depends, from (2.2.11) and the relation $\rho = D + D/\gamma^2$, on the value of γ and the ratio a/ρ. In figure 2.2.1 we graphically portray this dependence. The original Kelvin result, (2.2.8), required $D \ll a$, and is valid in a region approximately corresponding

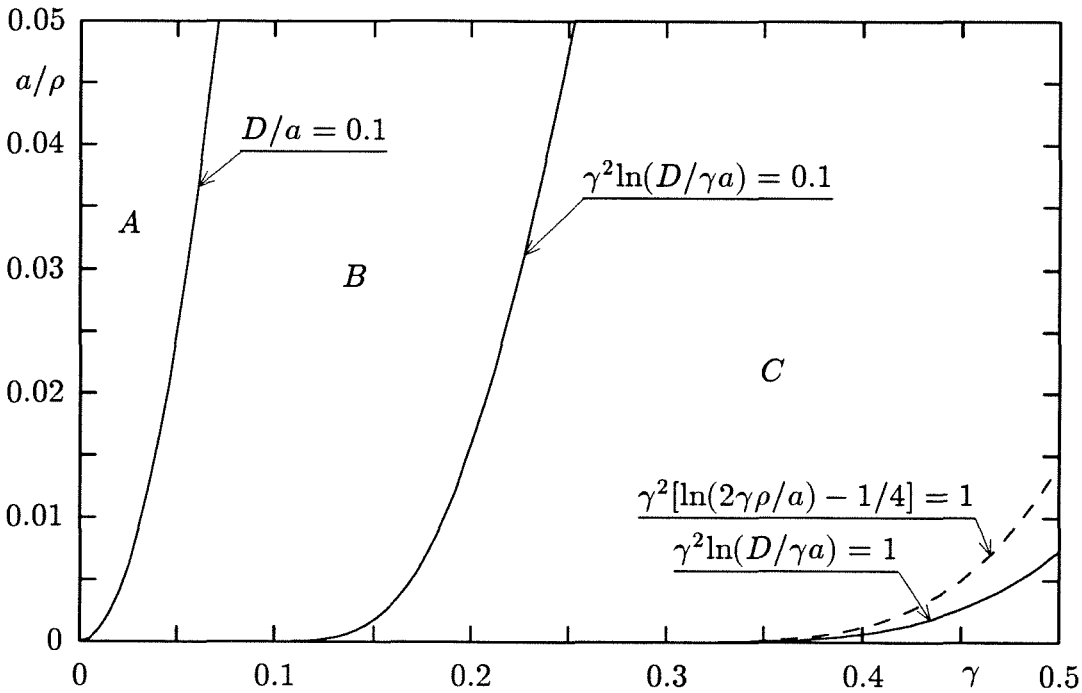

Figure 2.2.1 The rotation rate, Ω, as predicted by the cut–off equation (for a helical filament of large pitch with uniform vorticity in the core) depends on the values of a/ρ and the pitch $1/\gamma$. In regions A and B we have $\Omega = \Omega_K$, while in region C the cut–off equation indicates that there are corrections that become important (as explained in the text). The Klein–Majda regime applies on the dashed curve, near the boundary of region C.

to region A of the figure. The boundary of region A corresponds to $D/a = 0.1$. The extension of Kelvin's result, by Moore and Saffman, requires that $\gamma^2 \ln(D/a\gamma) \ll 1$. This means the extension is valid throughout a region approximately corresponding to region B, where the boundary of region B corresponds to $\gamma^2 \ln(D/a\gamma) = 0.1$. We depict another region C which has a boundary corresponding to $\gamma^2 \ln(D/a\gamma) = 1$. The equation (2.2.11) is valid throughout the region C. Clearly the error terms in (2.2.2) neglected by Moore and Saffman, become more significant as we move deeper into region C. Not surprisingly, the Klein and Majda case lies near the boundary of region C, and it is represented by the dashed curve. This curve corresponds to

$\gamma^2[\ln(2\gamma\rho/a) - 1/4] = 1$. We also note that since the helix is of large pitch, we require $\gamma \ll 1$ which means we should only consider the analyses in a thin strip parallel to the a/ρ axis. (However, in figure 2.2.1 we have taken a range in γ from 0.0 to 0.5, so as to allow a clear identification of the various regimes.)

The second feature of the helical motion considered by Klein and Majda was the stability of the helical filament. The stability question has been previously studied by Widnall (1972) and Fukumoto and Miyazaki (1991), both using the cut–off equation. (The analysis of Fukumoto and Miyazaki is a reworking of Widnall's analysis to include some of the second order effects, particularly the effect of an axial velocity.) Unfortunately, there is insufficient data available to make a direct comparison between the two results; however, qualitative agreement can be shown to exist if we consider figure 7 of Widnall's paper along with figures 3.1–2 of Klein and Majda's paper. The values of the parameters for the unperturbed helix in the Klein–Majda case are $\tilde{A} = 4.0$, $\tilde{\xi} = 2.0$ and $\epsilon = 0.5$. The helix of Widnall's paper is characterized by two parameters R and k, where R is the cylinder radius and $1/Rk$ is the pitch. Three parameters are used to characterize the helix in the Klein–Majda case, with the additional parameter specification setting the size of the core radius. The helix in the Klein–Majda case corresponds to a helix in Widnall's analysis with $Rk = 1$ and $a/R \approx 0.0019$. The perturbation wavenumber in the Widnall case is denoted by γ while the perturbation wave number relative to base helix wave number is given by β in the Klein–Majda case: these two quantities are related by $\gamma/k' = \beta/2$, where $k' = k/(1 + k^2R^2)$. For the Widnall analysis the ratio of core radius to helix radius ranges through the discrete set 0.01, 0.1, 0.22, 0.27, 0.33. For $Rk = 1$ we find two bands of instability on the Widnall graph, where one of the bands is for long waves and the other for short waves. The band for short waves corresponds to the so–called spurious instability mode. Both analyses confirm that the mutual inductance modes of instability are not present for the range of parameters considered by Klein and Majda, and overall the results of the Klein–Majda analysis closely mirror the Widnall results. In the Klein–Majda analysis greater detail is given of the boundaries of the instability bands. The individual boundaries, for the different values of a/R, for the

instability band corresponding to long waves were omitted in the Widnall analysis and were said to be characterized by the zero core–radius limit. Fukumoto and Miyazaki provide details of this instability band, which includes some of the effects of an axial flow in the core. For more details of the various analyses, the reader is referred to the respective papers.

2.3 The cut–off equation for the ultra–thin filament

We now show that the helix is not just a special case, but that the Klein and Majda equation follows from the cut–off equation for the appropriate type of filament. We apply the cut–off equation to the type of filament considered by Klein and Majda and show that their equations follow directly. On one level the calculations presented in this section are comparable to those of section 3 of Klein and Majda (1991a) since our calculation considers a reduced Biot–Savart type integral (the cut–off integral), while their calculation considers the full Biot–Savart integral. The fundamental difference between the calculations lies in the fact that our integral has no singular points, and as a consequence, the distance from the field point to the filament can be set to zero. This fact is vital to our calculations, since it allows us to make certain simplifications in the course of our calculation, simplifications which cannot be made when the distance to the filament is nonzero.

The filament Klein and Majda consider is upon suppression of the time dependence written as

$$\mathbf{X} = s\mathbf{s}_0 + \epsilon^2 \mathbf{X}^{(2)}(\sigma), \tag{2.3.1}$$

where now

$$\sigma = \frac{s}{\Lambda}, \tag{2.3.2}$$

with $\Lambda = \epsilon\rho_0$, from (2.1.12c). Now we use this filament along with the various assumptions to evaluate how the cut–off equation behaves. A careful consideration of the terms in the integrand of the cut–off equation allow us to write the cut–off equation as

$$\int_{[\delta]} \hat{\mathbf{s}}_* \times \frac{\mathbf{X}(\hat{s}) - \mathbf{X}(\hat{s}_*)}{|\mathbf{X}(\hat{s}) - \mathbf{X}(\hat{s}_*)|^3} d\hat{s}_* =$$

$$\left(\int_{-\infty}^{-a\delta\mu/\Lambda} + \int_{a\delta\mu/\Lambda}^{\infty}\right)\left(\mathbf{X}^{(2)}(\sigma+h) - \mathbf{X}^{(2)}(\sigma) - h\mathbf{X}_{\sigma}^{(2)}(\sigma+h)\right)\times$$

$$\left(\mathbf{s}_0 + \frac{\epsilon}{\rho_0}\mathbf{X}_{\sigma}^{(2)}(\sigma+h)\right)\left(1 + \frac{\epsilon^2}{\rho_0^2 h^2}\left|\mathbf{X}^{(2)}(\sigma+h) - \mathbf{X}^{(2)}(\sigma)\right|^2\right)^{-3/2}\frac{dh}{\rho_0^2\,|h|^3}. \quad (2.3.3)$$

In (2.3.3) we have an exact expression for the cut–off integral. The quantity μ appearing in the cut–off limits comes about since we have changed the variable of integration. A simple consideration of the relationship between the arclength along the unperturbed filament, s, and arclength along the perturbed filament, $\hat{s}$, tells us that $\mu = 1+O(\epsilon^2)$. If we use the fact that we are considering a situation where $a \ll \epsilon$, then we can be more precise in determining the dependence of μ on ϵ. However, for our situation the previous representation is adequate. We now show that (2.3.3) contains the equations of Klein and Majda. First we rewrite it as the sum of three separate integrals

$$\int_{[\delta]} \hat{\mathbf{s}}_* \times \frac{\mathbf{X}(\hat{s}) - \mathbf{X}(\hat{s}_*)}{|\mathbf{X}(\hat{s}) - \mathbf{X}(\hat{s}_*)|^3} d\hat{s}_* = \frac{1}{\rho_0^2}\left(I_1 + I_2 + I_3\right). \quad (2.3.4)$$

The first integral is

$$I_1 = \int_{-\infty}^{\infty}\left(\mathbf{X}^{(2)}(\sigma+h) - \mathbf{X}^{(2)}(\sigma) - h\mathbf{X}_{\sigma}^{(2)}(\sigma+h) + \frac{1}{2}h^2\mathcal{H}(1-|h|)\mathbf{X}_{\sigma\sigma}^{(2)}(\sigma)\right)\times$$

$$\left(\mathbf{s}_0 + \frac{\epsilon}{\rho_0}\mathbf{X}_{\sigma}^{(2)}(\sigma+h)\right)\left(1 + \frac{\epsilon^2}{\rho_0^2 h^2}\left|\mathbf{X}^{(2)}(\sigma+h) - \mathbf{X}^{(2)}(\sigma)\right|^2\right)^{-3/2}\frac{dh}{|h|^3}$$

$$= \mathcal{I}\left[\mathbf{X}^{(2)}\right]\times\mathbf{s}_0(1+O(\epsilon)), \quad (2.3.5)$$

where

$$\mathcal{I}\left[\mathbf{X}^{(2)}\right] =$$

$$\int_{-\infty}^{\infty}\left(\mathbf{X}^{(2)}(\sigma+h) - \mathbf{X}^{(2)}(\sigma) - h\mathbf{X}_{\sigma}^{(2)}(\sigma+h) + \frac{1}{2}h^2\mathcal{H}(1-|h|)\mathbf{X}_{\sigma\sigma}^{(2)}(\sigma)\right)\frac{dh}{|h|^3}, \quad (2.3.6)$$

and $\mathcal{H}$ is the Heaviside step function. The second integral is

$$I_2 = -\int_{-a\delta\mu/\lambda}^{a\delta\mu/\lambda}\left(\mathbf{X}^{(2)}(\sigma+h) - \mathbf{X}^{(2)}(\sigma) - h\mathbf{X}_{\sigma}^{(2)}(\sigma+h) + \frac{1}{2}h^2\mathbf{X}_{\sigma\sigma}^{(2)}(\sigma)\right)\times$$

$$\left(\mathbf{s}_0 + \frac{\epsilon}{\rho_0}\mathbf{X}_{\sigma}^{(2)}(\sigma+h)\right)\left(1 + \frac{\epsilon^2}{\rho_0^2 h^2}\left|\mathbf{X}^{(2)}(\sigma+h) - \mathbf{X}^{(2)}(\sigma)\right|^2\right)^{-3/2}\frac{dh}{|h|^3}$$

$$= O(\frac{a\delta}{\Lambda}). \quad (2.3.7)$$

Finally, the third integral is

$$I_3 = -\left(\int_{-1}^{-a\delta\mu/\Lambda} + \int_{a\delta\mu/\Lambda}^{1}\right)\left(\frac{1}{2}h^2\mathbf{X}^{(2)}_{\sigma\sigma}(\sigma)\right)\times\left(\mathbf{s}_0+\frac{\epsilon}{\rho_0}\mathbf{X}^{(2)}_{\sigma}(\sigma+h)\right)$$
$$\left(1+\frac{\epsilon^2}{\rho_0^2h^2}\left|\mathbf{X}^{(2)}(\sigma+h)-\mathbf{X}^{(2)}(\sigma)\right|^2\right)^{-3/2}\frac{dh}{|h|^3}$$
$$=\ln\left(\frac{\Lambda}{a\delta}\right)\left(1+\frac{\epsilon^2}{\rho_0^2}\left|\mathbf{X}^{(2)}_{\sigma}\right|^2\right)^{-3/2}\left(\mathbf{s}_0+\frac{\epsilon}{\rho_0}\mathbf{X}^{(2)}_{\sigma}\right)\times\mathbf{X}^{(2)}_{\sigma\sigma}+O(\epsilon). \qquad (2.3.8)$$

Using (2.3.5) and (2.3.7–8) in (2.3.4), we find that the cut–off integral reduces to the following expression:

$$\int_{[\delta]}\hat{\mathbf{s}}_*\times\frac{\mathbf{X}(\hat{s})-\mathbf{X}(\hat{s}_*)}{|\mathbf{X}(\hat{s})-\mathbf{X}(\hat{s}_*)|^3}d\hat{s}_*=\frac{1}{\rho_0^2}\mathcal{I}\left[\mathbf{X}^{(2)}\right]\times\mathbf{s}_0+$$
$$\frac{1}{\rho_0^2}\ln\left(\frac{\Lambda}{a\delta}\right)\left(1+\frac{\epsilon^2}{\rho_0^2}\left|\mathbf{X}^{(2)}_{\sigma}\right|^2\right)^{-3/2}\left(\mathbf{s}_0+\frac{\epsilon}{\rho_0}\mathbf{X}^{(2)}_{\sigma}\right)\times\mathbf{X}^{(2)}_{\sigma\sigma}+O(\epsilon,\frac{a\delta}{\epsilon}). \qquad (2.3.9)$$

Equation (2.3.9) can be simplified further by making use of the Frenet–Serret formulae. If we apply the Frenet–Serret formulae to the curve given in (2.3.2), then we find that the curvature κ and binormal $\hat{\mathbf{b}}$ satisfy

$$\kappa\hat{\mathbf{b}}=\hat{\mathbf{s}}\times(\kappa\hat{\mathbf{n}})$$
$$=\frac{1}{\rho_0^2}\left(1+\frac{\epsilon^2}{\rho_0^2}\left|\mathbf{X}^{(2)}_{\sigma}\right|^2\right)^{-3/2}\left(\mathbf{s}_0+\frac{\epsilon}{\rho_0}\mathbf{X}^{(2)}_{\sigma}\right)\times\mathbf{X}^{(2)}_{\sigma\sigma}. \qquad (2.3.10)$$

Using (2.3.10), in (2.3.9) we rewrite the equation of motion for the filament given by (2.3.1) as

$$\frac{\partial\mathbf{X}}{\partial t}=\frac{\Gamma}{4\pi\rho_0^2}\mathcal{I}\left[\mathbf{X}^{(2)}\right]\times\mathbf{s}_0+\frac{\Gamma}{4\pi}\left[\ln\left(\frac{2\epsilon\rho_0}{a}\right)-\ln(2\delta)\right]\kappa\hat{\mathbf{b}}+O(\epsilon,\frac{a\delta}{\epsilon}). \qquad (2.3.11)$$

The corresponding equation of the Klein and Majda analysis is (2.1.14). Clearly from (2.1.3) and (2.1.15) we have that $C=-\ln(2\delta)$. This leads to the conclusion that the cut–off equation reproduces the Klein and Majda equations upon application of their assumptions. Indeed, it is clear from (2.3.11) that the equation derived by Klein and Majda corresponds to the leading terms in an expansion, based on ϵ, of the cut–off equation. The fact that the cut–off equation reduces to the Klein and Majda equation means that both equations prescribe the same evolution for a filament belonging to the

Klein and Majda regime, but the Klein and Majda equation, because of its structure, may provide a more convenient tool for describing the evolution of suitable filaments. However, as demonstrated in Klein and Majda (1991b), filaments whose evolution is described by the Klein and Majda equations may eventually leave the regime of applicability of the equation. The cut–off equation, being more general, is able to describe the evolution of the filament outside the Klein and Majda regime. Also, it should be noted at this point that Moore and Saffman derived further equations which are more accurate than the cut–off equation. Needless to say, filaments that develop radii of curvature comparable to their core radius violate the assumptions for the applicability of any of the thin–cored filament theories.

2.4 Prescription of the cut-off length for viscous filaments

As we pointed out in section 2.1, the Klein and Majda analysis is for the viscous situation, so we must establish that the cut–off equation is asymptotically valid for the viscous situation. The procedure is essentially the same as that used by Moore and Saffman for the inviscid case (described in the introduction) in that we show that the asymptotic equations of Callegari and Ting are asymptotically equivalent to a specific cut–off equation. The Callegari and Ting asymptotic equation of motion takes the form

$$\frac{\partial \mathbf{X}}{\partial t} = \mathbf{Q}_0 + \frac{\Gamma}{4\pi\rho}\left[\ln\left(\frac{\rho}{a}\right)+C_1\right]\hat{\mathbf{b}}, \tag{2.4.1}$$

where

$$C_1 = \frac{4\pi}{\Gamma}\lim_{\overline{r}\to\infty}\left[\frac{v^{(0)}}{\overline{r}}\int_0^{\overline{r}}\frac{1}{\eta(v^{(0)})^2}\int_0^{\eta}\zeta v^{(0)}H(\zeta,t)d\zeta d\eta - \frac{\Gamma}{4\pi}\ln\overline{r}\right] \tag{2.4.2}$$

and where the various quantities appearing in (2.4.2) have the same meaning as their dimensionless counterparts in (2.1.5). As before we apply L'Hôpital's rule to obtain

$$C_1 = \left(\lim_{\overline{r}\to\infty}\left[\frac{4\pi^2}{\Gamma^2}\int_0^{\overline{r}}\zeta\left(v^{(0)}\right)^2 d\zeta - \ln\overline{r}\right] + \frac{1}{2} - \frac{8\pi^2}{\Gamma^2}\int_0^{\infty}\zeta\left(w^{(0)}\right)^2 d\zeta\right). \tag{2.4.3}$$

Also, in (2.4.1) we have $\mathbf{Q}_0 = \lim_{r\to 0}(\mathbf{Q}_2 + \mathbf{Q}_f)$ where $\mathbf{Q}_2$ is the externally induced velocity and $\mathbf{Q}_f$ is the finite part of the Biot–Savart integral

$$\mathbf{Q}_f = \frac{\Gamma}{4\pi}\int \hat{\mathbf{s}}_* \times \frac{(\mathbf{P}-\mathbf{X}(\hat{s}_*))}{|\mathbf{P}-\mathbf{X}(\hat{s}_*)|^3}d\hat{s}_*$$

$$- \left(\frac{\Gamma}{2\pi r} \hat{\mathbf{e}_\theta} + \frac{\Gamma}{4\pi\rho} \cos\phi \hat{\mathbf{e}_\theta} + \frac{\Gamma}{4\pi\rho} \ln\left(\frac{\rho}{r}\right) \hat{\mathbf{b}} \right), \tag{2.4.4}$$

with the point $\mathbf{P}$ lying at a distance r from the filament. The unit vector, $\hat{\mathbf{e}_\theta}$ is in the azimuthal direction of a polar coordinate system centered on the filament and oriented so that the radial unit vector makes an angle ϕ with the unit normal $\hat{\mathbf{n}}$. Essentially, the core radius a is taken to be $(\nu/\Gamma)^{1/2}$, so we see immediately that the concept of a nonzero inviscid vortex core is not permissible in the Callegari and Ting formulation (the classical Kelvin formula for the speed of a vortex ring requires such a core). To determine the cut–off length, assume $\mathbf{Q}_2 = 0$ (i.e., the filament motion is self–induced) and subtract the cut–off equation from (2.4.1). After some calculation we find that for the cut–off equation to be asymptotically equivalent to (2.4.1), we should choose the cut–off length to satisfy

$$\ln\left(\frac{\rho}{a}\right) + C_1 = 1 - \ln\left(\frac{2a\delta}{\rho}\right). \tag{2.4.5}$$

Solving for $\ln(2\delta)$ in (2.4.5) and using (2.4.3) we obtain

$$\ln(2\delta) = -\ln a - \lim_{r\to\infty} \left[\frac{4\pi^2}{\Gamma^2} \int_0^r \zeta(v)^2 \, d\zeta - \ln r \right] + \frac{1}{2} + \frac{8\pi^2}{\Gamma^2} \int_0^\infty \zeta(w)^2 \, d\zeta. \tag{2.4.6}$$

According to (2.1.6), the right–hand side of (2.4.6) is $-C$ and we have the result we require. Together with (2.3.11) this shows that the cut–off equation reduces to the equations of Klein and Majda when we use the cut–off length given by (2.4.6) and also make the same assumptions that they make.

CHAPTER 3

THE MOTION OF A VORTEX RING IN A PIPE AND AN ASSOCIATED INSTABILITY

3.1 Introduction

In this chapter we consider a thin–cored vortex ring moving inside and along the axis of a cylindrical pipe, which has a circular cross–section. We assume that the ring radius is R, the core radius is a and the strength is Γ. The pipe has radius D. The assumption of a thin core means that the ratio $a/R \ll 1$. In figure 3.1.1 we depict the geometry of this situation.

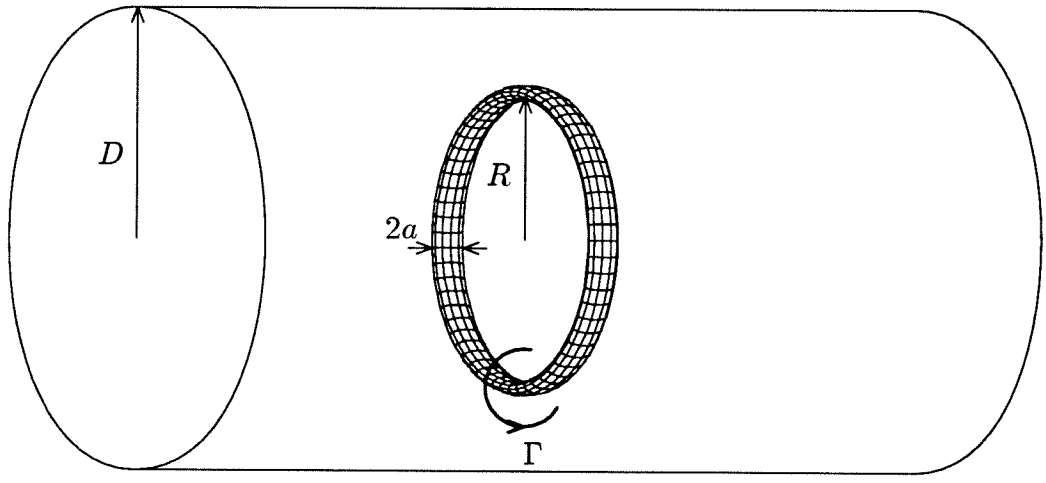

Figure 3.1.1 A vortex ring of radius R moving along the axis of a cylindrical pipe of radius D. The ring has core radius a and strength Γ.

Problems concerning the motion of vortex rings have received a lot of attention since the mid–eighteen hundreds. Interest in the motion of vortex rings was originally kindled by Kelvin's vortex–atom theory of matter. In this theory he proposed that

atoms were actually vortex rings in the so called ether, the ideal fluid which supposedly filled all space. Also, in a note added to Tait's (1867) translation of Helmholtz's (1858) paper, Kelvin gave an expression for the leading order velocity, U_K, of a vortex ring in an unbounded fluid. The expression, which is for a ring with uniform vorticity and no axial flow in the core, was given without proof and is

$$U_K = \frac{\Gamma}{4\pi R}\left[\ln\left(\frac{8R}{a}\right) - \frac{1}{4}\right]. \tag{3.1.1}$$

Amazingly, several notable fluid mechanicians attempted to derive the expression for U_K and failed. Indeed, Thomson (1883) wrote a treatise on the motion of vortex rings, in which he attempted to lay the groundwork for a complete mathematical theory of matter based on vortex ring atoms. However, in the treatise he derives an expression similar to (3.1.1), except it is of the form $(\Gamma/4\pi R)\left[\ln(8R/a) - 1\right]$ and when he compares this with Kelvin's formula he claims that Kelvin's result *agrees very approximately* with that just quoted. The reason that Thomson obtained a different formula stems from his assumption that the core radius was symmetric about the centerline of the ring. Hicks (1885) was the first to confirm Kelvin's result, and soon after Dyson (1893) computed the solution to the motion of the vortex ring to fourth order in the small parameter a/R. The modification of (3.1.1) to include the leading order effects of a general swirl velocity profile, in the core, were given by Fraenkel (1970) and also by Widnall, Bliss and Zalay (1970). Saffman (1970) gave the modifications which take account of the leading order effects of both a general swirl velocity profile and a general axial velocity profile, the expression for the steady speed being

$$U_0 = \frac{\Gamma}{4\pi R}\left[\ln\left(\frac{8R}{a}\right) - \ln(2\delta)\right], \tag{3.1.2}$$

where δ is given by

$$\begin{aligned}\ln(2a\delta) = \frac{1}{2} &+ \frac{8\pi^2}{\Gamma^2}\int_0^\infty \xi\left[w^{(0)}(\xi)\right]^2 d\xi \\ &- \lim_{r\to\infty}\left(\frac{4\pi^2}{\Gamma^2}\int_0^r \xi\left[v^{(0)}(\xi)\right]^2 d\xi - \ln\left(\frac{r}{a}\right)\right).\end{aligned} \tag{3.1.3}$$

In chapter 1 we considered equations of motion for more general shaped vortex filaments. We saw that the cut–off equation provided an asymptotically correct equation of motion for the filament and was relatively simple to employ. The equation of motion for a filament with centerline $\mathbf{X}(s,t)$ is

$$\frac{\partial \mathbf{X}}{\partial t} = -\frac{\Gamma}{4\pi}\int_{[\delta]} \mathbf{s}_* \times \frac{(\mathbf{X}(s,t) - \mathbf{X}(s_*,t))}{|\mathbf{X}(s,t) - \mathbf{X}(s_*,t)|^3} ds_*, \tag{3.1.4}$$

where the subscript $[\delta]$ indicates that a section of length $2a\delta$ centered on the point $s_* = s$ has been removed from the range of integration. If (3.1.4) is used to compute the speed of the vortex ring, then (3.1.2) is recovered.

Crow (1970) used the cut–off equation to examine the linear stability for the trailing vortex pair. Widnall and Sullivan (1973) used the cut–off equation to examine the linear stability of a vortex ring. We provide a brief description of these studies in sections 3.2 and 3.3, respectively. The goal of our analysis, presented in section 3.4, is to determine the effect the pipe wall has on the motion and stability. This involves computing the motion of the ring as a function of a/R, R/D and n, where n/R is the wavenumber of the perturbation. Accordingly, we use the cut–off equation and build on the results derived by Widnall and Sullivan. In section 3.5 we present the results of the computations. The main conclusion that will be drawn is that there is a critical value of the ratio of ring radius to pipe radius, R/D, above which the ring is subject to an instability where the ring tilts out of the plane normal to the pipe axis. In section 3.6 we reconsider the connection that the present problem has with the studies performed by Crow and by Widnall and Sullivan.

3.2 The stability of a pair of parallel line vortices

It is well known that large aircraft in flight generate a pair of strong counter rotating vortices originating at the wingtips and trailing behind the aircraft. As it evolves, this vortex pair undergoes a breakdown characterized by a growing sinusoidal disturbance on both of the filaments. Eventually the peaks of the disturbance on one filament touch those on the other filament and this is closely followed by the merging of the cores, which takes place in such a way that a sequence of crude vortex rings develops. Crow attempted to explain the mechanism which gives rise to the growing

sinusoidal disturbance. To do this he modeled the problem as the interaction between a pair of parallel line vortices. He assumed that the originally straight vortices were separated by a distance b, and on these he superimposed an infinitesimal sinusoidal type perturbation of wavelength $2\pi/k$. Although Crow allowed for either symmetrical or antisymmetrical disturbances (in the sense that for the symmetrical case either filament was a mirror image of the other with respect to the center plane), we shall only consider the symmetrical case and refer the reader to the original paper for details of the antisymmetrical case. (The reason we only consider the symmetrical case is that the ring in the pipe has a close connection with the symmetrical case when the ring and pipe radius are very large.) The geometry for the situation is depicted in figure 3.2.1. Assuming a perturbation proportional to $e^{\sigma_c t}$, where σ is the growth rate of the disturbance, Crow used the cut–off equation and obtained the following expression for the growth rate

$$\sigma_c^2 = \left(\frac{\Gamma}{2\pi b^2}\right)^2 \left[1 - \psi(kb) + k^2b^2\omega(ak\delta)\right]\left[1 + \chi(kb) - k^2b^2\omega(ak\delta)\right], \quad (3.2.1)$$

with

$$\psi(k\beta) = k\beta \mathrm{K}_1(k\beta), \quad (3.2.2)$$

$$\chi(k\beta) = k^2\beta^2 \mathrm{K}_0(k\beta) + k\beta \mathrm{K}_1(k\beta), \quad (3.2.3)$$

$$\omega(ak\delta) = \frac{1}{2}\left[\frac{\cos(ak\delta) - 1}{a^2k^2\delta^2} + \frac{\sin(ak\delta)}{ak\delta} - \mathrm{Ci}(ak\delta)\right], \quad (3.2.4)$$

where $\mathrm{K}_0(k\beta)$ and $\mathrm{K}_1(k\beta)$ are the zero and first order modified Bessel functions of the second kind, respectively, and $\mathrm{Ci}(ak\delta)$ is the cosine integral. For full details of the derivation of (3.2.1–4), see the original paper.

The expression (3.2.1) for the growth rate can be considered to be a function of the dimensionless parameters kb and $a\delta/b$. The boundary between stability and instability is constructed by computing the sign of (3.2.1) for ranges of values of the pair $(kb, a\delta/b)$. It suffices for us to say that there is a region of the $(kb, a\delta/b)$–plane at which (3.2.1) is positive (denoting instability).

The motion and stability of the vortex pair has a tenuous connection with the motion and stability of the ring in the pipe. To see this, consider the situation where

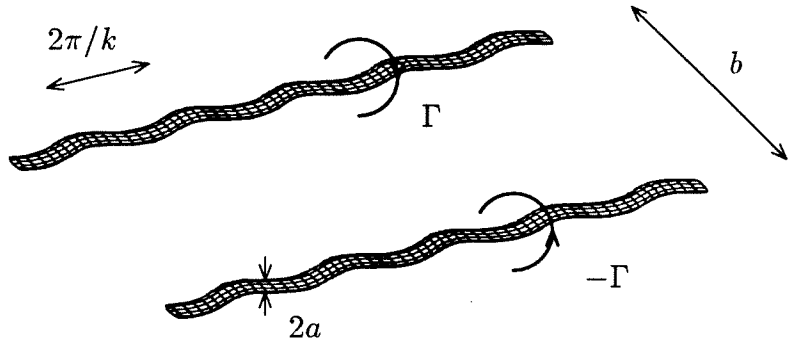

Figure 3.2.1 The geometry for the Crow problem. The originally straight vortex pair are separated by a distance b. A sinusoidal perturbation with wavenumber k has been superimposed on a pair of parallel vortices separated by a distance b.

the ring radius is the same order as the pipe radius, which is assumed to be very large. In this case the filament is straight (to first order) and is parallel to a plane wall (again to first order). The effect the wall has on the flow is the same as that which would be produced by an image vortex of equal and opposite strength positioned at the same distance behind the wall. Consequently, the instability described by the Crow analysis should occur for certain ranges of values of the ring parameters. In section 3.6 we return to this question, having fully analyzed the situation for the ring in the pipe.

3.3 The stability of a vortex ring in an unbounded fluid

As we mentioned in the section 3.1, Kelvin's model of the indestructible atom was a vortex ring moving through the ubiquitous ether. In his treatise on vortex motion, Thomson considered the stability of a vortex ring in an unbounded fluid, as a means of demonstrating the indestructibility of such atoms. The desingularization of the Biot–Savart integral adopted by Thomson is essentially the same as that used in the Rosenhead equation (c.f., equation (1.4.7)). By imposing an infinitesimal sinusoidal type perturbation on the centerline of the core and retaining only terms of order

$\ln(a/R)$, he derived the following expression for the growth rate,

$$\sigma_t = \frac{\Gamma}{4\pi R^2} n\sqrt{1-n^2}\ln\left(\frac{a}{R}\right), \tag{3.3.1}$$

where n is the number of waves on the perturbed ring. Clearly (3.3.1) predicts that for $n > 1$ the perturbation has a characteristic frequency of vibration or, expressed in another way, it says that vortex rings in an unbounded fluid are linearly stable to sinusoidal type disturbances.

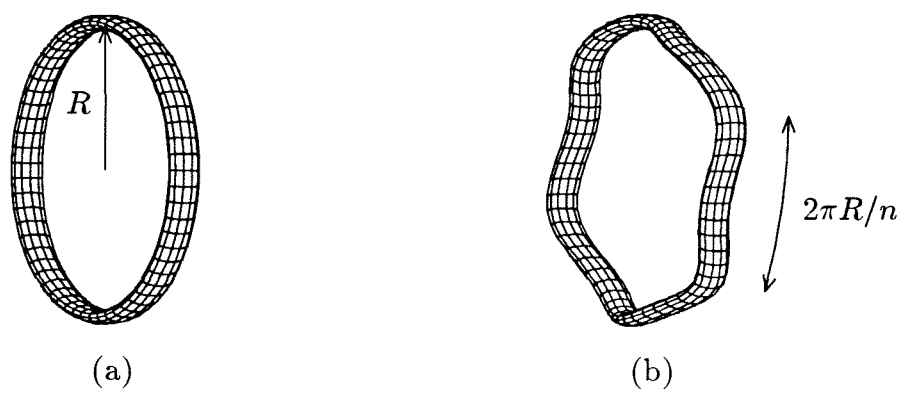

Figure 3.3.1 The vortex ring geometry considered by Widnall and Sullivan. The original ring, (a), has radius R, and the perturbed ring, (b), has a sinusoidal perturbation with wavenumber n/R.

The terms neglected by Thomson are $O(1)$, in terms of the small parameter a/R. The term $\ln(a/R)$ dominates the $O(1)$ terms only if a/R is exceedingly small. Widnall and Sullivan (1973) performed the analysis retaining all the $O(1)$ terms to see what effect, if any, they had on the stability of the ring. The desingularization of the Biot–Savart integral adopted by Widnall and Sullivan is essentially the cut–off method of desingularization. The sinusoidally perturbed core centerline took the form

$$\mathbf{R} = \left(R + \rho_0 e^{in\theta}\right)\mathbf{e}_r(\theta) + \xi_0 e^{in\theta}\mathbf{e}_z, \tag{3.3.2}$$

with respect to a cylindrical polar coordinate system. In figure 3.3.1 we depict the relative features of the original and perturbed ring.

The growth rate associated with the disturbance was assumed to σ_{ws}, so that $\partial/\partial t(\rho_0, \xi_0) = (\sigma_{ws}\rho_0, \sigma_{ws}\xi_0)$. Using the cut–off equation to determine the motion of the perturbed ring leads to the following eigenvalue equation

$$\sigma_{ws}\rho_0 = \frac{\Gamma}{4\pi R^2} S_r(\delta_*; n)\,\xi_0 \tag{3.3.3}$$

$$\sigma_{ws}\xi_0 = \frac{\Gamma}{4\pi R^2} S_z(\delta_*; n)\,\rho_0, \tag{3.3.4}$$

where the self interaction terms S_r and S_z are given by

$$S_r(\delta_*; n) = F(1) + \frac{1}{2}(n-1)F(n+1) - \frac{1}{2}(n+1)F(n-1) \tag{3.3.5}$$

$$S_z(\delta_*; n) = 1 - \frac{3}{2}F(0) + \frac{1}{2}F(1) + \frac{1}{2}F(n) + \frac{1}{4}(1-2n)F(n+1) + \frac{1}{4}(1+2n)F(n-1) \tag{3.3.6}$$

with

$$F(m) = \frac{1}{\sqrt{2}} \int_{\delta_*}^{\pi} \cos m\theta\,(1-\cos\theta)^{-3/2}\,d\theta. \tag{3.3.7}$$

The new parameter δ_* is given by

$$\delta_* = \frac{a\delta}{R}. \tag{3.3.8}$$

Clearly, a nontrivial solution to (3.3.3–4) exists only if σ_{ws} satisfies

$$\sigma_{ws}^2 = \left(\frac{\Gamma}{4\pi R^2}\right)^2 S_r(\delta_*; n)\,S_z(\delta_*; n). \tag{3.3.9}$$

When the right–hand side of (3.3.9) is positive, there is a corresponding instability associated with the values of the parameters (δ_*, n). Widnall and Sullivan found that for thin cores instability set in only at values of n which are very large. These large values of n correspond to very small values of the wavelength of the perturbation, which violates the assumptions needed for the application of the cut–off equation. (This fact was pointed out by Moore and Saffman (1974), who verified that the application of the cut–off equation predicted a spurious instability for short waves on a hollow thin–cored vortex ring. However, an analysis which does not use the cut–off

equation and predicts the short wave instabilities for a thin–cored vortex ring was presented by Widnall, Bliss and Tsai (1974) and in more detail by Widnall and Tsai (1977).) Alternatively, we may say that a thin cored vortex ring in an unbounded fluid is stable to long wavelength perturbations (i.e., perturbations that permit the application of the cut–off equation). Clearly, this problem has a simple connection to the stability of a ring in a pipe — take the case where the pipe radius is very large compared to the ring radius. In this case the ring essentially moves in an unbounded fluid and the stability results of Widnall and Sullivan can be applied. In section 3.6 we compare (3.3.9) to a corresponding result for the stability of a ring in a pipe and estimate the magnitude of the additional terms coming from the interaction of the wall and the ring.

3.4 Analysis for the vortex ring in a circular pipe

Before proceeding with the analysis, we note the work of Raja Gopal (1963), who computed the steady speed of propagation, U, of a circular ring in a cylindrical pipe. By assuming that the wall was equivalent to an image vortex system with cylindrical symmetry, he obtained the following expression for the speed

$$U = \frac{\Gamma}{4\pi R}\left[\ln\left(\frac{8R}{a}\right) - \frac{1}{4}\right] - \frac{\Gamma R}{\pi}\int_0^\infty t\frac{\mathrm{K}_1(Dt)}{\mathrm{I}_1(Dt)}\mathrm{I}_0(Rt)\mathrm{I}_1(Rt)dt, \qquad (3.4.1)$$

wher I_ν and K_ν are modified Bessel functions of order ν. The first term on the right–hand side of (3.4.1) is Kelvin's expression for the self–induced speed of a vortex ring. The second term is the component of the speed induced by the wall. The leading order effects of general axial and swirl velocity profiles, in the core, have not been included in (3.4.1), but will clearly only effect the self–induced part of the speed. We confirm this in what follows since a by–product of our analysis is an expression for the steady speed of propagation of a circular ring which includes the leading order effects of general axial and swirl velocity profiles in the core.

Now we proceed with a description of the geometry of the problem. We assume that the unperturbed ring moves along the axis of the pipe with a steady speed U. We adopt a cylindrical polar coordinate system, (r, θ, z), with the z–axis coinciding with the axis of the pipe. The frame of reference used is the frame in which the

unperturbed ring is stationary. Superimposing an infinitesimal perturbation on the centerline of the core leads to the following expression for a point on the filament

$$\mathbf{X} = \left(R + \epsilon r' e^{in\theta} e^{\sigma t}\right) \mathbf{e}_r(\theta) + \epsilon z' e^{in\theta} e^{\sigma t} \mathbf{e}_z. \tag{3.4.2}$$

Although the real part of the right–hand side of (3.4.2) is the physically meaningful part, the linear analysis means that products of complex terms will be ignored and so we can manipulate $\mathbf{X}$ as given. In figure 3.4.1 we give a sketch of the perturbed ring inside the pipe.

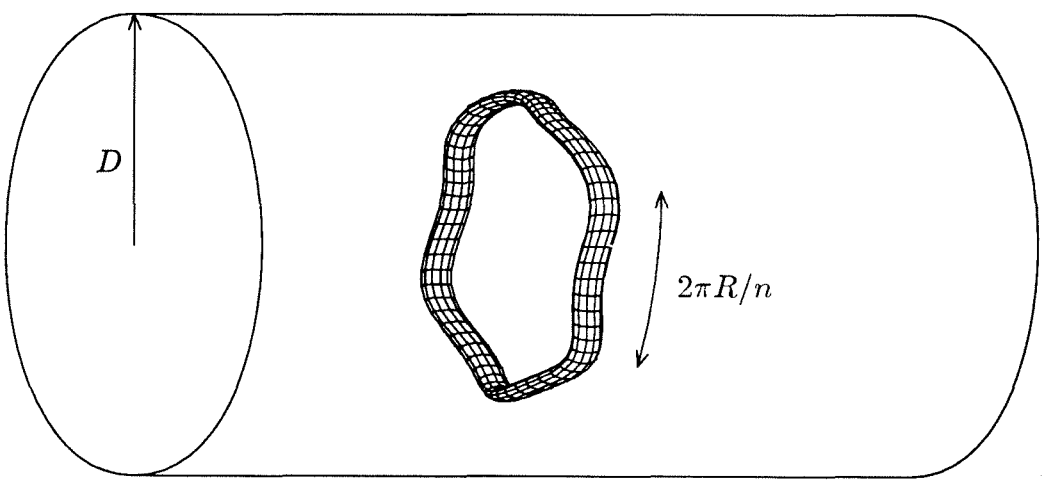

Figure 3.4.1 A sinusoidally perturbed ring inside a pipe. The perturbation has wavenumber n/R, where R is the original radius of the ring.

The velocity field of the fluid in the pipe is made up of two parts: the first part is induced by the vorticity in the ring, and the second part is induced by the wall (or equivalent image vortex system). The part induced by the wall can be written as the gradient of some potential field φ (i.e., the velocity field induced by the wall is irrotational in the pipe). Consequently, the velocity $\mathbf{u}(\mathbf{P})$ at some point $\mathbf{P} = (r, \theta, z)$, in the pipe and outside the vortex core, is given by

$$\mathbf{u}(\mathbf{P}) = \frac{\Gamma}{4\pi} \oint \mathbf{s}_* \times \frac{(\mathbf{P} - \mathbf{X}_*)}{|\mathbf{P} - \mathbf{X}_*|^3} ds_* + \nabla\varphi. \tag{3.4.3}$$

For a point $\mathbf{P} = \mathbf{X}$ on the centerline of the core, we must replace the closed integral $\oint$ by the cut–off integral $\int_{[\delta]}$.

The linearization assumption allows us to write the potential as

$$\varphi(r,\theta,z,t) = -Uz + \varphi_0(r,z) + \epsilon\varphi_n(r,z)e^{in\theta}e^{\sigma t} + O(\epsilon^2). \tag{3.4.4}$$

The first term on the right–hand side of (3.4.4) signifies that the fluid velocity is $-U\mathbf{e}_z$ as z goes to $\pm\infty$, in the frame of reference of the unperturbed ring. The remaining parts of the potential must vanish as $z \to \pm\infty$. Since φ satisfies Laplaces equation we can apply a Fourier transform and find that the potential can be rewritten as

$$\begin{aligned}\varphi = -Uz &+ \int_{-\infty}^{\infty} A_0(k)\mathrm{I}_0(kr)e^{-ikz}dk \\ &+ \epsilon e^{in\theta}e^{\sigma t}\int_{-\infty}^{\infty} A_n(k)\mathrm{I}_n(kr)e^{-ikz}dk + O(\epsilon^2).\end{aligned} \tag{3.4.5}$$

The unknown functions $A_0(k)$ and $A_n(k)$ follow from the condition that the normal velocity component vanishes on the pipe wall, i.e.,

$$\frac{\partial\varphi}{\partial r}(D,\theta,z) = -\frac{\Gamma}{4\pi}\left(\mathbf{e}_r(\theta)\cdot\oint \mathbf{s}_* \times \frac{(\mathbf{P}_W - \mathbf{X}_*)}{|\mathbf{P}_W - \mathbf{X}_*|^3}\right)ds_* \tag{3.4.6}$$

where the radial component of $\mathbf{P}_W$ is D. To get precise expressions for the functions $A_0(k)$ and $A_n(k)$, we linearize the Biot–Savart term

$$\frac{\Gamma}{4\pi}\left(\oint \mathbf{s}_* \times \frac{(\mathbf{P}_W - \mathbf{X}_*)}{|\mathbf{P}_W - \mathbf{X}_*|^3}ds_*\right)\cdot\mathbf{e}_r = u_0(D,z) + \epsilon e^{in\theta}e^{\sigma t}u_n(D,z) + O(\epsilon^2) \tag{3.4.7}$$

where

$$u_0(D,z) = \Gamma R/4\pi\int_{-\pi}^{\pi} z\cos\theta_*\left[\varpi^2 + z^2\right]^{-3/2}d\theta_* \tag{3.4.8}$$

$$\begin{aligned}u_n(D,z) = {} & 3\Gamma Rr'/4\pi\int_{-\pi}^{\pi} z\cos\theta_* e^{in\theta_*}\left[D\cos\theta_* - R\right]\left[\varpi^2 + z^2\right]^{-5/2}d\theta_* \\ & + 3\Gamma Rz'/4\pi\int_{-\pi}^{\pi} z^2\cos\theta_* e^{in\theta_*}\left[\varpi^2 + z^2\right]^{-5/2}d\theta_* \\ & + \Gamma Rz'/4\pi\int_{-\pi}^{\pi} e^{in\theta_*}\left[in\sin\theta_* - \cos\theta_*\right]\left[\varpi^2 + z^2\right]^{-3/2}d\theta_* \\ & + \Gamma r'/4\pi\int_{-\pi}^{\pi} ze^{in\theta_*}\left[in\sin\theta_* + \cos\theta_*\right]\left[\varpi^2 + z^2\right]^{-3/2}d\theta_*\end{aligned} \tag{3.4.9}$$

with

$$\varpi^2 = D^2 - 2DR\cos\theta_* + R^2. \tag{3.4.10}$$

Applying the inverse Fourier transform to (3.4.6) yields

$$kA_0(k)\mathrm{I}_0'(kD) = -\frac{1}{2\pi}\int_{-\infty}^{\infty} u_0(D,z)e^{ikz}dz \tag{3.4.11}$$

$$kA_n(k)\mathrm{I}_n'(kD) = -\frac{1}{2\pi}\int_{-\infty}^{\infty} u_n(D,z)e^{ikz}dz. \tag{3.4.12}$$

Substituting (3.4.8–9) into (3.4.11–12) yields expressions containing double integrals. Rearranging the order of integration leads to terms containing integrals of the form $\int_{-\infty}^{\infty} z^m e^{ikz}(\varpi^2+z^2)^{-n/2}dz$, where $m = 0$, 1 or 2 and $n = 3$ or 5. To evaluate such integrals we employ the Fourier transform of the order zero modified Bessel function of the second kind

$$\int_{-\infty}^{\infty} e^{ikz}\left(\varpi^2+z^2\right)^{-1/2}dz = 2\mathrm{K}_0(|k|\varpi). \tag{3.4.13}$$

We manipulate this to obtain the following expressions for the required integrals

$$\int_{-\infty}^{\infty} e^{ikz}(\varpi^2+z^2)^{-3/2}dz = \frac{2|k|}{\varpi}\mathrm{K}_1(|k|\varpi) \tag{3.4.14}$$

$$\int_{-\infty}^{\infty} ze^{ikz}(\varpi^2+z^2)^{-3/2}dz = 2ik\mathrm{K}_0(|k|\varpi) \tag{3.4.15}$$

$$\int_{-\infty}^{\infty} ze^{ikz}(\varpi^2+z^2)^{-5/2}dz = \frac{2ik|k|}{3}\mathrm{K}_1(|k|\varpi) \tag{3.4.16}$$

$$\int_{-\infty}^{\infty} z^2e^{ikz}(\varpi^2+z^2)^{-5/2}dz = \frac{2|k|}{3\varpi}\left[\mathrm{K}_1(|k|\varpi) - |k|\varpi\mathrm{K}_0(|k|\varpi)\right]. \tag{3.4.17}$$

Equations (3.1.14–17) yield the following expressions for the coefficients $A_0(k)$ and $A_n(k)$

$$A_0(k) = -i\frac{\Gamma R}{4\pi^2\mathrm{I}_0'(kD)}\int_{-\pi}^{\pi}\cos\theta_*\mathrm{K}_0(|k|\varpi)d\theta_* \tag{3.4.18}$$

$$\begin{aligned}A_n(k) = -i\frac{\Gamma r'}{4\pi^2\mathrm{I}_n'(kD)}\int_{-\pi}^{\pi}\Bigg(&|k|R\cos\theta_*\left[\frac{D\cos\theta_*-R}{\varpi}\right]\mathrm{K}_1(|k|\varpi)\\ &+\left[in\sin\theta_*+\cos\theta_*\right]\mathrm{K}_0(|k|\varpi)\Bigg)e^{in\theta_*}d\theta_*\\ -\frac{\Gamma|k|z'}{4\pi^2 k\mathrm{I}_n'(kD)}\int_{-\pi}^{\pi}\Bigg(&in\frac{R\sin\theta_*}{\varpi}\mathrm{K}_1(|k|\varpi)\\ &-kR\cos\theta_*\mathrm{K}_0(|k|\varpi)\Bigg)e^{in\theta_*}d\theta_*\end{aligned} \tag{3.4.19}$$

To reduce (3.4.18–19) we make use of the Gegenbauer summation expansion for Bessel functions

$$\mathrm{K}_\nu(|k|\varpi)e^{i\nu\psi} = \sum_{m=-\infty}^{\infty} \mathrm{K}_{\nu+m}(|k|D)\mathrm{I}_m(|k|R)e^{im\theta_*}, \tag{3.4.20}$$

where ψ satisfies

$$\begin{aligned} D - R\cos\theta_* &= \varpi\cos\psi \\ R\sin\theta_* &= \varpi\sin\psi. \end{aligned} \tag{3.4.21}$$

Using this expansion in (3.4.18–19) and employing the orthogonality property of the trigonometric functions yields expressions for $A_0(k)$ and $A_n(k)$ given by

$$A_0(k) = -i\frac{\Gamma R}{2\pi}\frac{\mathrm{K}_1(|k|D)\mathrm{I}_1(|k|R)}{\mathrm{I}_1(kD)} \tag{3.4.22}$$

$$A_n(k) = +i\frac{\Gamma Rr'}{2\pi}\frac{\mathrm{K}_n'(|k|D)\mathrm{I}_n(|k|R)}{\mathrm{I}_n'(kD)} - \frac{\Gamma Rz'}{2\pi}\frac{\mathrm{K}_n'(|k|D)\mathrm{I}_n'(|k|R)}{\mathrm{I}_n'(kD)}. \tag{3.4.23}$$

Equation (3.4.3) together with (3.4.22–23) completely expresses the potential, induced by the wall, in terms of known functions.

On account of (3.4.2) we can write the following expression for the motion of a point on the filament

$$\frac{\partial \mathbf{X}}{\partial t} = \sigma\left(\epsilon r' e^{in\theta}e^{\sigma t}\mathbf{e}_r(\theta) + \epsilon z' e^{in\theta}e^{\sigma t}\mathbf{e}_z\right). \tag{3.4.24}$$

But according to (3.4.3) we also have

$$\frac{\partial \mathbf{X}}{\partial t} = \frac{\Gamma}{4\pi}\int_{[\delta]} \mathbf{s}_* \frac{(\mathbf{X}-\mathbf{X}_*)}{|\mathbf{X}-\mathbf{X}_*|^3} ds_* + \nabla\varphi(\mathbf{X}). \tag{3.4.25}$$

The analysis of Widnall and Sullivan tells us that if we use (3.1.3) in the cut–off integral and carry out an expansion in terms of powers of ϵ, we obtain

$$\frac{\Gamma}{4\pi}\int_{[\delta]} \mathbf{s}_* \times \frac{(\mathbf{X}-\mathbf{X}_*)}{|\mathbf{X}-\mathbf{X}_*|^3} ds_* = \mathbf{q}_0 + \epsilon\mathbf{q}_n e^{in\theta}e^{\sigma t} + O(\epsilon^2), \tag{3.4.26}$$

with

$$\mathbf{q}_0 = \frac{\Gamma}{4\pi R}\left[F(0) - F(1)\right]\mathbf{e}_z, \tag{3.4.27}$$

$$\mathbf{q}_n = \frac{\Gamma z'}{4\pi R^2}S_r\left(\delta_*; n\right)\mathbf{e}_r + \frac{\Gamma r'}{4\pi R^2}S_z\left(\delta_*; n\right)\mathbf{e}_z, \tag{3.4.28}$$

where S_r and S_z are given by equations (3.3.5–6) and the function $F(m)$ is given by (3.3.7). Using (3.4.24–25) and (3.4.4) we obtain the following leading order equation

$$U = \frac{\Gamma}{4\pi R}\left[F(0) - F(1)\right] - \frac{\Gamma R}{\pi D^2}\int_0^\infty k\frac{\mathrm{K}_1(k)}{\mathrm{I}_1(k)}\mathrm{I}_0(k\lambda)\mathrm{I}_1(k\lambda)dk, \tag{3.4.29}$$

where $\lambda = R/D$. The next order terms are linear in ϵ and yield the following eigenvalue equation for the growth rate

$$\sigma r' = \frac{\Gamma}{4\pi R^2}\left[S_r\left(\delta_*; n\right) - 4\lambda^3 I_r\left(\lambda; n\right)\right] z' \tag{3.4.30}$$

$$\sigma z' = \frac{\Gamma}{4\pi R^2}\left[S_z\left(\delta_*; n\right) - 4\lambda^3 I_z\left(\lambda; n\right)\right] r' \tag{3.4.31}$$

where the terms I_r and I_z are the terms induced by the wall, given by

$$I_r\left(\lambda; n\right) = \int_0^\infty k^2\left[\left(\mathrm{I}_1(k\lambda)\right)^2\frac{\mathrm{K}_1(k)}{\mathrm{I}_1(k)} + \left(\mathrm{I}_n'(k\lambda)\right)^2\frac{\mathrm{K}_n'(k)}{\mathrm{I}_n'(k)}\right]dk \tag{3.4.32}$$

$$I_z\left(\lambda; n\right) = \int_0^\infty k^2\left[\left(\mathrm{I}_1(k\lambda)\right)^2\frac{\mathrm{K}_1(k)}{\mathrm{I}_1(k)} - \left(\mathrm{I}_n(k\lambda)\right)^2\frac{\mathrm{K}_n'(k)}{\mathrm{I}_n'(k)}\right]dk. \tag{3.4.33}$$

Solving for σ, from (3.4.30–31), leads to

$$\sigma^2 = \left(\frac{\Gamma}{4\pi R^2}\right)^2\left[S_r\left(\delta_*; n\right) - 4\lambda^3 I_r\left(\lambda; n\right)\right]\left[S_z\left(\delta_*; n\right) - 4\lambda^3 I_z\left(\lambda; n\right)\right]. \tag{3.4.34}$$

The growth rate given by (3.4.34) is a function of the dimensionless parameters (λ, δ_*, n). Conveniently, the parameter n is discrete so it is advantageous to compute the growth rate for each value of n as a function of λ and δ_*, which is done in the next section.

3.5 Numerical computation of the growth rate

To compute the growth rates, we need to compute the integrals given by $I_r(\lambda; n)$, $I_z(\lambda; n)$ and $F(m)$, where m takes on several values between 0 and $n+1$. The integrals corresponding to $F(m)$ for the first few values of m can be written down relatively easily and are

$$F(0) = \frac{1}{4}\frac{\cos\frac{\delta_*}{2}}{\sin^2\frac{\delta_*}{2}} + \frac{1}{8}\ln\left(\frac{1+\cos\frac{\delta_*}{2}}{1-\cos\frac{\delta_*}{2}}\right) \tag{3.5.1}$$

$$F(1) = \frac{1}{4}\frac{\cos\frac{\delta_*}{2}}{\sin^2\frac{\delta_*}{2}} - \frac{3}{8}\ln\left(\frac{1+\cos\frac{\delta_*}{2}}{1-\cos\frac{\delta_*}{2}}\right) \tag{3.5.2}$$

$$F(2) = \frac{1}{4}\frac{\cos\frac{\delta_*}{2}}{\sin^2\frac{\delta_*}{2}} - \frac{15}{8}\ln\left(\frac{1+\cos\frac{\delta_*}{2}}{1-\cos\frac{\delta_*}{2}}\right) + 4\cos\frac{\delta_*}{2}. \tag{3.5.3}$$

For higher values of m, a recurrence relation can be constructed for computing $F(m)$ in terms of the functions $F(0)$ to $F(m-1)$. However, the recurrence relation is extremely unstable and does not provide a reliable method for constructing the functions. Widnall and Sullivan computed the integrals by first writing them as

$$F(m) = 2\int_{\delta_*}^{\infty} \cos(m\theta)\left(\frac{\mathcal{H}(\pi-\theta)}{2(1-\cos\theta)^{3/2}} - \frac{1}{\theta^3} - \frac{1}{8}\frac{e^{-\theta}}{\theta}\right) d\theta + 2\int_{\delta_*}^{\infty} \cos(m\theta)\left(\frac{1}{\theta^3} + \frac{1}{8}\frac{e^{-\theta}}{\theta}\right) d\theta \tag{3.5.4}$$

where $\mathcal{H}$ is the Heaviside step function. The integrand in the first integral is regular, and consequently the integral can be computed by allowing $\delta_* \to 0$ and using an FFT to compute the corresponding Fourier transform. The second integral can be expressed in terms of known functions

$$2\int_{\delta_*}^{\infty} \cos(m\theta)\left(\frac{1}{\theta^3} + \frac{1}{8}\frac{e^{-\theta}}{\theta}\right) d\theta = \frac{\cos m\delta}{\delta^2} - \frac{m\sin m\delta}{\delta} + m^2\mathrm{Ci}(m\delta) - \frac{1}{4}\mathrm{Ci}(\delta\sqrt{1+m^2}). \tag{3.5.5}$$

We adopt a slightly different tact and write

$$F(m) = 2\int_{\delta_*}^{\pi} \cos(m\theta)\left(\frac{1}{2(1-\cos\theta)^{3/2}} - \frac{1}{\theta^3} - \frac{1}{8}\frac{e^{-\theta}}{\theta}\right) d\theta + 2\int_{\delta_*}^{\pi} \cos(m\theta)\left(\frac{1}{\theta^3} + \frac{1}{8}\frac{e^{-\theta}}{\theta}\right) d\theta. \tag{3.5.6}$$

Again we can allow $\delta_* \to 0$ in the first integral and compute the resulting integral using standard quadrature rules. The second integral can also be expressed in terms of elementary functions

$$2\int_{\delta_*}^{\pi} \cos(m\theta)\left(\frac{1}{\theta^3} + \frac{1}{8}\frac{e^{-\theta}}{\theta}\right) d\theta = -\frac{(-1)^m}{\pi^2} + \frac{\cos m\delta}{\delta^2} - \frac{m\sin m\delta}{\delta} + \left(m^2 + \frac{1}{4}\right)\left(\mathrm{Ci}(m\delta) - \mathrm{Ci}(m\pi)\right). \tag{3.5.7}$$

In table 3.5.1 we give values of $F(n)$ and the self–induction terms $S_r(\delta_*, n)$ and $S_z(\delta_*, n)$ for a ring with $\delta_* = 0.1$ and for a range of m between 1 and 13. Examination of the entries show a change in sign of the self–induction terms as n increases from 10

to 11. This sign change is a result of a spurious instability associated with the cut-off equation when the wavelength of the perturbation is $O(a)$. Variation of the parameter δ_* about the value 0.1 will allow one to find a small range of values of δ_* at which the self–induction terms are the same sign, for $n = 10$ or 11, implying instability for an unbounded ring. This is the instability regime obtained by Widnall and Sullivan, but which was later shown by Moore and Saffman (1974) to be a spurious effect associated with the cut–off equation. Also from the table we take note of the signs on the self–induction terms, which for $n < 1/\delta_*$ are that $S_r < 0$ and $S_z > 0$.

Next we consider the integral terms induced by the wall. The integrand in $I_z(\lambda; n)$ is readily shown to be positive, which implies that $I_z(\lambda; n)$ is also positive. Moreover, it is easy to show that the integrand is asymptotic to $\frac{k}{\lambda}e^{-2k(1-\lambda)}$, for large k. This means that as $\lambda \to 1$ the integral diverges to $+\infty$. Since both S_z and I_z are of opposite signs and I_z increases with λ, it follows that the factor $S_z - 4\lambda^3 I_z$ undergoes a change in sign, from positive to negative, as λ increases from 0 to 1. The point at which this sign change occurs corresponds to a point of transition from stability to instability, or vice–versa, for the ring in the pipe. On the other hand the sign of the integral $I_r(\lambda; n)$ is not so easily determined, since both of the terms making up the integrand are of opposite signs. However, the asymptotic form of the integrand can be shown to be given by

$$k^2\left[(\mathrm{I}_1(k\lambda))^2\,\frac{\mathrm{K}_1(k)}{\mathrm{I}_1(k)} + (\mathrm{I}_n'(k\lambda))^2\,\frac{\mathrm{K}_n'(k)}{\mathrm{I}_n'(k)}\right] \sim \frac{k}{2\lambda}e^{-2k(1-\lambda)}\left[\frac{n^2}{k\lambda}(1-\lambda) - \frac{n^2}{4k^2\lambda^2}\left((3+3n^2)(1-\lambda)^2+2\right)\right], \quad (3.5.8)$$

and in figure 3.5.1 we give a plot of the integrand for a value of $\lambda = 0.5$. It is obvious from the detail insert in the figure that the integrand of $I_r(0.5; 1)$ is positive for large values of k. The general character of the integrand remains the same for other values of λ and n. Since we are really interested in $\lambda < (1 + a/R)^{-1}$, we argue that the integral $I_r(\lambda; n)$ will only diverge to $-\infty$ outside the range of physical interest (i.e., for $\lambda > (1 + a/R)^{-1}$). Consequently, the factor $S_r - 4\lambda^3 I_r$ has no zeroes for any physically meaningful value of λ. The numerics provide a confirmation of this assertion.

n	F	S_r	S_z
0	100.880	0.0	-2.689
1	97.192	-3.689	1.250×10^{-3}
2	90.121	-8.103	4.086
3	80.986	-12.488	8.277
4	70.562	-16.194	11.849
5	59.386	-18.778	14.332
6	47.858	-19.938	15.415
7	36.289	-19.475	14.891
8	24.922	-17.269	12.636
9	13.954	-13.263	8.592
10	3.539	-7.454	2.752
11	-6.200	.1178	-4.843
12	-15.168	9.372	-14.115
13	-23.294	20.197	-24.953

Table 3.5.1 Variations in the values of the function $F(n)$ and the self-induction terms for various numbers of waves, n, on a vortex ring with $\delta_* = 0.1$.

In figure 3.4.2 we plot some of the growth rates for various values of n. From this we see that the instability associated with the higher mode numbers comes into play when the ring is closer to the pipe wall. However, the $n = 1$ mode is the most unstable over most of the range of values of λ. The transition points for instability are recorded in table 3.5.2, and in figure 3.5.3 we plot the regions of instability for each mode number.

3.6 The limiting regimes of large and small pipe radius

In section 3.2 we described the stability analysis carried out by Crow for a pair of parallel line vortices. We also described how in the limit of large ring and pipe radius we could have a situation equivalent to a particular case of the Crow problem. Unfortunately, the image vortex system equivalent to the pipe wall cannot simply be taken to be a vortex ring coincident with the image curve and having an appropriate strength. To illustrate this we shall replace the wall by a concentric ring of radius R_I and strength Γ_I and show that the resulting system is not equivalent to the ring inside the pipe. The velocity induced by the coplanar vortex ring pair is

$$\begin{aligned}\mathbf{u}(r,\theta,z) = \frac{\Gamma}{4\pi}\int_{-\pi}^{\pi}\left(\frac{zR\cos\theta_*}{\mathcal{D}^3}\mathbf{e}_r + \frac{R^2 - rR\cos\theta_*}{\mathcal{D}^3}\mathbf{e}_z\right)d\theta_* \\ + \frac{\Gamma_I}{4\pi}\int_{-\pi}^{\pi}\left(\frac{zR_I\cos\theta_*}{\mathcal{D}_I^3}\mathbf{e}_r + \frac{R_I^2 - rR_I\cos\theta_*}{\mathcal{D}_I^3}\mathbf{e}_z\right)d\theta_* \qquad (3.6.1)\end{aligned}$$

where

$$\begin{aligned}\mathcal{D}^2 &= R^2 - 2rR\cos\theta_* + r^2 + z^2 \\ \mathcal{D}_I^2 &= R_I^2 - 2rR_I\cos\theta_* + r^2 + z^2.\end{aligned} \qquad (3.6.2)$$

The vortex pair must satisfy two constraints; the first is that the pair must move as a coherent unit, i.e., the velocity of each ring should be the same, and the second constraint is that the radial component of the velocity evaluated on the cylindrical surface $r = D$ must be zero. The second condition is simply the requirement that the vortex pair is equivalent to the vortex inside the pipe.

Addressing the first constraint we find that the velocity of the inner ring is

$$\begin{aligned}\mathbf{u}(R,\theta,0) = \frac{\Gamma}{4\pi R}\left(F(0) - F(1)\right)\mathbf{e}_z \\ + \frac{\Gamma_I R_I}{4\pi}\left(\int_{-\pi}^{\pi}\frac{1}{\left(R_I - R\cos\theta_*\right)^2}d\theta_*\right)\mathbf{e}_z. \qquad (3.6.3)\end{aligned}$$

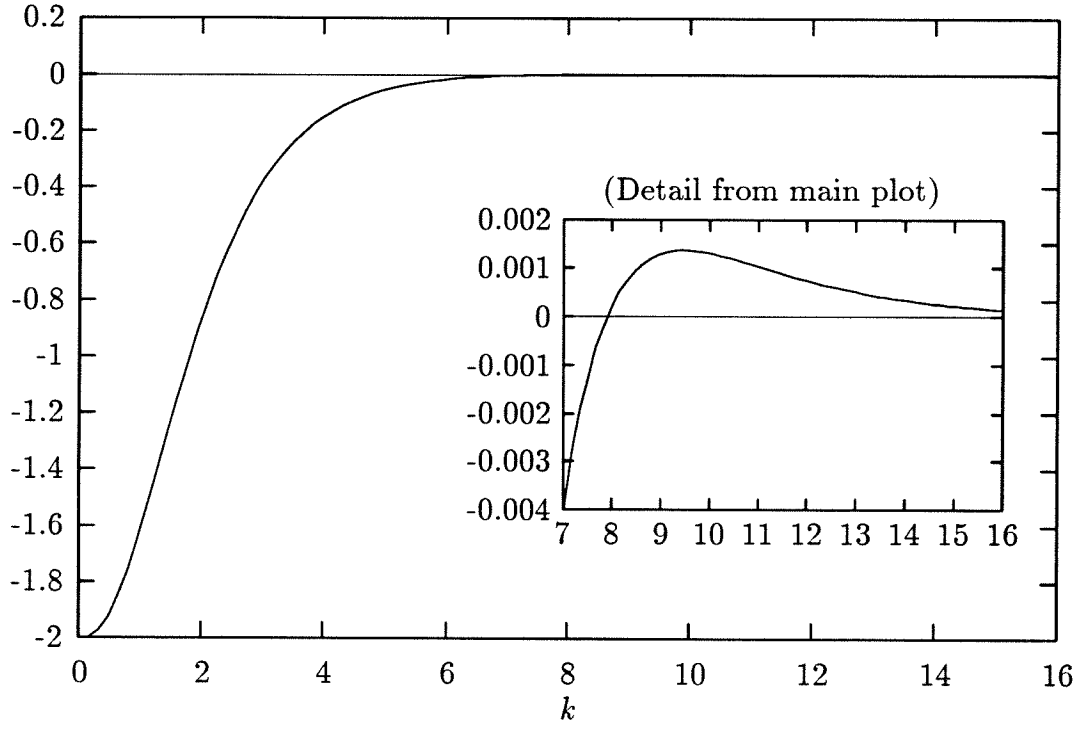

Figure 3.5.1 A plot of the integrand of $I_r(\lambda; 1)$ for $\lambda = 0.5$. This plot illustrates the general character of the integrand for any value of λ. The only significant change is that as λ tends to 1, the loop of the curve lying above the k–axis (detail) falls below the axis.

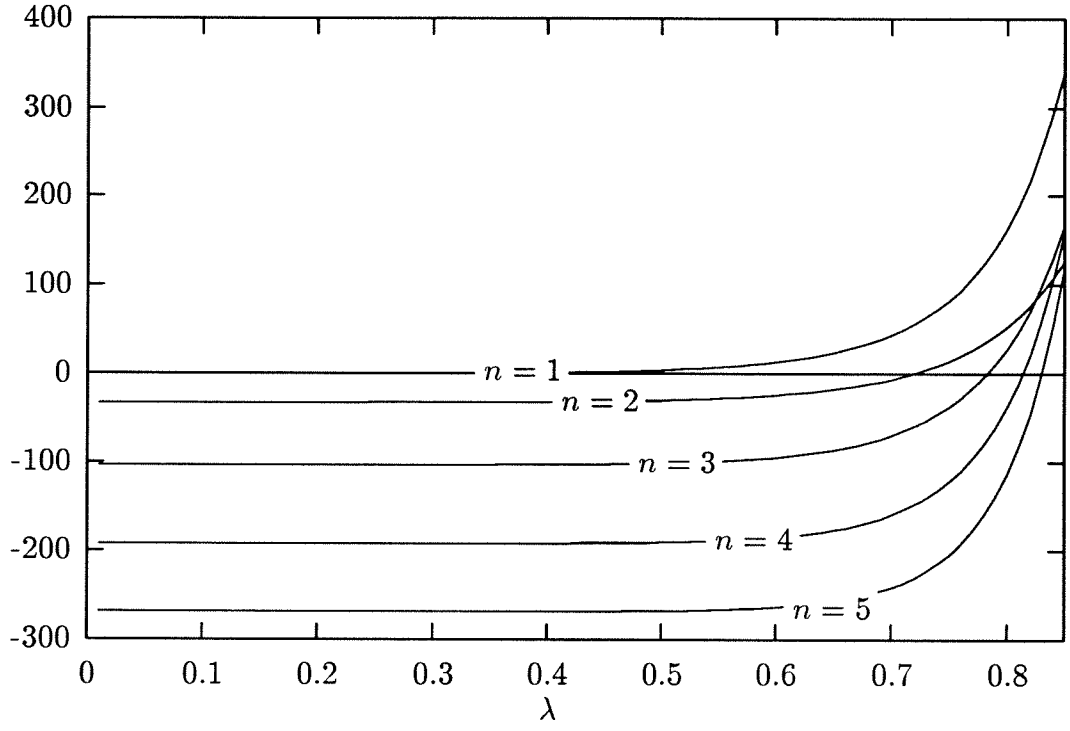

Figure 3.5.2 The square of the growth rate for perturbations $n = 1 \ldots 5$ as a function of $\lambda = R/D$, the ratio of ring radius to pipe radius. The plot is for a ring with $\delta_* = 0.1$.

δ_*	$n=1$	$n=2$	$n=3$
0.01	0.057	0.791	0.853
0.02	0.075	0.776	0.840
0.03	0.089	0.766	0.831
0.04	0.100	0.758	0.822
0.05	0.109	0.750	0.815
0.06	0.117	0.743	0.809
0.07	0.124	0.737	0.802
0.08	0.131	0.731	0.795
0.09	0.137	0.725	0.790
0.10	0.143	0.720	0.783

Table 3.5.2 The critical values of the parameter $\lambda = R/D$, the ratio of ring radius to pipe radius, for different values of n and δ_*. These critical values mark the point of change in stability for a vortex ring characterized by δ_* perturbed by sinusoidal perturbation with wavenumber n/R.

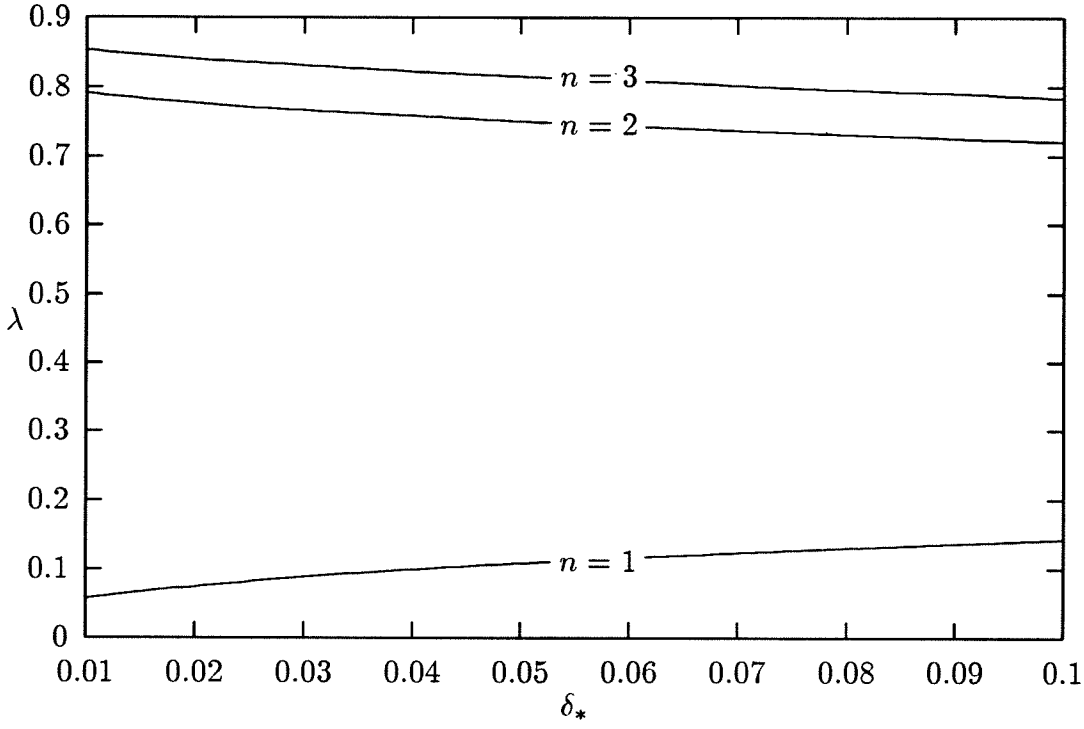

Figure 3.5.3 Plot of the (λ, δ_*) plane and the curves marking the location of the transition from stability to instability for sinusoidal perturbations with n crests on the perturbed centerline (where $n = 1$, 2 or 3). Each curve is labeled with a value of n which indicates that below the curve the corresponding perturbation is stable, while above the curve the perturbation is unstable.

Similarly, the velocity of the outer ring is

$$\mathbf{u}(R_I,\theta,0) = \frac{\Gamma R}{4\pi}\left(\int_{-\pi}^{\pi}\frac{1}{\left(R - R_I\cos\theta_*\right)^2}d\theta_*\right)\mathbf{e}_z + \frac{\Gamma_I}{4\pi R_I}\left(F^{(I)}(0) - F^{(I)}(1)\right)\mathbf{e}_z \tag{3.6.4}$$

where $F^{(I)}(n)$ is the integral appearing in (3.3.7) with the parameter δ_* replaced by $a\delta/R_I$. The other integrals which explicitly appear in (3.6.3–4) can be written as complete elliptic integrals. Clearly, equating the velocities of the vortex rings leads to an expression for the strength Γ_I in terms of Γ, R and R_I. In fact this situation has been looked at by Weidman and Riley (1993). They considered, from both the numerical and experimental point of view, the problem of a pair of concentric coplanar vortex rings moving down a pipe of circular cross section. In the paper they present an expression for the relationship between the strengths and the radii of the vortex rings for the pair to propagate as a single unit. Also, in the paper they claim that the vortex ring pair, produced in their experiments, lost its coherency through an instability where the innermost ring tilted out of the common plane and subsequently broke away from the outer ring moving off in a different direction. They attributed the instability to a flexural disturbance in the apparatus used to produce the rings. However, it may be that this is a manifestation of the same type of instability that was predicted by the numerical results. (In appendix E we examine this possibility in more detail and we also estimate the growth rate of the tilting instability associated with the inner ring for one of the experimental test cases.)

Addressing the second constraint we find the radial velocity component on the cylindrical surface $r = D$ to be given by

$$\mathbf{u}(D,\theta,z)\cdot\mathbf{e}_r = \frac{z}{4\pi}\int_{-\pi}^{\pi}\left(\frac{\Gamma R\cos\theta_*}{\left(D^2 - 2RD\cos\theta_* + R^2 + z^2\right)^{3/2}} - \frac{\Gamma_I R_I\cos\theta_*}{\left(D^2 - 2R_I D\cos\theta_* + R_I^2 + z^2\right)^{3/2}}\right)d\theta_*. \tag{3.6.5}$$

Clearly, the right–hand side of (3.6.5) cannot vanish identically if the outer ring coincides with the image curve, i.e., $R_I = D^2/R$, or any other concentric ring. The

failure of the lone vortex ring to represent the image vorticity stems from the geometry of the problem. When the radius of the ring and pipe become very large, the effects of curvature are reduced so that the representation of the image vorticity as a ring, of large radius, is quite good.

To compare our results with those of Widnall and Sullivan, we must take the limit of infinite pipe radius. When the pipe radius is very large compared with the ring radius, the ratio R/D $(= \lambda)$ is very small and we can represent the effect of the pipe wall on the growth rate as a series in λ. To do this we make use of the formal power series expansion for Bessel functions. For small λ the leading order behavior of the image terms is

$$\begin{aligned} I_r(\lambda; n) &\approx 0.942855\lambda^2 \\ I_z(\lambda; n) &\approx 0.942855\lambda^2 \end{aligned} \tag{3.6.6}$$

for $n > 1$ and

$$\begin{aligned} I_r(\lambda; 1) &\approx 0.158272\lambda^2 \\ I_z(\lambda; 1) &\approx 2.220510\lambda^2 \end{aligned} \tag{3.6.7}$$

for $n = 1$. Consequently, the growth rate given by (3.4.34) reduces to

$$\sigma^2 \approx \left(\frac{\Gamma}{4\pi R^2}\right)^2 \left[S_r S_z - 16C_n(S_r + S_z)\lambda^5\right] \tag{3.6.8}$$

where the constant $C_n \approx 2.378782$ when $n > 1$ and $C_1 \approx 1.885710$. In (3.6.8) we can simply see the effect that the wall has on the growth rate of a sinusoidal disturbance for the case when the pipe radius is very large compared to the ring radius: the first term in the brackets is the term derived by Widnall and Sullivan, and the second term is the approximation for the effect of the wall when the ratio $R/D \ll 1$. When $n > 1$ both S_r and S_z are large and are of opposite signs. This allows us to conclude that for small λ the wall has a very small effect on the growth rate of disturbances with mode numbers $n > 1$. However, for the case $n = 1$, we see that S_z is much smaller than S_r, allowing the wall to have a stronger influence on the growth rate, through the factor $S_z - 4\lambda^3 I_z$. For example, for a ring with core radius 0.1, the value of the Widnall and Sullivan term is $S_r S_z = -0.00461$ when $n = 1$. The term $-16C_1(S_r + S_z)\lambda^5 = 0.00461$ when $\lambda = 0.1329$ so according to (3.6.8) $\sigma \approx 0$. For the same ring with a perturbation having $n = 2$, we have $S_r S_z = -33.1089$ and this is

only balanced by $-16C_2(S_r + S_z)\lambda^5$ if $\lambda = 0.7364$, which is certainly not small. To find the point at which the ring becomes unstable to the $n = 1$ perturbation, we find the approximate value of λ at which the factor $S_z - 4\lambda^3 I_z$ is zero and this is

$$\lambda = \left(\frac{S_z}{8.882040}\right)^{1/5}. \tag{3.6.9}$$

When $\delta_* = 0.01$ this yields a value of $\lambda \approx 0.065$ while $\delta_* = 0.1$ yields a value of $\lambda \approx 0.162$. Both of these values agree closely with the numerical computed values presented in table 3.5.2.

CHAPTER 4

PLANAR THIN–CORED VORTEX FILAMENTS OF PERMANENT SHAPE

4.1 Introduction

In this chapter we focus on the problem of determining the shapes of thin–cored vortex filaments which are planar, have steady periodic shapes and rotate along with the plane about some axis fixed in space. A picture of the situation being considered is given in figure 4.1.1.

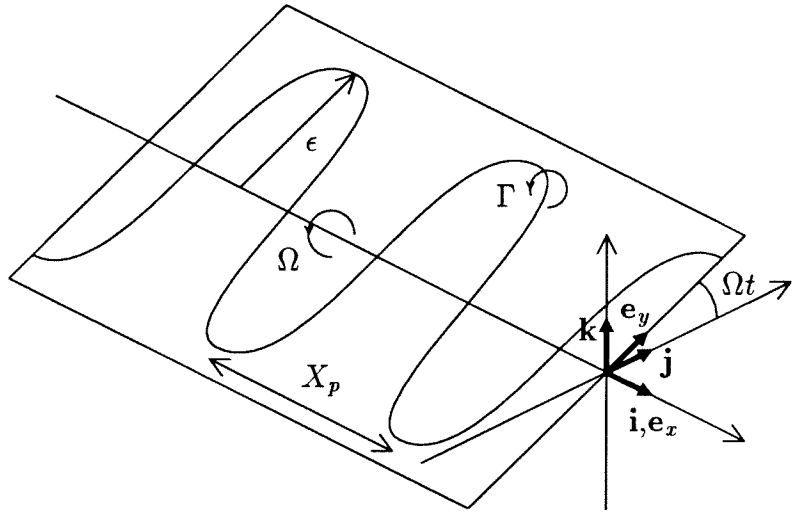

Figure 4.1.1 The geometry for the thin–cored planar filament.

Kelvin (1880), in his classic paper on the vibrations of a columnar vortex, stated that for the solution of the problem, "crowds of exceedingly interesting cases present themselves." A member of this crowd is a planar filament of infinitesimal amplitude.

The equation for the filament can be written as

$$\mathbf{X} = x\mathbf{e}_x + \epsilon F(x,\epsilon)\mathbf{e}_y, \tag{4.1.1}$$

where $F(x,\epsilon)$ is a periodic function of x with period X_p, as indicated in figure 4.1.1. The pair $\{\mathbf{e}_x,\ \mathbf{e}_y\}$ are orthonormal vectors in the rotating plane (with $\mathbf{e}_x$ oriented along the axis of rotation). The parameter ϵ is a small parameter indicating that the amplitude of the displacement of the curve from the axis is small. Using these assumptions the leading order solution to this problem is to take F as

$$F(x,\epsilon) = \cos(x) + O(\epsilon) \tag{4.1.2}$$

from which it follows that the rotation rate is given by

$$\Omega = \ln\left(\frac{a}{2}\right) + \gamma - \frac{1}{4} + O(\epsilon) \tag{4.1.3}$$

where a is the core radius and $\gamma = 0.5772\ldots$ is Euler's constant.

We will determine the rotation rate and the curve shape to higher order in ϵ using the cut–off equation

$$\frac{\partial \mathbf{X}(s,t)}{\partial t} = \frac{\Gamma}{4\pi}\int_{[\delta]} \mathbf{s}_* \times \frac{\mathbf{X}(s,t) - \mathbf{X}(s_*,t)}{|\mathbf{X}(s,t) - \mathbf{X}(s_*,t)|^3} ds_*. \tag{4.1.4}$$

As we originally saw in chapter 1, this describes the motion of the filament curve $\mathbf{X}(s,t)$, where s is arclength and t is time. The cut–off length δ satisfies (1.4.6). The equation for the filament will be taken to be given by

$$\mathbf{X}(s,t) = \left(X_p(\epsilon)\frac{s}{2\pi} + X(s,\epsilon)\right)\mathbf{e}_x + Y(s,\epsilon)\mathbf{e}_y \tag{4.1.5}$$

where X and Y are 2π–periodic functions of s and $X_p(\epsilon)$ is the axial wavelength. The time dependence, which is explicitly shown on the left–hand side of (4.1.5), resides completely in $\mathbf{e}_y$. To see this consider a non–rotating cartesian coordinate system with unit vectors $\{\mathbf{i}, \mathbf{j}, \mathbf{k}\}$. Now assume that the plane containing the filament rotates with angular speed $\Omega(\epsilon)$ about the $\mathbf{i}$ axis. Accordingly, we must have the following

relationships between the pair $\{\mathbf{e}_x, \mathbf{e}_y\}$ in the rotating plane and the triple $\{\mathbf{i}, \mathbf{j}, \mathbf{k}\}$ in the fixed cartesian frame

$$\mathbf{e}_x = \mathbf{i} \tag{4.1.6}$$

$$\mathbf{e}_y = \mathbf{j}\cos(\Omega t) + \mathbf{k}\sin(\Omega t)\,. \tag{4.1.7}$$

From (4.1.6–7) we see how the time enters on the right–hand side of (4.1.5). Substituting (4.1.5) into (4.1.4) and taking the component normal to the plane (which is the only relevant component of the equation) leads to the following equation of motion

$$\Omega(\epsilon)Y(s,\epsilon) = \frac{\Gamma}{4\pi}\int_{[\delta]} \frac{\left(\frac{X_p(\epsilon)}{2\pi} + X'(s_*,\epsilon)\right)\left(Y(s,\epsilon) - Y(s_*,\epsilon)\right)}{\mathcal{D}^3} - \frac{Y'(s_*,\epsilon)\left(X_p(\epsilon)\frac{(s-s_*)}{2\pi} + X(s,\epsilon) - X(s_*,\epsilon)\right)}{\mathcal{D}^3} ds_* \tag{4.1.8}$$

where the denominator in the integrand is given by

$$\mathcal{D}^2 = \left(X_p(\epsilon)\frac{(s-s_*)}{2\pi} + X(s,\epsilon) - X(s_*,\epsilon)\right)^2 + \left(Y(s,\epsilon) - Y(s_*,\epsilon)\right)^2 \tag{4.1.9}$$

and the primed superscript denotes differentiation with respect to the arclength parameter. Along with solving (4.1.8) we also impose conditions on $X(s)$ and $Y(s)$ at $s = 0$, which are

$$\begin{aligned} X(0) &= 0 \\ Y(0) &= \epsilon. \end{aligned} \tag{4.1.10}$$

In addition we must also ensure that s is the true arclength, which follows if

$$\left(\frac{X_p(\epsilon)}{2\pi} + X'(s,\epsilon)\right)^2 + \left(Y'(s,\epsilon)\right)^2 = 1. \tag{4.1.11}$$

Since we are looking for an ϵ–expansion for the solution, we assume the following form for the various unknown quantities

$$X_p(\epsilon) = x_0 + \epsilon x_1 + \epsilon^2 x_2 + \epsilon^3 x_3 + \epsilon^4 x_4 + \epsilon^5 x_5 + O(\epsilon^6) \tag{4.1.12}$$

$$\begin{aligned} X(s,\epsilon) &= \epsilon a_0 \sin(s) \\ &\quad + \epsilon^2(a_1 \sin(s) + b_1 \sin(2s)) \end{aligned}$$

$$+ \epsilon^3(a_2 \sin(s) + b_2 \sin(2s) + c_2 \sin(3s))$$
$$+ \epsilon^4(a_3 \sin(s) + b_3 \sin(2s) + c_3 \sin(3s) + d_3 \sin(4s))$$
$$+ \epsilon^5(a_4 \sin(s) + b_4 \sin(2s) + c_4 \sin(3s) + d_4 \sin(4s) + e_4 \sin(5s))$$
$$+ O(\epsilon^6) \tag{4.1.13}$$

$$Y(s,\epsilon) = \epsilon A_0 \cos(s)$$
$$+ \epsilon^2(A_1 \cos(s) + B_1 \cos(2s))$$
$$+ \epsilon^3(A_2 \cos(s) + B_2 \cos(2s) + C_2 \cos(3s))$$
$$+ \epsilon^4(A_3 \cos(s) + B_3 \cos(2s) + C_3 \cos(3s) + D_3 \cos(4s))$$
$$+ \epsilon^5(A_4 \cos(s) + B_4 \cos(2s) + C_4 \cos(3s) + D_4 \cos(4s) + E_4 \cos(5s))$$
$$+ O(\epsilon^6) \tag{4.1.14}$$

$$\Omega = \Omega_0 + \epsilon\Omega_1 + \epsilon^2\Omega_2 + \epsilon^3\Omega_3 + \epsilon^4\Omega_4 + O(\epsilon^5) \tag{4.1.15}$$

Substituting (4.1.12–15) into the equations (4.1.8–11) allows us to determine all the unknowns. We carry out this step using the symbolic manipulator Maple. The nonzero coefficients for the rotation rate are

$$\Omega_0 = \ln\left(\frac{a}{2}\right) + \gamma - \frac{1}{4}$$
$$\Omega_2 = \frac{1}{32}\left(4\Omega_0 + 11 - 16\ln 2\right),$$

The nonzero coefficients for the axial coordinate are

$$x_0 = 2\pi$$
$$x2 = -\frac{\pi}{2}$$
$$x4 = \frac{\pi}{32}\left(\frac{-20\Omega_0 + 3 - 36\ln 3 + 16\ln 2}{8\Omega_0 + 9\ln 3}\right)$$
$$b_1 = \frac{1}{8}$$
$$b_3 = -\frac{1}{32}\left(\frac{-4\Omega_0 + 3 - 18\ln 3 + 16\ln 2}{8\Omega_0 + 9\ln 3}\right)$$
$$d_3 = \frac{1}{256}\left(\frac{4\Omega_0 + 5 - 36\ln 3 + 48\ln 2}{8\Omega_0 + 9\ln 3}\right),$$

Finally, the nonzero coefficients for $Y(s,\epsilon)$, the displacement of a point on the filament

from the axis, are

$$A_0 = 1$$

$$A_2 = -\frac{1}{32}\left(\frac{4\Omega_0 + 3 - 9\ln 3 + 16\ln 2}{8\Omega_0 + 9\ln 3}\right)$$

$$C_2 = -A_2$$

$$A_4 = \frac{1}{512}\left(\frac{(4\Omega_0+3)^2 - 9\ln 3(4\Omega_0+11) + 8 - 128\ln 2 - 144\ln 2\ln 3 - 256(\ln 2)^2}{16\Omega_0^2 - 32\Omega_0 + 18\Omega_0\ln 3}\right)$$

$$C_4 = -A_4.$$

All the remaining coefficients in (4.1.12–15) are identically zero.

4.2 A numerical algorithm for finding plane wave solutions

In the previous section we saw that, in principle, Kelvin's analysis in the case of small amplitude could be extended to yield a solution as a regular power series in the amplitude, and we used the symbolic manipulator Maple to compute the first 5 terms in the expansion of the solution. Naturally, such solutions are limited to the case where the amplitude is small. To obtain finite amplitude wave solutions, we must solve the equations numerically. Since the solutions are periodic in the arclength, our numerical algorithm adopts a Fourier series based pseudo–spectral approach, using Newton's method to converge on the Fourier coefficients of the solution.

The form of the solution is the same as that assumed for the perturbation series

$$\mathbf{X}(s) = \left(X_p\frac{s}{2\pi} + X(s)\right)\mathbf{e}_x + Y(s)\mathbf{e}_y \tag{4.2.1}$$

where we have dropped the explicit dependence on the amplitude ϵ. We use the Rosenhead approximation (1.4.7) to describe the self–induced motion of the filament. For our problem, this reduces to the single equation

$$\Omega Y(s) = \frac{\Gamma}{4\pi}\int_{-\infty}^{\infty} \frac{\left(\frac{X_p}{2\pi} + X'(s_*)\right)(Y(s) - Y(s_*))}{(\mathcal{D}(0))^3} - \frac{Y'(s_*)\left(X_p\frac{(s-s_*)}{2\pi} + X(s) - X(s_*)\right)}{(\mathcal{D}(0))^3} ds_* \tag{4.2.2}$$

where the denominator in the integrand is given by

$$(\mathcal{D}(\nu))^2 = \left(X_p\frac{(s - s_* - 2\nu\pi)}{2\pi} + X(s) - X(s_*)\right)^2 + (Y(s) - Y(s_*))^2 + \mu^2 \tag{4.2.3}$$

and $\mu = ae^{-3/4}$ is the value of the Rosenhead parameter (assuming the core has uniform vorticity and no axial flow). The remaining equations describing the solution are (4.1.10) and (4.1.11), as in the case of the perturbation solution.

We can construct a $2p$–periodic solution by scaling a 2π–periodic solution. The appropriate scaled filament is

$$\hat{\mathbf{X}}(\sigma) = \frac{p}{\pi}\mathbf{X}\left(\frac{\pi\sigma}{p}\right) \tag{4.2.4}$$

which is a $2p$–periodic filament that rotates with angular speed

$$\hat{\Omega} = \left(\frac{\pi}{p}\right)^2 \Omega, \tag{4.2.5}$$

has amplitude

$$\hat{\epsilon} = \left(\frac{p}{\pi}\right)\epsilon, \tag{4.2.6}$$

and core radius

$$\hat{a} = \left(\frac{p}{\pi}\right)a. \tag{4.2.7}$$

Clearly, because we can relate an arbitrary periodic filament to a 2π–periodic filament, we need only consider the case of filaments which are 2π periodic in the arclength.

Although the form of the solution essentially remains the same as it did in section 4.1, we write the 2π–periodic functions $X(s)$ and $Y(s)$ in the following way:

$$\begin{aligned} X(s) &= \sum_{n=-\infty}^{\infty} x_n e^{ins} \\ Y(s) &= \sum_{n=-\infty}^{\infty} y_n e^{ins}, \end{aligned} \tag{4.2.8}$$

To facilitate the use of the Fourier pseudo–spectral method, we rewrite (4.2.2) as a finite integral

$$\begin{aligned} \Omega Y(s) = \frac{\Gamma}{4\pi}\int_{-\pi}^{\pi} \sum_{\nu=-\infty}^{\infty} & \frac{\left(\frac{X_p}{2\pi} + X'(s_*)\right)(Y(s) - Y(s_*))}{(\mathcal{D}(\nu))^3} \\ & - \sum_{\nu=-\infty}^{\infty} \frac{Y'(s_*)\left(X_p\frac{(s-s_*-2\nu\pi)}{2\pi} + X(s) - X(s_*)\right)}{(\mathcal{D}(\nu))^3} ds_*. \end{aligned} \tag{4.2.9}$$

From (4.2.6) we see that the kernel, $H(s, s_*)$, of the integral is periodic, in both s and s_*, and consequently has the Fourier decomposition

$$H(s, s_*) = \sum_{n=-\infty}^{\infty} \sum_{m=-\infty}^{\infty} h_{n,m} \mathrm{e}^{ins} \mathrm{e}^{ims_*} \tag{4.2.10}$$

where the Fourier coefficients $h_{n,m}$ are functions of X_p, the Fourier coefficients of $X(s)$ and the Fourier coefficients of $Y(s)$.

At this point we can write down the Fourier representation of our equations. From equation (4.1.11) we get

$$\begin{aligned} &\left(\frac{X_p}{2\pi}\right)^2 + \sum_{m=-\infty}^{\infty} m^2 \left(|x_m|^2 + |y_m|^2\right) - 1 = 0 \quad \text{for } n = 0 \\ &i\frac{nX_p x_n}{\pi} - \sum_{m=-\infty}^{\infty} m(n-m)(x_{n-m}x_m + y_{n-m}y_m) = 0 \quad \text{for } n \neq 0,\ n \in \mathbf{Z} \end{aligned} \tag{4.2.11}$$

where $\mathbf{Z}$ is the set of integers. Equation (4.2.9), along with (4.2.10), yields the deceivingly simple equation

$$\Omega y_n - \frac{\Gamma}{2} h_{n,0} = 0 \quad \text{for } n \in \mathbf{Z}. \tag{4.2.12}$$

The conditions at the origin expressed as (4.1.10) become

$$\begin{aligned} \sum_{m=-\infty}^{\infty} x_m &= 0 \\ \sum_{m=-\infty}^{\infty} y_m - \epsilon &= 0. \end{aligned} \tag{4.2.13}$$

Our unknowns are X_p, Ω, $\{x_n\}_{n=-\infty}^{\infty}$ and $\{y_n\}_{n=-\infty}^{\infty}$. From (4.2.11–13) we can see that we have the same number of equations as unknowns.

The equations, as they stand in (4.2.11–13), are infinite–dimensional and cannot be represented on a computer. If we truncate the Fourier series and retain the corresponding finite number of equations from (4.2.11–13), then we can represent this new system on a computer. The truncation of the Fourier series allows us to use Fast Fourier Transforms to relate sampled function values in real space to coefficients in Fourier space and vice versa. The sampled function values in real space and the

corresponding Fourier coefficients form a discrete transform pair. To set up a discrete transform pair $\{F(s_j) \mid j = 0, \ldots, N-1\}$ and $\{f_n \mid n = -N/2, \ldots, N/2-1\}$, we define a set of N nodal points, $\{s_j = 2\pi j/N \mid j = 0, \ldots, N-1\}$, in the independent variable s. Consequently, for an arbitrary periodic function $F(s)$, we can compute a set of N sampled values $F(s_j)$. These can be related to the values f_n in Fourier space by the following relation:

$$F(s_j) = \sum_{n=-\frac{N}{2}}^{\frac{N}{2}-1} f_n e^{i\frac{2\pi jn}{N}} \tag{4.2.14}$$

The inversion formula is

$$f_n = \frac{1}{N} \sum_{j=0}^{N-1} F(s_j) e^{-i\frac{2\pi jn}{N}} \tag{4.2.15}$$

The relations (4.2.14–15) allow us to compute representations for derivatives of the function $F(s)$ at the nodal points s_j. For example, the discrete spectral representation of the first derivate $F'(s)$ at a nodal point is

$$F'(s_j) = \sum_{n=-\frac{N}{2}}^{\frac{N}{2}-1} inf_n e^{i\frac{2\pi jn}{N}}. \tag{4.2.13}$$

This is the main idea behind the pseudo–spectral approach, which assumes that a representation for the value of a nonlinear term at the nodal points can be computed from the representations for the values of all of its factors. For our problem this allows us to compute a discrete representation for the kernel $H(s, s_*)$ at $s = s_j$ and $s_* = s_k$, for $j, k = 0, \ldots, N-1$ (the discrete Fourier coefficients follow).

In using the truncated Fourier series we require values for the $2N+2$ unknowns X_p, Ω, $\{x_n\}_{n=-N/2}^{N/2-1}$ and $\{y_n\}_{n=-N/2}^{N/2-1}$, which satisfy the $2N+2$ equations, obtained by taking the pseudo–spectral representations for (4.2.11–12) and truncating the series in (4.2.13). Symbolically, this yields a nonlinear vector function $\vec{g}(\vec{u})$, where $\vec{g}$ is a $2N+2$ dimensional vector representing the left–hand side of our equations and $\vec{u}$, also a $2N+2$ dimensional vector, represents our unknowns. Newton's method for finding a root of $\vec{g}$ employs the following two step algorithm:

(*i*) Pick an initial guess $\vec{u}_0$

(*ii*) **If** $\|\vec{g}(\vec{u}_r)\| < tolerance$, for some chosen norm and tolerance, **then** $\vec{u}_r$ is our approximation of the solution.

Else compute the update vector $\vec{u}_{r+1}$ given by

$$\vec{u}_{r+1} = \vec{u}_r - J(\vec{u}_r)\vec{g}(\vec{u}_r)$$

where $J(\vec{u}_r)$ is the inverse of the jacobian of $\vec{g}$ evaluated at $\vec{u}_r$. **Repeat** step (ii).

If an analytic (i.e., accurate) jacobian can be calculated, then the Newton iteration part of the algorithm converges quadratically, when the initial guess is near enough to the actual solution.

4.3 Efficient implementation of the numerical algorithm

The numerical algorithm, as it was described in the previous section, cannot be translated simply into an efficient code. Essentially, there are three problem areas that need to be addressed. The first concerns the kernel of the integral, which has a strong non–uniform behavior near the singular point. The second problem area concerns the representation of the infinite sum that makes up the kernel of the integral. The third problem area concerns the computation of the jacobian matrix used in the Newton iteration section of the code.

The problem associated with the non–uniform behavior of the integrand is easily seen by approximating the kernel of the Rosenhead formula for s_* close to s, which yields

$$\mathbf{s}_* \times \frac{(\mathbf{X}(s) - \mathbf{X}(s_*))}{\left(|\mathbf{X}(s) - \mathbf{X}(s_*)|^2 + \mu^2\right)^{3/2}} \approx H^{(0)}(s, s_*)\kappa\mathbf{b} \tag{4.3.1}$$

where

$$H^{(0)}(s, s_*) = \frac{1}{2}\frac{(s - s_*)^2}{((s - s_*)^2 + \mu^2)^{3/2}}. \tag{4.3.2}$$

$H^{(0)}(s, s_*)\kappa(s)$ is the approximation for the kernel of (4.2.2) when s_* is close to s. In figure 4.3.1 we plot $H^{(0)}(s, s_*)$, for a core radius of $a = 0.1$. The non–uniform behavior of the kernel is clearly evident in the figure by the presence of the peaks on either side of the point $s_* = s$, where $H^{(0)}(s, s_*)$ vanishes. The distance between the

peaks scales like a and their height scales like $1/a$. Consequently, the non–uniform behavior becomes more severe for smaller values of the core radius. Moore (1974) used the Rosenhead approximation to follow the evolution of a trailing vortex pair, subject to an initial sinusoidal perturbation, which was unstable according to Crow's linear stability analysis. The geometry of the situation was somewhat similar to the one we consider here, since both filaments had a periodic shape. To remove the strong non–uniformity from the Rosenhead kernel, Moore chose to rewrite the integral as

$$\begin{aligned}
&\int_{-\infty}^{\infty} \mathbf{s}_* \times \frac{(\mathbf{X}(s)-\mathbf{X}(s_*))}{\left(|\mathbf{X}(s)-\mathbf{X}(s_*)|^2+\mu^2\right)^{3/2}} ds_* \\
&= \int_{-\infty}^{\infty} \left(\mathbf{s}_* \times \frac{(\mathbf{X}(s)-\mathbf{X}(s_*))}{\left(|\mathbf{X}(s)-\mathbf{X}(s_*)|^2+\mu^2\right)^{3/2}} - H^{(0)}(s,s_*)\mathcal{H}(2\pi-|s-s_*|)\,\kappa\mathbf{b} \right) ds_* \\
&\quad + \frac{1}{2}\left(\ln\left(\frac{\sqrt{(s-2\pi)^2+\mu^2}-(s-2\pi)}{\sqrt{(s+2\pi)^2+\mu^2}-(s+2\pi)} \right) \right. \\
&\qquad \left. + \frac{(s-2\pi)}{\sqrt{(s-2\pi)^2+\mu^2}} - \frac{(s+2\pi)}{\sqrt{(s+2\pi)^2+\mu^2}} \right) \kappa\mathbf{b}
\end{aligned} \tag{4.3.3}$$

where $\mathcal{H}$ is the heaviside step function and the term outside the integral compensates for making the kernel smoother. Immediately we can see that this procedure for making the kernel smoother is not appropriate for our problem, because the smoothed kernel is no longer periodic in s and s_*. (Also, the term outside the integral in (4.3.3) is not periodic in s.) Furthermore, the smoothing term decays like $1/|s-s_*|$, when s_* is far from s, so the range of s_* for which the smoothing function may be subtracted from the original integral cannot be extended from $\pm 2\pi$ to $\pm\infty$.

To circumvent this problem we construct a smoothing function which has the correct behavior for s_* near s and decays faster than $1/|s-s_*|$ for s_* far from s. A smoothing function which has these properties is

$$\bar{H}^{(0)}(s,s_*) = \frac{(1-\cos(s-s_*))}{((s-s_*)^2+\mu^2)^{3/2}}. \tag{4.3.4}$$

Figure 4.3.1 also contains a plot of this new smoothing function. Clearly it has the correct behavior for s_* close to s and decays like $1/|s-s_*|^3$ for s_* far from s.

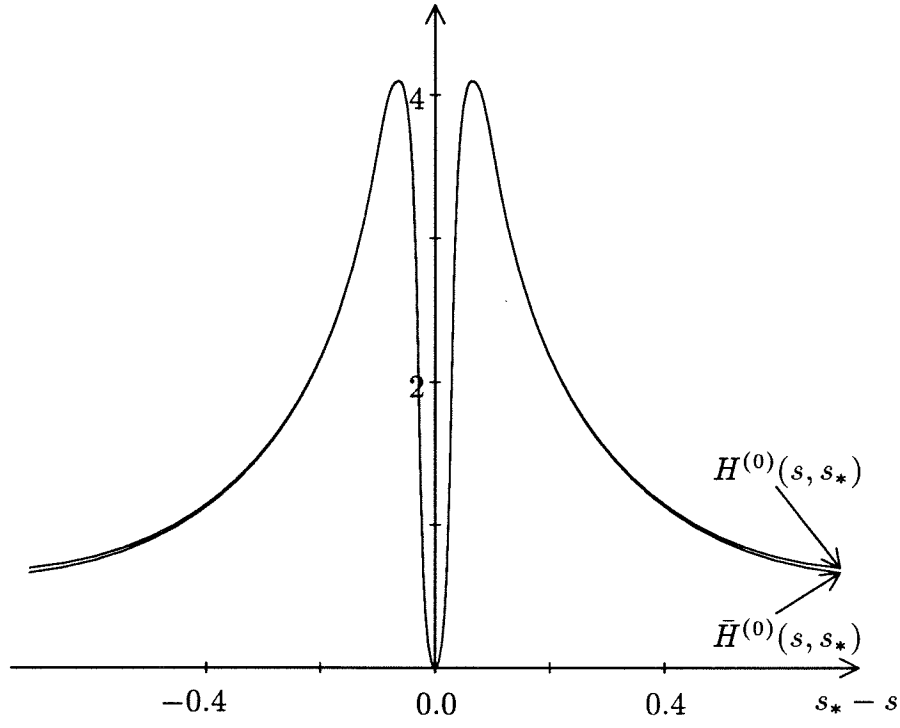

Figure 4.3.1 Plot showing the behaviors of the approximations $H^{(0)}(s, s_*)$ and $\bar{H}^{(0)}(s, s_*)$ of the Rosenhead kernel for s_* near s.

Furthermore, if $\mathrm{K}_1(z)$ is the first order modified Bessel function of the second kind, then we can rewrite the integral in the Rosenhead formula as

$$\begin{aligned}
&\int_{-\infty}^{\infty} \mathbf{s}_* \times \frac{(\mathbf{X}(s) - \mathbf{X}(s_*))}{\left(|\mathbf{X}(s) - \mathbf{X}(s_*)|^2 + \mu^2\right)^{3/2}} ds_* \\
&= \int_{-\infty}^{\infty} \left(\mathbf{s}_* \times \frac{(\mathbf{X}(s) - \mathbf{X}(s_*))}{\left(|\mathbf{X}(s) - \mathbf{X}(s_*)|^2 + \mu^2\right)^{3/2}} - \bar{H}^{(0)}(s, s_*)\kappa\mathbf{b} \right) ds_* \\
&\qquad + \frac{2}{\mu}\left(\frac{1}{\mu} - \mathrm{K}_1(\mu)\right)\kappa.\mathbf{b}
\end{aligned} \tag{4.3.5}$$

This new formulation, for the integral term, has the required periodicity for using the Fourier series approach in solving the problem. The expression (4.3.5) also has the advantage that it expresses the Rosenhead formula as the sum of an integral part and a part resembling the local induction term (i.e., the part proportional to $\kappa\mathbf{b}$, outside

the integral).

The second problem area that prohibits the effective implementation of the numerical algorithm is the representation of the infinite sums that appear when an integral over an infinite range is transformed into an integral over a finite range, as in (4.2.6). We shall abstract things for a moment and note that the type of summations that we require are of the form

$$\Sigma(\alpha,\beta) = \sum_{\nu=-\infty}^{\infty} \frac{\nu^{\alpha}}{((c-2\nu\pi)^2+d^2)^{\beta/2}} \tag{4.3.6}$$

where in general c and d are functions of s and s_* and α and β are integers. One approach for representing the solution is to truncate the series so that it sums from $-M$ to $+M$, for some integer M. In essence this is equivalent to ignoring the effect that portions of the filament separated by a distance of more than MX_p have on each other. Unfortunately, the terms in the series converge rather slowly, decaying like $1/\nu^{(\beta-\alpha)}$ (for the slowest converging case $\beta-\alpha=2$), and consequently M must be very large to get an accurate representation for the sum.

One simple way of circumventing this problem is to use an asymptotic representation for the difference between the actual sum and the truncation

$$\begin{aligned}
&\Sigma(\alpha,\beta) - \sum_{\nu=-M}^{M} \frac{\nu^{\alpha}}{((c-2\nu\pi)^2+d^2)^{\beta/2}} \\
&\quad = \sum_{\nu=M+1}^{\infty} \left(\frac{(-\nu)^{\alpha}}{((c+2\nu\pi)^2+d^2)^{\beta/2}} + \frac{\nu^{\alpha}}{((c-2\nu\pi)^2+d^2)^{\beta/2}} \right) \\
&\quad \sim \frac{(1+(-1)^{\alpha})}{(2\pi)^{\beta}} \left(\zeta(\beta-\alpha) - \sum_{\nu=1}^{M} \frac{1}{\nu^{\beta-\alpha}} \right) \\
&\quad + c\beta \frac{(1-(-1)^{\alpha})}{(2\pi)^{\beta+1}} \left(\zeta(\beta-\alpha+1) - \sum_{\nu=1}^{M} \frac{1}{\nu^{\beta-\alpha+1}} \right) \\
&\qquad + o(M^{-(\beta-\alpha+1)})
\end{aligned} \tag{4.3.7}$$

where $\zeta(z) = \sum_{\nu=1}^{\infty} \nu^{-z}$ is the Riemann Zeta function. By retaining higher order terms in the asymptotic expansion, $\Sigma(\alpha,\beta)$ can be computed very accurately. The values of the Riemann Zeta function will only be required for integer values of the argument between 2 and 20 (at most), and the corresponding values can be assigned

using any of the standard tables. Moreover, the partial sums that appear in the asymptotic expansion can be computed at the same time as the truncated sum. Using ten terms of the asymptotic expansion along with a modest value of M (10, say) yields values of the summation with an accuracy on the order of the machine precision.

Our final problem area concerns the computation of a representation for the jacobian to be used in the Newton iteration section of the code. Equations (4.2.13) are linear, so their jacobian entries are trivial to compute. Equation (4.2.11) is essentially quadratic, and the corresponding entries in the jacobian can be computed, without the aliasing error, using either the "padding" technique or by using the "phase shift" technique (see sections 3.2.2–3 of *Spectral Methods in Fluid Mechanics* by Canuto, Hussaini, Quarteroni and Zang (1986)). Equation (4.2.12) is the most troublesome, since the nonlinearity is so strong. Attempts at computing the jacobian entries using two–sided finite differences fail miserably. We adopt a different approach based on the pseudo–spectral representation of our problem. To illustrate this, suppose we have a nonlinear function, $V(Z(s))$, of a periodic function, $Z(s)$. Then the pseudo–spectral representation of the situation yields the truncated Fourier series

$$\begin{aligned} Z(s) &= \sum_{n=-\frac{N}{2}}^{\frac{N}{2}-1} z_n \mathrm{e}^{ins} \\ V(s) &= \sum_{n=-\frac{N}{2}}^{\frac{N}{2}-1} v_n \mathrm{e}^{ins} \end{aligned} \tag{4.3.8}$$

where the vector of Fourier coefficients $\vec{v}$ is a nonlinear function of the vector of Fourier coefficients $\vec{z}$. What we wish to compute is the jacobian of $\vec{v}(\vec{z})$, i.e., the quantities $\partial v_n/\partial z_m$ for $n,m = -N/2, \ldots, N/2-1$. First we note that the jacobian entries are the Fourier coefficients of $\partial V/\partial z_m$, i.e.,

$$\frac{\partial V}{\partial z_m} = \sum_{n=-\frac{N}{2}}^{\frac{N}{2}-1} \frac{\partial v_n}{\partial z_m} \mathrm{e}^{ins}. \tag{4.3.9}$$

Secondly, we note that we can also write

$$\frac{\partial V}{\partial z_m} = \frac{\partial V}{\partial Z} \mathrm{e}^{ims} \tag{4.3.10}$$

Consequently, if we denote the vector of Fourier coefficients of $\partial V/\partial Z$ by $\vec{v}^{(z)}$, then from (4.3.9) and (4.3.10) we must have

$$\sum_{n=-\frac{N}{2}}^{\frac{N}{2}-1} \frac{\partial v_n}{\partial z_m} e^{ins} = \sum_{n=-\frac{N}{2}}^{\frac{N}{2}-1} v_n^{(z)} e^{i(n+m)s} \tag{4.3.11}$$

or

$$\frac{\partial v_n}{\partial z_m} = v_{[n-m]}^{(z)} \tag{4.3.12}$$

where

$$\begin{aligned} [n-m] &= n-m+N \quad \text{if} \quad n-m < -\frac{N}{2} \\ [n-m] &= n-m \qquad\quad \text{if} \quad -\frac{N}{2} \le n-m < \frac{N}{2} \\ [n-m] &= n-m-N \quad \text{if} \quad \frac{N}{2} \le n-m. \end{aligned} \tag{4.3.13}$$

This says that the entries in the jacobian of $\vec{v}(\vec{z})$ can be found by cyclically permuting the Fourier coefficients of $\partial V/\partial Z$. Since equation (4.2.12) is a function of two periodic functions $X(s)$ and $Y(s)$, we need to extend (4.3.13). Our extension also takes account of the fact that our nonlinear function depends on the first and second derivatives of $X(s)$ and $Y(s)$. This procedure provides us with a complete representation for the jacobian to be used in the Newton iteration.

4.4 Numerical extension of the perturbation results to finite amplitude and comparison with the solution to the local induction equation

In this section we do two things: we compute the numerical solution for finite values of the amplitude and we compare the results with the solution to the local induction equation. The latter comparison tells us how the non–local terms from the integral affect the solution. With regard to the solution to the local induction equation, Kida (1981) derived an analytic expression for the general solution for a three dimensional periodic filament whose motion was governed by the local induction equation. The plane rotator is a special case of this type of solution, and we now outline the solution procedure for this particular case. The local induction equation yields the following

equation for the plane rotator

$$\begin{aligned}\Omega Y(s) &= C\kappa(s) \\ &= C\left(\left(\frac{X_p}{2\pi} + X'(s)\right)Y''(s) - Y'(s)X''(s)\right)\end{aligned} \tag{4.4.1}$$

where $\kappa(s)$ is the position dependent curvature and C is a constant of proportionality which in our case is

$$C = \frac{\Gamma}{2\pi\mu}\left(\frac{1}{\mu} - \mathrm{K}_1(\mu)\right) \tag{4.4.2}$$

(see expression (4.3.5)). The prime superscripts in (4.4.1) denote differentiation with respect to arclength. C is positive and it follows that the rotation rate Ω is negative. To see this we need only consider a point on the rotator where $Y(s)$ is a maximum, which implies that $Y' = 0$ and Y'' is negative. Since the axial coordinate has been assumed to increase with s, it follows that $X_p/\pi + X'$ is positive and consequently Ω must be negative.

Equation (4.1.11), which expresses that s is the arclength for the curve, is directly applicable in this case. Multiplying (4.4.1) by Y' and using (4.1.11) leads to

$$\Omega YY' = C\left(\left(\frac{X_p}{2\pi} + X'\right)Y'Y'' - X'' + \left(\frac{X_p}{2\pi} + X'\right)^2 X''\right). \tag{4.4.3}$$

Differentiating (4.1.11) yields

$$\left(\frac{X_p}{2\pi} + X'\right)X'' + Y'Y'' = 0 \tag{4.4.4}$$

which upon substitution into (4.4.3) yields

$$\Omega YY' = -CX''. \tag{4.4.5}$$

Integrating (4.4.5) we obtain

$$X' = \frac{\Omega}{2C}\left(A - Y^2\right) \tag{4.4.6}$$

for some arbitrary constant A. Introducing (4.4.6) into (4.1.11) leads to the following differential equation for Y

$$\left(\frac{X_p}{2\pi} + \frac{\Omega}{2C}\left(A - Y^2\right)\right)^2 + Y'^2 = 1. \tag{4.4.7}$$

Multiplying by $4Y^2$ and introducing $y = Y^2$ leads to

$$y'^2 = \left(\frac{\Omega}{C}\right)^2 \left(y - \left(A + \frac{CX_p}{\pi\Omega} - \frac{2C}{\Omega}\right)\right)\left(\left(A + \frac{CX_p}{\pi\Omega} + \frac{2C}{\Omega}\right) - y\right) y. \quad (4.4.8)$$

The solution to this equation is in terms of Jacobi elliptic functions

$$Y^2(s) = y(s) = \left(A + \frac{CX_p}{\pi\Omega} - \frac{2C}{\Omega}\right) \mathrm{cn}^2\left(\sqrt{\frac{-\Omega}{C}}s, k\right) \quad (4.4.9)$$

where the modulus k is

$$k = \frac{1}{2}\sqrt{2 - \frac{X_p}{\pi} - \frac{\Omega A}{C}} \quad (4.4.10)$$

Integrating (4.4.6) yields

$$X(s) = \frac{\Omega A}{2C}s + \sqrt{\frac{C}{-\Omega}}\left(1 - \frac{X_p}{2\pi} - \frac{\Omega A}{2C}\right) \mathrm{E}\left(\sqrt{\frac{-\Omega}{C}}s, k\right) \quad (4.4.11)$$

where $\mathrm{E}(\theta, k)$ is the incomplete elliptic integral of the second kind. We have been assuming that the linear part of the axial coordinate is represented completely by $X_p s/2\pi$ and that $X(s)$ is periodic. Consequently, we must have

$$\frac{\Omega A}{2C} + \sqrt{\frac{C}{-\Omega}}\left(1 - \frac{X_p}{2\pi} - \frac{\Omega A}{2C}\right)\frac{\mathrm{E}(k)}{2\pi} = 0 \quad (4.4.12)$$

where $\mathrm{E}(k)$ is the complete elliptic integral of the second kind. The amplitude, ϵ, of the solution is

$$\begin{aligned}\epsilon &= \sqrt{A + \frac{CX_p}{\pi\Omega} - \frac{2C}{\Omega}} \\ &= 2\sqrt{\frac{C}{-\Omega}}k.\end{aligned} \quad (4.4.13)$$

Similarly, the period has been assumed to be 2π, so we must have

$$2\pi = 2\sqrt{\frac{C}{-\Omega}}\mathrm{K}(k) \quad (4.4.14)$$

where $\mathrm{K}(k)$ is the complete elliptic integral of the first kind. Equations (4.4.9-14) provide a complete prescription for the solution in the case where the local induction equation is used as the equation of motion. We note that the constant C, which

contains the information about the core radius, essentially has the effect of rescaling the rotation rate.

In figure 4.4.1 we plot the axial wavelength as a function of amplitude, for the local induction solution, the perturbation solution and the numerical solution. The axial wavelength for the numerical and perturbation solutions is depicted for a core radius of 0.001 — the results for core radii of 0.01 and 0.1 being indistinguishable from the results plotted. Also, for the local induction solution, the axial wavelength is independent of the core radius. (As we explained at the end of the previous paragraph, changing the core radius causes a rescaling of the rotation rate.) It is clear that the numerical solution and the perturbation solution are almost coincident for an amplitude less than $\epsilon = 0.7$, but thereafter the axial wavelength for the numerical solution contracts faster than that for the perturbation solution, indicating that higher order terms in the perturbation solution become important. Furthermore, the axial wavelength for both the perturbation solution and the numerical solution exhibit a stronger dependence on the amplitude than exhibited by that for the solution to the local induction equation.

In figure 4.4.2 we depict the results for the rotation rate scaled with respect to C. As we described above the rotation rate, for the local induction solution, scaled with respect to C is independent of the core radius. The scaled numerical and perturbation solutions show that in these cases the integral term forces the dependence of the rotation rate on the core radius to be more complicated than a simple scaling of the rotation rate. The numerical solution for the rotation rate, when compared to the perturbation solution for the rotation rate, has the same characteristics as the solutions for the axial wavelength, i.e., they begin to deviate from one another for amplitudes greater than $\epsilon = 0.7$. The large difference between the rotation rate for the solution to the local induction equation and the perturbation or numerical solution (especially for the smaller core radius) would seem to indicate that $C\kappa\mathbf{b}$ is a very conservative measure for the local part when the Rosenhead integral is split into a local part plus an integral term (as was done in equation (4.3.5)).

In tables 4.4.1 and 4.4.2 we present more detailed results for the axial wavelength

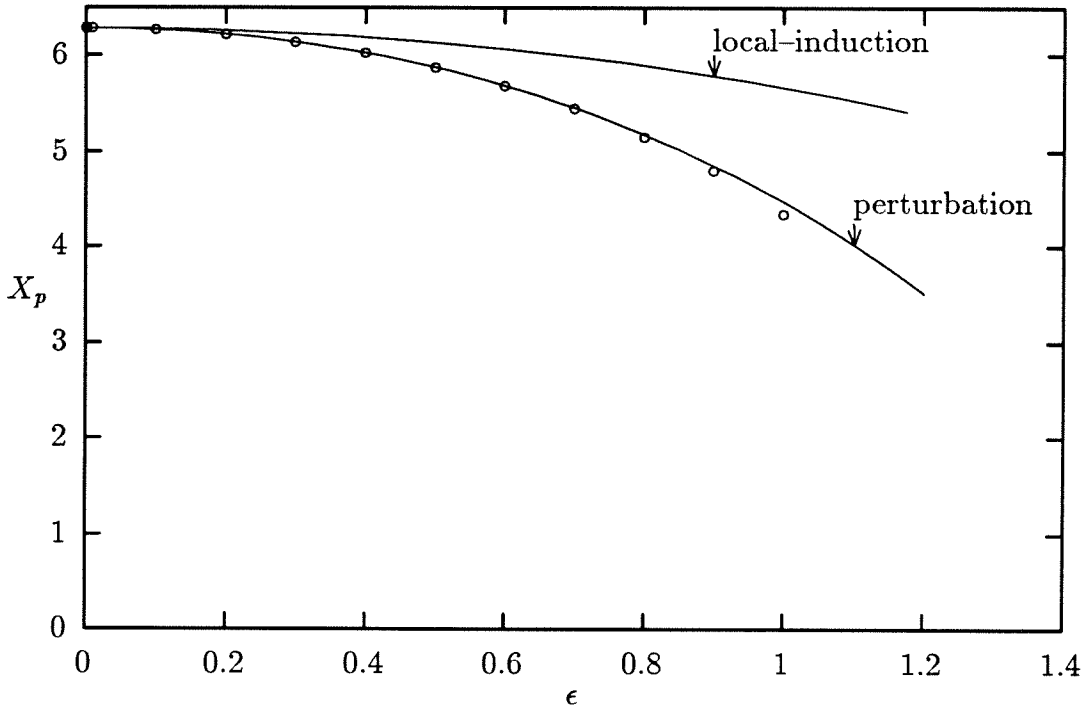

Figure 4.4.1 The axial wavelength as a function of amplitude for a core radius of 0.001. The numerical results are indicated by the open circles.

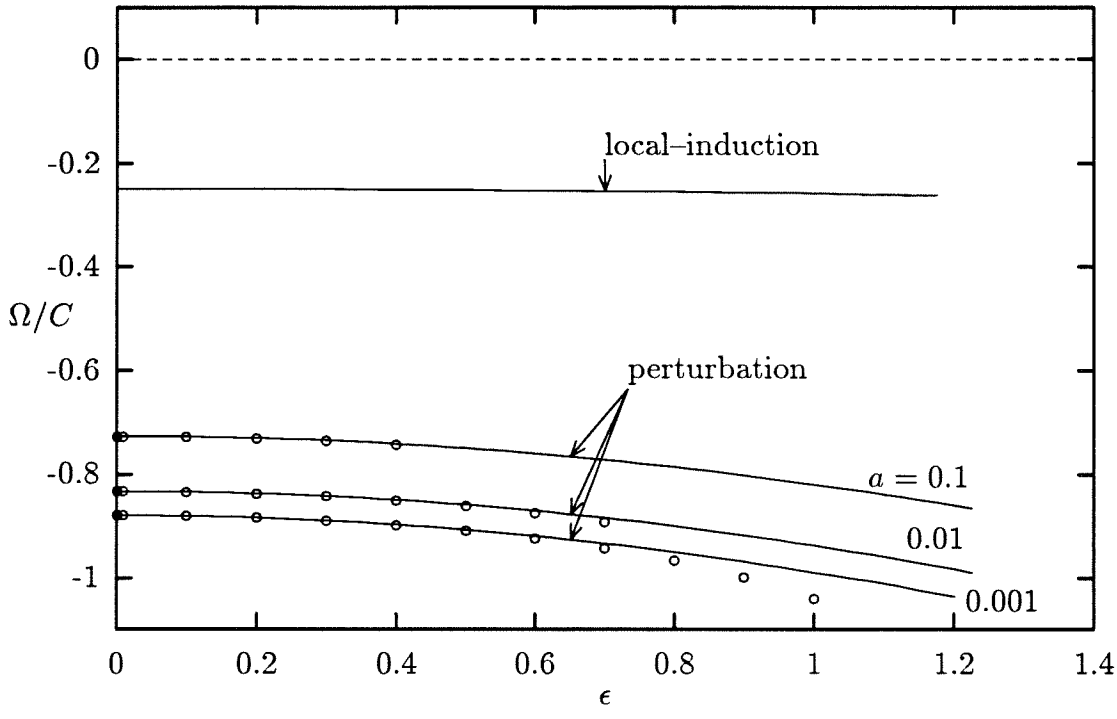

Figure 4.4.2 The rotation rate as a function of amplitude for core radii of 0.001, 0.01 and 0.1. The numerical results are indicated by the open circles.

and the rotation rate obtained from the numerical solution. The results for three distinct values of the core radius are presented ($a = 0.001$, $a = 0.01$ and $a = 0.1$) for amplitudes ranging from $\epsilon = 0.001$ to $\epsilon = 1.1$. The entries indicated by $*$ indicate that no results were obtained for the corresponding values of a and ϵ, i.e., the Newton procedure failed to converge. As is typical in such situations, the rate of convergence of the Newton procedure deteriorated as the amplitude was increased. The convergence criterion chosen for the Newton procedure was to assume convergence if the magnitude of the residual (the square root of the sum of the square of the Fourier coefficients) was less than 10^{-12}. The relative error in the solution was also monitored (the relative error, at each step of the Newton procedure, is taken to be the ratio between the magnitude of the current update and the magnitude of the current approximation to the solution). When the residual decreased toward the tolerance, the relative error was driven down toward a value on the order of the machine precision. In table 4.4.3 we detail the convergence properties for a filament with core radius $a = 0.001$ for filament amplitudes of 0.001, 0.01, 0.1 and 1.0. The magnitude of the residual associated with the initial guess (the perturbation solution, ranges from 10^{-6} to 10^{-1}. Clearly, the code has no difficulties converging on the numerical solution until the amplitude gets close to $\epsilon = 1.0$ at which point the number of iterations required increases dramatically. The only noticeable difference between the solutions as the amplitude approached the limiting value was a gradual decrease in the rate of decay of the Fourier coefficients, i.e., many of the Fourier coefficients in the upper part of spectrum (64 modes were being used) were on the order of 10^{-13}. (For the solutions that showed no problems in converging, the Fourier coefficients of the solution exhibited a rapid decay to values on the order of $10^{-16} - -10^{-17}$.) Doubling the number of modes once more, provided no increase in the limiting value of the amplitude, and the Fourier coefficients in the upper half of the spectrum still exhibited the poor decay rate.

In figure 4.4.3 we plot the filament shape for the maximum amplitude for which a solution was obtained (i.e., $\epsilon = 1.1$ for a core radius $a = 0.001$). For comparison we have also plotted a simple sinusoid having the same amplitude and wavelength. The broadening of the loop is clearly evident. Such a feature should be expected, since

the distance along the curve between two peaks has been fixed at 2π. Consequently, as the ampitude is increased, the wavelength must contract, and correspondingly the shape must alter to account for the fact that the velocity induced by neighboring loops is relatively stronger because the loops are physically closer.

4.5 Period doubling as a special case of a subharmonic bifurcation

A subharmonic of any wave is a wave whose wavelength is greater than the wavelength of the fundamental wave. Clearly, a search for bifurcations of our regular solutions to an arbitrary subharmonic is not feasible. However, with minor modifications to our algorithm (really just the initial guess), it is possible to search for bifurcations to subharmonic solutions that have periods equal to some integer multiple of 2π. In this section we will do this for a subharmonic (of a 2π–periodic solution) with period 4π — a so–called period doubling bifurcation.

Suppose $\hat{\mathbf{X}}(s)$ is a $2m\pi$–periodic solution, where m is a prime number. This filament rotates with angular speed $\hat{\Omega}$, has axial wavelength $\hat{X}_p$ and amplitude $\hat{\epsilon}$, with an assumed core radius of $\hat{a}$. Equations (4.2.4–7) state that there is a related 2π–periodic solution given by $\widetilde{\mathbf{X}}(s) = \frac{1}{m}\hat{\mathbf{X}}(ms)$, which rotates with angular speed $\widetilde{\Omega} = m^2\hat{\Omega}$, has amplitude $\tilde{\epsilon} = \hat{\epsilon}/m$ and core radius $\tilde{a} = \hat{a}/m$. Using the numerical algorithm described in the previous sections, the solution $\widetilde{\mathbf{X}}(s)$ can be continued in the amplitude $\tilde{\epsilon}$. Any bifurcations in the solution, including period altering bifurcations, will be manifested by the presence of a null space for the jacobian used in the Newton iteration.

We use a 2π–periodic solution to construct a $2m\pi$–periodic solution. Take $\mathbf{X}(s)$ to be a 2π–periodic solution, with rotation rate Ω, axial wavelength X_p, amplitude ϵ and core radius a. The equation for the filament is given by

$$\mathbf{X}(s) = \left(X_p \frac{s}{2\pi} + \sum_{n=-\infty}^{\infty} x_n e^{ins} \right) \mathbf{e}_x + \left(\sum_{n=-\infty}^{\infty} y_n e^{ins} \right) \mathbf{e}_y. \qquad (4.5.1)$$

The equation for a $2m\pi$–periodic filament is given by

$$\hat{\mathbf{X}}(s) = \left(\hat{X}_p \frac{s}{2m\pi} + \sum_{n=-\infty}^{\infty} \hat{x}_n e^{ins/m} \right) \mathbf{e}_x + \left(\sum_{n=-\infty}^{\infty} \hat{y}_n e^{ins/m} \right) \mathbf{e}_y. \qquad (4.5.2)$$

ϵ	$a = 0.001$	$a = 0.01$	$a = 0.1$
0.001	6.2831837363830	6.2831837363830	6.2831837363830
0.010	6.2830282251073	6.2830282251163	6.2830282251530
0.100	6.2674528742975	6.2674529635708	6.2674533334372
0.200	6.2199582404432	6.2199597608728	6.2199659679372
0.300	6.1397806428943	6.1397886396445	6.1398212893874
0.400	6.0252828736467	6.0253095801321	6.0254186352626
0.500	5.8739307486642	5.8740009600230	*
0.600	5.6819739870536	5.6821342150529	*
0.700	5.4438803792005	5.4442157005006	*
0.800	5.1512806255512	*	*
0.900	4.7908220342149	*	*
1.000	4.3390875658206	*	*
1.100	3.7475792399359	*	*

Table 4.4.1 The axial wavelength for a range of values of the amplitude and the core radius.

ϵ	$a = 0.001$	$a = 0.01$	$a = 0.1$
0.001	-7.2758321459987	-4.9732791692148	-2.6732869750548
0.010	-7.2759224267209	-4.9733409544451	-2.6733202433467
0.100	-7.2833694500251	-4.9795373231557	-2.6766563738745
0.200	-7.3111335792637	-4.9969326331145	-2.6856222272614
0.300	-7.3585256394153	-5.0293545567051	-2.7030527870274
0.400	-7.4273648763356	-5.0764294899765	-2.7283285600755
0.500	-7.5205201672469	-5.1400936893308	*
0.600	-7.6423426478239	-5.2232762607771	*
0.700	-7.7994477234613	-5.3304141670334	*
0.800	-8.0022036959466	*	*
0.900	-8.2674514110978	*	*
1.000	-8.6274068745677	*	*
1.100	-9.1493242589823	*	*

Table 4.4.2 The rotation rate for a range of values of the amplitude and the core radius. The quantity $C = C(a)$, used to scale the rotation rate in figure 4.4.2 takes the values $C(0.001) = 8.273236062$, $C(0.01) = 5.971125566$ and $C(0.1) = 3.669748820$.

amplitude	$\epsilon = 0.001$	$\epsilon = 0.01$	$\epsilon = 0.1$	$\epsilon = 1.0$
initial residual	$1.596^{(-6)}$	$1.596^{(-5)}$	$3.750^{(-5)}$	$1.939^{(-1)}$
# of iterations	1	2	3	20
final residual	$2.894^{(-16)}$	$1.305^{(-16)}$	$5.653^{(-15)}$	$5.916^{(-13)}$
relative error	$5.667^{(-15)}$	$1.563^{(-16)}$	$6.118^{(-14)}$	$3.062^{(-14)}$

Table 4.4.3 Convergence properties of the algorithm for a range of amplitudes, for a filament with core radius $a = 0.001$. The superscripted numbers $x^{(y)}$, appearing in the table, are shorthand for $x \times 10^y$.

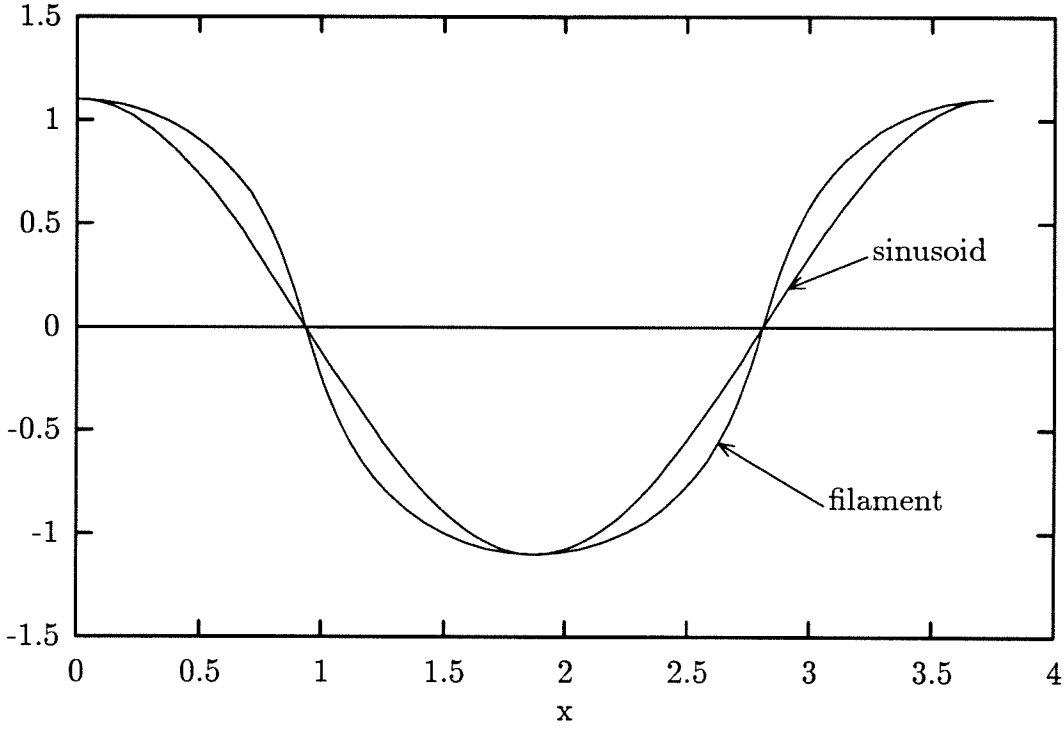

Figure 4.4.3 A plot of the filament shape, over one period, for a core radius of 0.001 and amplitude of 1.1. A simple sinusoid, with the same amplitude and wavelength, is also plotted for comparison.

Clearly, the filament $\mathbf{X}(s)$ can be considered to be a $2m\pi$–periodic filament also, which involves taking

$$\begin{aligned}
\hat{x}_n &= x_{n/m} \quad \text{if } n \bmod m = 0 \\
&= 0 \quad \text{otherwise} \\
\hat{y}_n &= y_{n/m} \quad \text{if } n \bmod m = 0 \\
&= 0 \quad \text{otherwise} \\
\hat{X}_p &= mX_p \\
\hat{\Omega} &= \Omega \\
\hat{\epsilon} &= \epsilon \\
\hat{a} &= a.
\end{aligned} \tag{4.5.3}$$

Finally we map this solution onto a 2π–periodic solution $\widetilde{\mathbf{X}}(s)$ by taking

$$\begin{aligned}
\tilde{x}_n &= \frac{x_{n/m}}{m} \quad \text{if } n \bmod m = 0 \\
&= 0 \quad \text{otherwise} \\
\tilde{y}_n &= \frac{y_{n/m}}{m} \quad \text{if } n \bmod m = 0 \\
&= 0 \quad \text{otherwise} \\
\tilde{X}_p &= X_p \\
\tilde{\Omega} &= m^2\Omega \\
\tilde{\epsilon} &= \frac{\epsilon}{m} \\
\tilde{a} &= \frac{a}{m}.
\end{aligned} \tag{4.5.4}$$

The solution $\widetilde{\mathbf{X}}(s)$ really has period $2\pi/m$, because we have mapped m periods of a 2π–periodic solution onto a 2π interval. In what follows, we take $m = 2$ and look for a period doubling bifurcation.

In the previous section we showed that we could construct a 2π–periodic solution for a filament with a core radius of 0.001 for amplitudes up to $\epsilon = 1.1$. According to the formulas given by (4.5.4), we can map these solutions onto π-periodic solutions. Stated in another way, we can construct periodic solutions for a filament with core radius of 0.0005 with amplitudes up to $\epsilon = 0.55$. (In fact, by relaxing the tolerance

used in the Newton iteration section to 10^{-10}, we were able to compute solutions for amplitudes up to $\epsilon = 0.6$.) Although the spectrum of the jacobian exhibited an eigenvalue that appeared to be heading toward zero (for $\epsilon = 0.5$ this eigenvalue was -0.1152 and for $\epsilon = 0.6$ it had changed to -0.0777), the eigenvector corresponding to this, the smallest eigenvalue, was not of the type that would support period doubling. Consequently, we must conclude that there is no period doubling bifurcation in the range of amplitudes for which a solution was computed.

CHAPTER 5

SUMMARY AND CHAPTER CONCLUSIONS

5.1 Summary

In this thesis we focused on several aspects of the dynamics associated with the motion of thin–cored vortex filaments. Essentially, we limited ourselves to problems involving inviscid fluid flow. When viscosity is present, the structure of the flow in the vortex core is an important feature of the flow. In chapter 1, where we present our most general description of thin–cored vortex filament dynamics, we have not provided any detail of how the flow in the core evolves. A complete description of the dynamics of thin–cored vortex filaments must supplement the material presented in the first two sections of chapter 1 (in conjunction with the material from appendix A and appendix B) with a description of how the core flow couples to the motion of the centerline. If the viscous effects in the flow occur on a time scale much longer than the time scale of interest, the assumption of an inviscid flow is justified.

5.2 Thin filament dynamics

In the first chapter we presented an overview of the type of fluid flow problems to be considered in the thesis. We went on to detail some of the assumptions adopted in the analysis of such flows, from the point of view of thin–cored vortex filament dynamics. In the process we outlined some of the matching procedures used in deriving the equations of motion. Besides providing a brief description of the equations of motion used in the subsequent chapters, we emphasised that the cut–off equation is a formally correct asymptotic equation of motion for thin–cored vortex filaments. This is a very important point since many investigators have made the implicit assumption that the application of the cut–off equation to describe the motion of a thin–cored vortex filament, with a centerline of arbitrary shape, is ad–hoc.

5.3 Ultra–thin filaments

The main focus of chapter 2 was to analyze the asymptotic equations of motion derived by Klein and Majda (1991a,b). Their equations purported to provide a mathematical description of some of the physics of the self–stretching of a vortex filament. Briefly, their equation expressed the velocity of a point on the centerline of the filament as the sum of the local induction term plus a nonlocal integral term. It was clear that the nonlocal term originated with the Biot–Savart integral, but it remained unclear exactly what had been extracted from the integral. We essentially showed that their equation comprised the leading order terms of an expansion, based on a small parameter, of the cut–off equation. The small parameter in this case was the ratio of the axial wavelength to the radius of curvature, of the underlying filament. There are two important conclusions that can be drawn from the connection that has been established between the two equations. The first conclusion is the obvious one, in that the origin of the terms that make up the *new* equation have been clearly identified. The second conclusion is a little more subtle and concerns the claims made by Klein and Majda that the new terms isolated in their equation account for hairpin shaped centerlines arising during the evolution of certain filaments. We do not dispute this claim, but assert that the hairpins that develop from filaments that are evolved using this equation may be spurious in nature. Moore and Saffman (1974) showed that the cut–off equation predicts a spurious instability for short waves on a hollow thin–cored vortex ring. It is generally accepted that a prediction, by the cut–off equation, of a short wave instability on a filament is quite likely a spurious prediction. Unless these short waves are filtered out in the numerical evolution of the filament (the nonlinearity will provide a seed from which these waves can grow), the centerline may evolve into a nonphysical shape. Consequently, the hairpins observed by Klein and Majda may be spurious, since their equation is essentially the cut–off equation in disguise.

5.4 Vortex ring in a pipe

Chapter 3 focused on the motion of a vortex ring, a paradigm of vortex filament motion. The thrust of the analysis was to determine the effect that a boundary had

on the stability of a filament centerline. Such knowledge is crucial since boundaries are present in all experimental situations. The main prediction, in the chapter, is that the ring inside the pipe is subject to a tilting type instability. This should not be too surprising, since in an unbounded fluid a ring tilted out of its original plane simply propagates at the same speed in the new direction, i.e., the tilting mode is neutrally stable. The presence of the boundary provides a preferred direction of orientation in space (in this case it is along the axis of the pipe). Generally, it should be expected that a boundary will induce a tilting type instability in the motion of a vortex ring. The study carried out for the current problem may also have some important consequences for vortex breakdown. It has been noted that when bubble–type breakdown occurs, there is often an entrained vortex ring at the downstream side of the bubble. If the ring is subject to the tilting mode instability, the resulting asymmetry could lead to a transition from bubble–type to spiral–type breakdown.

5.5 Planar rotator

In chapter 4, we focused on a very interesting problem in vortex filament dynamics: filaments that propagate without a change in shape of the centerline. Trivial examples of such filaments are the vortex ring and the helical vortex filament, which are filaments whose centerlines have constant curvature and constant torsion (for the ring the torsion is zero). We attempted to concentrate on the simple nontrivial example of a filament which was planar and had steady periodic shape parameters (i.e., the curvature and torsion). We extended the perturbation analysis (based on small amplitude) put forward by Kelvin and derived an expansion correct to fifth order in this small parameter. We proposed a numerical procedure, which used Newton's method coupled with a pseudo–spectral representation of the equations to solve the problem for finite amplitude waves. Unfortunately, the nonlinearities present in the problem seem to have prohibited a complete solution to the problem and the numerical procedure only provided solutions which were slightly more accurate than the perturbation approach. A search for period doubling bifurcations merely demonstrated that there were no such bifurcations in the range of parameters for which a solution could be obtained.

APPENDIX A

FLOW DESCRIPTION IN THE INNER REGION

A.1 The natural curvilinear coordinate system for the neighborhood of the vortex filament

For an arbitrary space curve $\mathbf{X} = \mathbf{R}(\xi, t)$ parametrized by ξ and dependent on time t we can establish an arclength coordinate $s = s(\xi, t)$, by defining s to be the distance along the curve between the points $\mathbf{R}(0, t)$ and $\mathbf{R}(\xi, t)$. This is expressed as

$$s(\xi, t) = \int_0^{\xi} \left| \frac{\partial \mathbf{R}(\xi', t)}{\partial \xi'} \right| d\xi'.$$

The introduction of s allows us to construct an arclength parameterization of $\mathbf{X}$ at each instant, i.e., $\mathbf{X} = \mathbf{X}(s(\xi, t), t)$. We have deliberately distinguished between the parametrizations of $\mathbf{X}$ in terms of ξ and s, because we will need an unambiguous way of describing the velocity of a point on the filament. Such a description is available with the Lagrangian parameterization in terms of ξ. The arclength parametrization along with the Frenet–Serret formulae provide a prescription for constructing a triad of unit vectors $\{\mathbf{s}, \mathbf{n}, \mathbf{b}\}$ for the space curve. These unit vectors are called the tangent, principal normal and binormal, respectively. The Frenet–Serret formulae express the interrelationship between $\mathbf{X}$ and the triad in the following way:

$$\begin{aligned} \mathbf{s} &= \frac{\partial \mathbf{X}}{\partial s} \\ \frac{\partial \mathbf{s}}{\partial s} &= \kappa \mathbf{n} \\ \frac{\partial \mathbf{n}}{\partial s} &= \tau \mathbf{b} - \kappa \mathbf{s} \\ \frac{\partial \mathbf{b}}{\partial s} &= -\tau \mathbf{n} \end{aligned} \qquad (A.1.1)$$

The geometry of the situation is illustrated in figure A.1.1. In the figure the radius of curvature, ρ, is clearly indicated, and its inverse, κ, appearing in (A.1.1) is called

the curvature. The torsion, τ, which also appears in (A.1.1) is a measure of the rate at which the triad $\{\mathbf{s}, \mathbf{n}, \mathbf{b}\}$ twists about the curve as one moves in the direction of increasing arc–length.

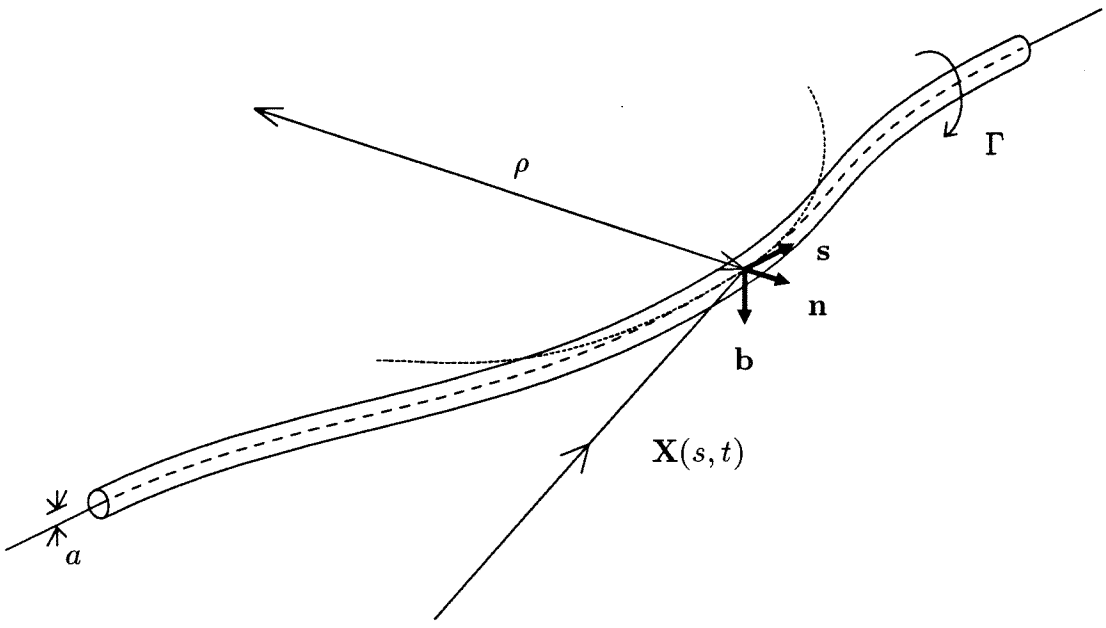

Figure A.1.1 A vortex filament with core radius a and strength Γ centered on a time dependent space curve $\mathbf{X}(s,t)$. The orientation of the unit vectors $\mathbf{s}$, $\mathbf{n}$ and $\mathbf{b}$ are indicated for an arbitrary point on the curve. We also indicate the radius of curvature, ρ, and part of the osculating circle at $\mathbf{X}(s,t)$.

We now construct a quasi–cylindrical coordinate system, (s, r, θ), centered on the space curve. This involves introducing two new unit vectors $\{\mathbf{e}_r, \mathbf{e}_\theta\}$ which span the plane normal to the curve, i.e., they lie in the plane spanned by $\mathbf{n}$ and $\mathbf{b}$. In particular, the pair $\{\mathbf{e}_r, \mathbf{e}_\theta\}$ make an angle ϕ with the pair $\{\mathbf{n}, \mathbf{b}\}$, as indicated in figure A.1.2.

The precise relationship between both pairs of vectors is expressed as

$$\begin{aligned} \mathbf{e}_r &= \cos\phi\mathbf{n} + \sin\phi\mathbf{b} \\ \mathbf{e}_\theta &= -\sin\phi\mathbf{n} + \cos\phi.\mathbf{b} \end{aligned} \qquad (A.1.2)$$

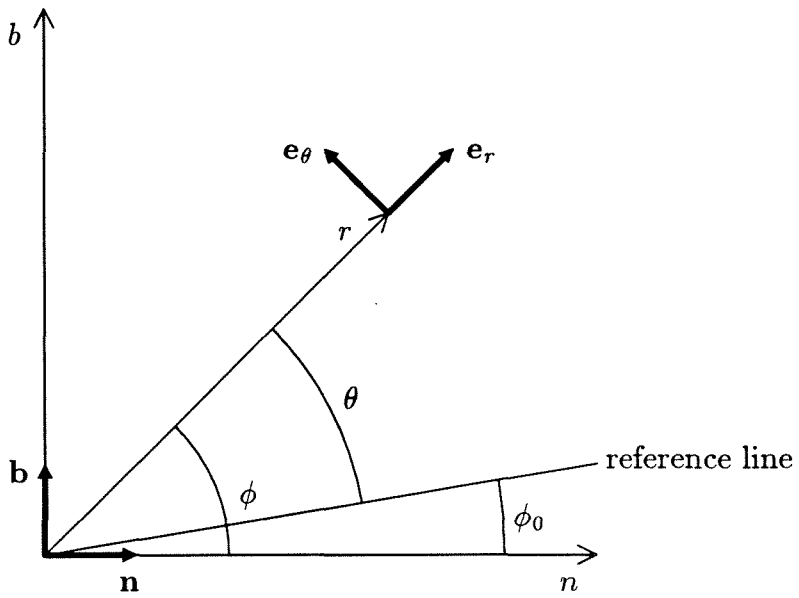

Figure A.1.2 The polar coordinate system in the normal plane.

The coordinate r, in the quasi–cylindrical coordinate system, is the perpendicular distance from an arbitrary point $\mathbf{x}$ to the curve $\mathbf{X}$. The coordinate θ is the angle made between some reference line and the unit vector $\mathbf{e}_r$. Both r and θ are indicated in figure A.1.2. The reference line marking the origin of the theta coordinate lies in the plane perpendicular to the curve and makes and angle ϕ_0 with the normal, $\mathbf{n}$. This angle is chosen to ensure that the curvilinear coordinate system (s, r, θ) is an orthogonal coordinate system. The pair $\{\mathbf{e}_r, \mathbf{e}_\theta\}$ are functions of s and θ only. An arbitrary point $\mathbf{x}$ has the following representation in our quasi–cylindrical coordinate system

$$\mathbf{x}(s, r, \theta) = \mathbf{X} + r\mathbf{e}_r(s, \theta). \qquad (A.1.3)$$

If (s, r, θ) is an orthogonal curvilinear coordinate system, then the differential $d\mathbf{x}$ can be written as

$$d\mathbf{x} = h_s \mathbf{s} ds + h_r \mathbf{e}_r dr + h_\theta \mathbf{e}_\theta d\theta, \qquad (A.1.4)$$

where h_s, h_r and h_θ are called the scale factors of the coordinated system. Using

(A.1.1), (A.1.3) and the usual polar relations

$$\begin{aligned} \frac{\partial \mathbf{e}_r}{\partial \theta} &= \mathbf{e}_\theta \\ \frac{\partial \mathbf{e}_\theta}{\partial \theta} &= -\mathbf{e}_r. \end{aligned} \tag{A.1.5}$$

we find

$$d\mathbf{x} = \left(\mathbf{s} + r\frac{\partial \mathbf{e}_r}{\partial s}\right) ds + \mathbf{e}_r dr + r\mathbf{e}_\theta d\theta. \tag{A.1.6}$$

Now according to (A.1.2) and (A.1.1)

$$\frac{\partial \mathbf{e}_r}{\partial s} = -\kappa \cos\phi \mathbf{s} - \left(\frac{\partial \phi}{\partial s} + \tau\right)(\sin\phi \mathbf{n} - \cos\phi \mathbf{b}). \tag{A.1.7}$$

Clearly, if (A.1.6) is to correspond to (A.1.4), then we must have

$$\frac{\partial \phi}{\partial s} = -\tau \tag{A.1.8}$$

and it follows that the scale factors are given by

$$\begin{aligned} h_s &= 1 - \kappa r \cos\phi \\ h_r &= 1 \\ h_\theta &= r \end{aligned} \tag{A.1.9}$$

We have introduced three angles at this stage ϕ, ϕ_0 and θ, which are not independent but are related through

$$\theta = \phi - \phi_0. \tag{A.1.9}$$

Since θ and s are independent coordinates, we must have

$$\frac{\partial \phi_0}{\partial s} = -\tau. \tag{A.1.10}$$

The derivatives of the triad $\{\mathbf{s}, \mathbf{e}_r, \mathbf{e}_\theta\}$ are easily written down using the information accumulated so far,

$$\begin{aligned} \frac{\partial}{\partial s}(\mathbf{s}, \mathbf{e}_r, \mathbf{e}_\theta) &= (\kappa(\cos\phi \mathbf{e}_r - \sin\phi \mathbf{e}_\theta), -\kappa\cos\phi \mathbf{s}, \kappa \sin\phi \mathbf{s}) \\ \frac{\partial}{\partial r}(\mathbf{s}, \mathbf{e}_r, \mathbf{e}_\theta) &= (\mathbf{0}, \mathbf{0}, \mathbf{0}) \\ \frac{\partial}{\partial \theta}(\mathbf{s}, \mathbf{e}_r, \mathbf{e}_\theta) &= (\mathbf{e}_\theta, -\mathbf{e}_r, \mathbf{0}) \end{aligned} \tag{A.1.11}$$

some of which will be needed in what follows.

We return now to a consideration of the time dependent nature of the problem. This is necessary, since our ultimate aim is to express the Euler or Navier–Stokes equations in terms of the quasi–cylindrical coordinate system constructed above. The coordinates (s, r, θ) are attatched to the space curve $\mathbf{X}(s, t)$ and are consequently time dependent. Suppose the point $\mathbf{x}$ given by (A.1.3) is fixed in space, i.e., is not dependent on time, then we can take the derivate with respect to t to find

$$\mathbf{0} = \left(\frac{\partial \mathbf{X}}{\partial t} + r\frac{\partial \mathbf{e}_r}{\partial t}\right) + (1 - \kappa r\cos\phi)\mathbf{s}\frac{\partial s}{\partial t} + \mathbf{e}_r\frac{\partial r}{\partial t} + r\mathbf{e}_\theta\frac{\partial \theta}{\partial t}. \qquad (A.1.12)$$

Taking the scalar product of (A.1.12) with the individual vectors of the triad $\{\mathbf{s}, \mathbf{e}_r, \mathbf{e}_\theta\}$ yields the following equations:

$$\begin{aligned}
\frac{\partial s}{\partial t} &= -\frac{1}{1 - \kappa r\cos\phi}\left(\frac{\partial \mathbf{X}}{\partial t} + r\frac{\partial \mathbf{e}_r}{\partial t}\right)\cdot \mathbf{s} \\
\frac{\partial r}{\partial t} &= -\frac{\partial \mathbf{X}}{\partial t}\cdot \mathbf{e}_r \\
\frac{\partial \theta}{\partial t} &= -\frac{1}{r}\left(\frac{\partial \mathbf{X}}{\partial t} + r\frac{\partial \mathbf{e}_r}{\partial t}\right)\cdot \mathbf{e}_\theta
\end{aligned} \qquad (A.1.13)$$

Now we are in a position to write down the equations of motion in terms of the quasi–cylindrical coordinates. Suppose the velocity field of the fluid is represented by $\mathbf{u}(\mathbf{x}, t)$ and the corresponding pressure field is $p(\mathbf{x}, t)$, then the Euler equations are

$$\frac{D\mathbf{u}}{Dt} = -\nabla p \qquad (A.1.14)$$

$$\nabla\cdot\mathbf{u} = 0 \qquad (A.1.15)$$

where $D/Dt = \partial/\partial t + \mathbf{u}\cdot\nabla$ represents the total derivative operator. We have already constructed a coordinate system relative to the space curve, and we can decompose the velocity field in an analagous manner. This involves introducing a relative velocity field $\mathbf{V} = u\mathbf{e}_r + v\mathbf{e}_\theta + w\mathbf{s}$ so that

$$\mathbf{u}(\mathbf{x}, t) = \frac{\partial \mathbf{X}}{\partial t} + \mathbf{V}(s, r, \theta, t). \qquad (A.1.16)$$

For a scalar function $q(s, r, \theta, t)$, the total derivative is

$$\begin{aligned}
\frac{Dq}{Dt} = \frac{\partial q}{\partial t} + \frac{\partial q}{\partial s}\frac{\partial s}{\partial t} + \frac{\partial q}{\partial r}\frac{\partial r}{\partial t} + \frac{\partial q}{\partial \theta}\frac{\partial \theta}{\partial t} + \\
\left(\frac{\partial \mathbf{X}}{\partial t} + \mathbf{V}\right)\cdot\left(\frac{1}{h_s}\frac{\partial q}{\partial s}\mathbf{s} + \frac{1}{h_r}\frac{\partial q}{\partial r}\mathbf{e}_r + \frac{1}{h_\theta}\frac{\partial q}{\partial \theta}\mathbf{e}_\theta\right).
\end{aligned} \qquad (A.1.17)$$

Using (A.1.13) this is rewritten as

$$\frac{Dq}{Dt} = \frac{\partial q}{\partial t} + \left(\mathbf{V} - r\frac{\partial \mathbf{e}_r}{\partial t}\right) \cdot \left(\frac{1}{h_s}\frac{\partial q}{\partial s}\mathbf{s} + \frac{\partial q}{\partial r}\mathbf{e}_r + \frac{1}{r}\frac{\partial q}{\partial \theta}\mathbf{e}_\theta\right). \qquad (A.1.18)$$

We can apply (A.1.18) to the components, with respect to a fixed cartesian frame, of the unit vectors $\{\mathbf{s}, \mathbf{n}, \mathbf{b}\}$, to find

$$\frac{D\mathbf{s}}{Dt} = \frac{\partial \mathbf{s}}{\partial t} + \frac{1}{h_s}\left(w - r\frac{\partial \mathbf{e}_r}{\partial t} \cdot \mathbf{s}\right)\left(\frac{\partial \mathbf{s}}{\partial s}\right) \qquad (A.1.19)$$

$$\frac{D\mathbf{n}}{Dt} = \frac{\partial \mathbf{n}}{\partial t} + \frac{1}{h_s}\left(w - r\frac{\partial \mathbf{e}_r}{\partial t} \cdot \mathbf{s}\right)\left(\frac{\partial \mathbf{n}}{\partial s}\right) \qquad (A.1.21)$$

$$\frac{D\mathbf{b}}{Dt} = \frac{\partial \mathbf{b}}{\partial t} + \frac{1}{h_s}\left(w - r\frac{\partial \mathbf{e}_r}{\partial t} \cdot \mathbf{s}\right)\left(\frac{\partial \mathbf{b}}{\partial s}\right) \qquad (A.1.22)$$

where we have used the fact that $\{\mathbf{s}, \mathbf{n}, \mathbf{b}\}$ are independent of r and θ. The components of the velocity $\partial\mathbf{X}/\partial t$ relative to the triad $\{\mathbf{s}, \mathbf{n}, \mathbf{b}\}$ are also independent of r and θ, so we can write

$$\frac{D}{Dt}\left(\frac{\partial \mathbf{X}}{\partial t}\right) = \frac{\partial^2 \mathbf{X}}{\partial t^2} + \frac{1}{h_s}\left(w - r\frac{\partial \mathbf{e}_r}{\partial t} \cdot \mathbf{s}\right)\frac{\partial}{\partial s}\left(\frac{\partial \mathbf{X}}{\partial t}\right). \qquad (A.1.23)$$

The total derivatives of the unit vectors $\mathbf{e}_r$ and $\mathbf{e}_\theta$ are given by

$$\frac{D\mathbf{e}_r}{Dt} = \frac{\partial \mathbf{e}_r}{\partial t} - \frac{\kappa\cos\phi}{h_s}\left(w - r\frac{\partial \mathbf{e}_r}{\partial t} \cdot \mathbf{s}\right)\mathbf{s} + \frac{1}{r}\left(v - r\frac{\partial \mathbf{e}_r}{\partial t} \cdot \mathbf{e}_\theta\right)\mathbf{e}_\theta \qquad (A.1.24)$$

$$\frac{D\mathbf{e}_\theta}{Dt} = \frac{\partial \mathbf{e}_\theta}{\partial t} + \frac{\kappa\sin\phi}{h_s}\left(w - r\frac{\partial \mathbf{e}_r}{\partial t} \cdot \mathbf{s}\right)\mathbf{s} - \frac{1}{r}\left(v - r\frac{\partial \mathbf{e}_r}{\partial t} \cdot \mathbf{e}_\theta\right)\mathbf{e}_r. \qquad (A.1.25)$$

Using (A.1.19) and (A.1.24–25) leads to the following expression for the total derivative of the velocity field $\mathbf{V}(s, r, \theta, t)$ (after some algebraic steps):

$$\begin{aligned}
\frac{D\mathbf{V}}{Dt} = {} & \left[\frac{\partial w}{\partial t} - u\frac{\partial \mathbf{s}}{\partial t} \cdot \mathbf{e}_r - v\frac{\partial \mathbf{s}}{\partial t} \cdot \mathbf{e}_\theta + u\frac{\partial w}{\partial r} + \frac{1}{r}\left(v - r\frac{\partial \mathbf{e}_r}{\partial t} \cdot \mathbf{e}_\theta\right)\frac{\partial w}{\partial \theta}\right. \\
& \left. + \frac{1}{h_s}\left(w + r\frac{\partial \mathbf{s}}{\partial t} \cdot \mathbf{e}_r\right)\left(\frac{\partial w}{\partial s} - u\kappa\cos\phi + v\kappa\sin\phi\right)\right]\mathbf{s} \\
& + \left[\frac{\partial u}{\partial t} + w\frac{\partial \mathbf{s}}{\partial t} \cdot \mathbf{e}_r + u\frac{\partial u}{\partial r} + \frac{1}{r}\left(v - r\frac{\partial \mathbf{e}_r}{\partial t} \cdot \mathbf{e}_\theta\right)\frac{\partial u}{\partial \theta} - \frac{v^2}{r}\right. \\
& \left. + \frac{1}{h_s}\left(w + r\frac{\partial \mathbf{s}}{\partial t} \cdot \mathbf{e}_r\right)\left(\frac{\partial u}{\partial s} + w\kappa\cos\phi\right)\right]\mathbf{e}_r \\
& + \left[\frac{\partial v}{\partial t} + w\frac{\partial \mathbf{s}}{\partial t} \cdot \mathbf{e}_\theta + u\frac{\partial v}{\partial r} + \frac{1}{r}\left(v - r\frac{\partial \mathbf{e}_r}{\partial t} \cdot \mathbf{e}_\theta\right)\frac{\partial v}{\partial \theta} + \frac{uv}{r}\right. \\
& \left. + \frac{1}{h_s}\left(w + r\frac{\partial \mathbf{s}}{\partial t} \cdot \mathbf{e}_r\right)\left(\frac{\partial v}{\partial s} - w\kappa\sin\phi\right)\right]\mathbf{e}_\theta \qquad (A.1.26)
\end{aligned}$$

The gradient of the pressure field is

$$\nabla p = \frac{1}{h_s}\frac{\partial p}{\partial s} + \frac{\partial p}{\partial r} + \frac{1}{r}\frac{\partial p}{\partial \theta}. \qquad (A.1.27)$$

Equations (A.1.23) and (A.1.26–7) allow us to express the Euler equations in terms of the quasi–cylindrical coordinates.

$$\frac{\partial^2 \mathbf{X}}{\partial t^2} + \frac{1}{h_s}\left(w + r\frac{\partial \mathbf{s}}{\partial t}\cdot \mathbf{e}_r\right)\frac{\partial}{\partial s}\left(\frac{\partial \mathbf{X}}{\partial t}\right) + \frac{D\mathbf{V}}{Dt} = -\nabla p \qquad (A.1.28)$$

The continuity equation becomes

$$\begin{aligned}
0 = \; & \frac{\partial}{\partial s}(h_r h_\theta \mathbf{u}\cdot\mathbf{s}) + \frac{\partial}{\partial r}(h_s h_\theta \mathbf{u}\cdot\mathbf{e}_r) + \frac{\partial}{\partial \theta}(h_s h_r \mathbf{u}\cdot\mathbf{e}_\theta) \\
= \; & r\frac{\partial}{\partial s}\left(w + \frac{\partial \mathbf{X}}{\partial t}\cdot\mathbf{s}\right) + \frac{\partial}{\partial r}\left(r h_s\left(u + \frac{\partial \mathbf{X}}{\partial t}\cdot\mathbf{e}_r\right)\right) + \frac{\partial}{\partial \theta}\left(h_s\left(v + \frac{\partial \mathbf{X}}{\partial t}\cdot\mathbf{e}_\theta\right)\right) \\
= \; & r\frac{\partial w}{\partial s} + r\frac{\partial}{\partial s}\left(\frac{\partial \mathbf{X}}{\partial t}\right)\cdot\mathbf{s} + \kappa r\frac{\partial \mathbf{X}}{\partial t}\cdot\mathbf{n} + \frac{\partial}{\partial r}(r h_s u) + (h_s - \kappa r\cos\phi)\frac{\partial \mathbf{X}}{\partial t}\cdot\mathbf{e}_r \\
& \qquad + \frac{\partial}{\partial \theta}(h_s v) - h_s\frac{\partial \mathbf{X}}{\partial t}\cdot\mathbf{e}_r + \kappa r\sin\phi\frac{\partial \mathbf{X}}{\partial t}\cdot\mathbf{e}_\theta \\
= \; & r\frac{\partial w}{\partial s} + r\frac{\partial}{\partial s}\left(\frac{\partial \mathbf{X}}{\partial t}\right)\cdot\mathbf{s} + \frac{\partial}{\partial r}(r h_s u) + \frac{\partial}{\partial \theta}(h_s v). \qquad (A.1.29)
\end{aligned}$$

Equations (A.1.26–29) provide a complete description of the Euler equations in the new coordinate system.

A.2 The perturbation series expansion for the flow in the neighborhood of the vortex filament

In section A.1 we expressed the Euler equations in terms of a natural quasi–cylindrical coordinate system fixed with respect to the filament curve. The resulting equations are certainly no simpler than the original equations, so to get a handle on the solution, we must appeal to another tool from the applied mathematician's bag of tricks. Since the filament is assumed to be a thin–cored filament, we can say that the ratio of the core radius to the radius of curvature of the filament curve is a small quantity, and we can look for a solution for the flow field in terms of a regular perturbation expansion in $\epsilon = a/\rho_0$, the ratio of core radius to radius of curvature.

Before introducing the perturbation series for the flow field, we must perform a scaling of the variables in the problem. The radial coordinate of the quasi–cylindrical

coordinate system is scaled with respect to the core radius, and the remaining coordinates having dimensions of length are scaled with respect to the radius of curvature. In the neighborhood of the vortex core, the characteristic speed is the azimuthal speed $\Gamma/2\pi a$ on the boundary of the core, and we scale all speeds relative to the velocity of the filament with respect to this speed. The natural time scale for the problem is given by $\Gamma/2\pi\rho_0^2$, which is a crude approxiamtion of the time required by a vortex ring of radius ρ_0 to move a distance equal to its radius. Finally, the pressure, according to Bernoulli's law, should scale like $(\Gamma/2\pi a)^2$. These scaling rules are summarized as follows:

$$\begin{aligned}(s', \xi', \mathbf{X}', \rho') &= \frac{1}{\rho_0}(s, \xi, \mathbf{X}, \rho) \\ r' &= \frac{r}{a} \\ t' &= \frac{\Gamma}{2\pi\rho_0^2}t \\ \mathbf{V}' &= \frac{2\pi a}{\Gamma}\mathbf{V} \\ p' &= \frac{4\pi^2 a^2}{\Gamma^2}p\end{aligned} \tag{A.2.1}$$

It turns out to be convenient to consider $4\pi^2 a^3/\Gamma^2$ times each term in equation (A.1.28). The gradient of the pressure term appearing in (A.1.28) becomes

$$\frac{4\pi^2 a^3}{\Gamma^2}\nabla p = \epsilon\frac{\partial p'}{\partial s'}\mathbf{s} + \frac{\partial p'}{\partial r'}\mathbf{e}_r + \frac{1}{r'}\frac{\partial p'}{\partial \theta}\mathbf{e}_r. \tag{A.2.2}$$

We also find

$$\begin{aligned}\frac{4\pi^2 a^3}{\Gamma^2}\left(\frac{\partial^2 \mathbf{X}}{\partial t^2} + \frac{1}{h_s}\left(w + r\frac{\partial \mathbf{s}}{\partial t}\cdot\mathbf{e}_r\right)\frac{\partial}{\partial s}\left(\frac{\partial \mathbf{X}}{\partial t}\right)\right) &= \\ \epsilon^3\frac{\partial^2 \mathbf{X}'}{\partial t'^2} + \epsilon^2\frac{1}{1-\epsilon\kappa' r'\cos\phi}\left(w' + \epsilon^2 r'\frac{\partial \mathbf{s}}{\partial t'}\cdot\mathbf{e}_r\right)\frac{\partial}{\partial s'}\left(\frac{\partial \mathbf{X}'}{\partial t'}\right).\end{aligned} \tag{A.2.3}$$

For the total derivative of $\mathbf{V}$, it is easier to work with the individual components. For the tangential component we get

$$\begin{aligned}\frac{4\pi^2 a^3}{\Gamma^2}\frac{D\mathbf{V}}{Dt}\cdot\mathbf{s} = \epsilon^2\frac{\partial w'}{\partial t'} - \epsilon^2 u'\frac{\partial \mathbf{s}}{\partial t'}\cdot\mathbf{e}_r - \epsilon^2 v'\frac{\partial \mathbf{s}}{\partial t'}\cdot\mathbf{e}_\theta \\ + u'\frac{\partial w'}{\partial r'} + \frac{1}{r'}\left(v' - \epsilon^2 r'\frac{\partial \mathbf{e}_r}{\partial t'}\cdot\mathbf{e}_\theta\right)\frac{\partial w'}{\partial \theta} \\ + \frac{\epsilon}{1-\epsilon\kappa' r'\cos\phi}\left(w' + \epsilon^2 r'\frac{\partial \mathbf{s}}{\partial t'}\cdot\mathbf{e}_r\right)\left(\frac{\partial w'}{\partial s'} - u'\kappa'\cos\phi + v'\kappa'\sin\phi\right).\end{aligned} \tag{A.2.4}$$

For the radial component we get

$$\frac{4\pi^2 a^3}{\Gamma^2}\frac{D\mathbf{V}}{Dt}\cdot\mathbf{e}_r = \epsilon^2\frac{\partial u'}{\partial t'} + \epsilon^2 w'\frac{\partial \mathbf{s}}{\partial t'}\cdot\mathbf{e}_r + u'\frac{\partial u'}{\partial r'} + \frac{1}{r'}\left(v' - \epsilon^2 r'\frac{\partial \mathbf{e}_r}{\partial t'}\cdot\mathbf{e}_\theta\right)\frac{\partial u'}{\partial \theta} + \frac{v'^2}{r'} + \frac{\epsilon}{1-\epsilon\kappa' r'\cos\phi}\left(w' + \epsilon^2 r'\frac{\partial \mathbf{s}}{\partial t'}\cdot\mathbf{e}_r\right)\left(\frac{\partial u'}{\partial s'} + w'\kappa'\cos\phi\right). \quad (A.2.5)$$

For the azimuthal component we get

$$\frac{4\pi^2 a^3}{\Gamma^2}\frac{D\mathbf{V}}{Dt}\cdot\mathbf{e}_\theta = \epsilon^2\frac{\partial v'}{\partial t'} + \epsilon^2 w'\frac{\partial \mathbf{s}}{\partial t'}\cdot\mathbf{e}_\theta + u'\frac{\partial v'}{\partial r'} + \frac{1}{r'}\left(v' - \epsilon^2 r'\frac{\partial \mathbf{e}_r}{\partial t'}\cdot\mathbf{e}_\theta\right)\frac{\partial v'}{\partial \theta} + \frac{u'v'}{r'} + \frac{\epsilon}{1-\epsilon\kappa' r'\cos\phi}\left(w' + \epsilon^2 r'\frac{\partial \mathbf{s}}{\partial t'}\cdot\mathbf{e}_r\right)\left(\frac{\partial v'}{\partial s'} - w'\kappa'\sin\phi\right). \quad (A.2.6)$$

Equations (A.2.2–6) provide a complete description of the transformed Euler equtions in terms of the scaled variables. Finally, the conitinuity equation (A.1.29) becomes

$$\epsilon r'\frac{\partial w'}{\partial s} + \epsilon^2 r'\frac{\partial}{\partial s'}\left(\frac{\partial \mathbf{X}'}{\partial t'}\right)\cdot\mathbf{s} + \frac{\partial}{\partial r'}\left(r'\left(1-\epsilon\kappa' r'\cos\phi\right)u'\right) + \frac{\partial}{\partial \theta}\left(\left(1-\epsilon\kappa' r'\cos\phi\right)v'\right) = 0. \quad (A.2.7)$$

Our next step is to write perturbation series for the field quantities that appear in our equations.

$$\mathbf{V} = \left(w^{(0)}, 0, v^{(0)}\right) + \epsilon\left(w^{(1)}, u^{(1)}, v^{(1)}\right) + \epsilon^2\left(w^{(2)}, u^{(2)}, v^{(2)}\right) + O(\epsilon^3) \quad (A.2.8)$$

$$p' = p^{(0)} + \epsilon p^{(1)} + \epsilon^2 p^{(2)} + O(\epsilon^3) \quad (A.2.9)$$

$$\frac{\partial \mathbf{X}'}{\partial t'} = \left(\frac{\partial \mathbf{X}'}{\partial t'}\right)^{(0)} + \epsilon\left(\frac{\partial \mathbf{X}'}{\partial t'}\right)^{(1)} + \epsilon^2\left(\frac{\partial \mathbf{X}'}{\partial t'}\right)^{(2)} + O(\epsilon^3). \quad (A.2.10)$$

Substituting (A.2.8–10) into the transformed equations and ignoring terms of $O(\epsilon^3)$ and higher leads to a new system of equations. The terms that are independent of ϵ are given by

$$\begin{aligned} \frac{v^{(0)}}{r'}\frac{\partial w^{(0)}}{\partial \theta} &= 0 \\ -\frac{\left(v^{(0)}\right)^2}{r'} &= -\frac{\partial p^{(0)}}{\partial r'} \\ \frac{v^{(0)}}{r'}\frac{\partial v^{(0)}}{\partial \theta} &= -\frac{1}{r'}\frac{\partial p^{(0)}}{\partial \theta} \\ \frac{\partial v^{(0)}}{\partial \theta} &= 0 \end{aligned} \quad (A.2.11)$$

which come from the axial–momentum, radial–momentum, azimuthal–momentum and continuity equations, respectively. The corresponding terms proportional to ϵ are

$$\begin{aligned}
u^{(1)}\frac{\partial w^{(0)}}{\partial r'} + \frac{v^{(0)}}{r'}\frac{\partial w^{(1)}}{\partial \theta} + \frac{v^{(1)}}{r'}\frac{\partial w^{(0)}}{\partial \theta} + w^{(0)}\frac{\partial w^{(0)}}{\partial s'} \\
+ \kappa' v^{(0)} w^{(0)} \sin\phi = -\frac{\partial p^{(0)}}{\partial s'} \\
\frac{v^{(0)}}{r'}\frac{\partial u^{(1)}}{\partial \theta} - \frac{2v^{(0)}v^{(1)}}{r'} + \kappa'\left(w^{(0)}\right)^2 \cos\phi = -\frac{\partial p^{(1)}}{\partial r'} \\
u^{(1)}\frac{\partial v^{(0)}}{\partial r'}\frac{v^{(0)}}{r'}\left(\frac{\partial v^{(1)}}{\partial \theta} + u^{(1)}\right) + \frac{v^{(1)}}{r'}\frac{\partial v^{(0)}}{\partial \theta} + w^{(0)}\frac{\partial v^{(0)}}{\partial s'} \\
- \kappa'\left(w^{(0)}\right)^2 \sin\phi = -\frac{1}{r'}\frac{\partial p^{(1)}}{\partial \theta} \\
\frac{\partial}{\partial r'}\left(r' u^{(1)}\right)\frac{\partial v^{(1)}}{\partial \theta} - \kappa' r' \frac{\partial}{\partial \theta}\left(v^{(0)}\cos\phi\right) + r'\frac{\partial w^{(0)}}{\partial s'} = 0.
\end{aligned} \tag{A.2.12}$$

Finally, the equations proportional to ϵ^2 are

$$\begin{aligned}
w^{(0)}\frac{\partial}{\partial s'}\left(\left(\frac{\partial \mathbf{X}'}{\partial t'}\right)^{(0)}\right)\cdot\mathbf{s} + \frac{\partial w^{(0)}}{\partial t'} - v^{(0)}\frac{\partial \mathbf{s}}{\partial t'}\cdot\mathbf{e}_\theta + u^{(1)}\frac{\partial w^{(1)}}{\partial r'} \\
+ u^{(2)}\frac{\partial w^{(0)}}{\partial r'} + \frac{v^{(0)}}{r'}\frac{\partial w^{(2)}}{\partial \theta} + \frac{v^{(1)}}{r'}\frac{\partial w^{(1)}}{\partial \theta} + \frac{1}{r'}\left(v^{(2)} - r'\frac{\partial \mathbf{e}_r}{\partial t'}\cdot\mathbf{e}_\theta\right)\frac{\partial w^{(0)}}{\partial \theta} \\
+ w^{(0)}\left(\frac{\partial w^{(1)}}{\partial s'} + \kappa' v^{(1)}\sin\phi - \kappa' u^{(1)}\cos\phi\right) + w^{(1)}\left(\frac{\partial w^{(0)}}{\partial s'} + \kappa' v^{(0)}\sin\phi\right) \\
+ \kappa' r' w^{(0)}\left(\frac{\partial w^{(0)}}{\partial s'} + \kappa' v^{(0)}\sin\phi\right)\cos\phi = -\frac{\partial p^{(1)}}{\partial s'}
\end{aligned} \tag{A.2.13}$$

from the axial–momentum equation,

$$\begin{aligned}
2w^{(0)}\frac{\partial}{\partial s'}\left(\left(\frac{\partial \mathbf{X}'}{\partial t'}\right)^{(0)}\right)\cdot\mathbf{e}_r + u^{(1)}\frac{\partial u^{(1)}}{\partial r'} + \frac{v^{(0)}}{r'}\frac{\partial u^{(2)}}{\partial \theta} + \frac{v^{(1)}}{r'}\frac{\partial u^{(1)}}{\partial \theta} \\
- \frac{1}{r'}\left(\left(v^{(1)}\right)^2 + 2v^{(0)}v^{(2)}\right) + \kappa'^2 r'\left(w^{(0)}\right)^2\cos^2\phi + 2\kappa' w^{(0)}w^{(1)}\cos\phi \\
+ w^{(0)}\frac{\partial u^{(1)}}{\partial s'} = -\frac{\partial p^{(2)}}{\partial r'}
\end{aligned} \tag{A.2.14}$$

from the radial–momentum equation,

$$2w^{(0)}\frac{\partial}{\partial s'}\left(\left(\frac{\partial \mathbf{X}'}{\partial t'}\right)^{(0)}\right)\cdot\mathbf{e}_\theta + \frac{\partial v^{(0)}}{\partial t'} + u^{(1)}\frac{\partial v^{(1)}}{\partial r'} + u^{(2)}\frac{\partial v^{(0)}}{\partial r'}$$

$$+\frac{1}{r'}\left(v^{(0)}\left(\frac{\partial v^{(2)}}{\partial\theta}+u^{(2)}\right)+v^{(1)}\left(\frac{\partial v^{(1)}}{\partial\theta}+u^{(1)}\right)+\left(v^{(2)}-r'\frac{\partial \mathbf{e}_r}{\partial t'}\cdot\mathbf{e}_\theta\right)\frac{\partial v^{(0)}}{\partial\theta}\right)$$
$$+w^{(0)}\left(\frac{\partial v^{(1)}}{\partial s'}-\kappa' w^{(1)}\sin\phi\right)+w^{(1)}\left(\frac{\partial v^{(0)}}{\partial s'}-\kappa' w^{(0)}\sin\phi\right)$$
$$+\kappa' r' w^{(0)}\left(\frac{\partial v^{(0)}}{\partial s'}-\kappa' w^{(0)}\sin\phi\right)\cos\phi=-\frac{1}{r'}\frac{\partial p^{(2)}}{\partial\theta} \quad (A.2.15)$$

from the azimuthal–momentum equations and

$$\frac{\partial}{\partial r'}\left(r'u^{(2)}\right)-\kappa'\frac{\partial}{\partial r'}\left(r'^2u^{(1)}\right)\cos\phi+\frac{\partial v^{(2)}}{\partial\theta}-\kappa' r'\frac{\partial}{\partial\theta}\left(v^{(1)}\cos\phi\right)$$
$$+r'\frac{\partial w^{(1)}}{\partial s'}+r'\frac{\partial}{\partial s'}\left(\left(\frac{\partial\mathbf{X}'}{\partial t'}\right)^{(0)}\right)\cdot\mathbf{s}=0 \quad (A.2.14)$$

from the continuity equation.

A.3 Solution of the leading order perturbation equations

The leading order equations (A.2.11) are readily solved to yield

$$p^{(0)}=p_\infty-\int_{r'}^{\infty}\frac{\left(v^{(0)}(\xi)\right)^2}{\xi}d\xi \quad (A.3.1)$$

and

$$\begin{aligned}\frac{\partial w^{(0)}}{\partial\theta}&=0\\ \frac{\partial v^{(0)}}{\partial\theta}&=0\\ \frac{\partial p^{(0)}}{\partial\theta}&=0.\end{aligned} \quad (A.3.2)$$

This clearly shows that to leading order the effects of curvature are absent from the flow at infinity; the leading order flow is axisymmetric.

A.4 Solution of the order ϵ equations

To solve the order ϵ equations, we require more information about the leading order flow structure. We deduce from the asymptotic behavior of $v^{(0)}$, which being like $1/r'$ is independent of s', that $v^{(0)}$ is independent of s'. Furthermore, if we average the first order equations over the azimuthal direction (i.e., compute the integral

$1/2\pi \int_0^{2\pi}(\cdot)d\theta)$, we find

$$\begin{aligned} u_0^{(1)}\frac{\partial w^{(0)}}{\partial r'} + w^{(0)}\frac{\partial w^{(0)}}{\partial s'} &= -\frac{\partial p^{(0)}}{\partial s'} \\ -2\frac{v^{(0)}v_0^{(1)}}{r'} &= -\frac{\partial p_0^{(1)}}{\partial r'} \\ u_0^{(1)}\frac{\partial v^{(0)}}{\partial r'} + \frac{u_0^{(1)}v^{(0)}}{r'} + w^{(0)}\frac{\partial v^{(0)}}{\partial s'} &= 0 \\ \frac{\partial}{\partial r'}\left(r'u_0^{(1)}\right) + r'\frac{\partial w^{(0)}}{\partial s'} &= 0 \end{aligned} \tag{A.4.1}$$

where the quantities with subscript 0 denote the azimuthal averages of the corresponding quantity. Using the fact that $v^{(0)}$ is independent of s' yields

$$\begin{aligned} \frac{\partial v^{(0)}}{\partial s'} &= 0 \\ u_0^{(1)} &= 0 \\ \frac{\partial w^{(0)}}{\partial s'} &= 0 \\ \frac{\partial p^{(0)}}{\partial s'} &= 0. \end{aligned} \tag{A.4.2}$$

This allows the first order equations to be rewritten as

$$\begin{aligned} u^{(1)}\frac{\partial w^{(0)}}{\partial r'} + \frac{v^{(0)}}{r'}\frac{\partial w^{(1)}}{\partial \theta} + \kappa' v^{(0)}w^{(0)}\sin\phi &= 0 \\ \frac{v^{(0)}}{r'}\frac{\partial u^{(1)}}{\partial \theta} - 2\frac{v^{(0)}v^{(1)}}{r'} + \kappa'\left(w^{(0)}\right)^2\cos\phi &= -\frac{\partial p^{(1)}}{\partial r'} \\ u^{(1)}\frac{\partial v^{(0)}}{\partial r'} + \frac{v^{(0)}}{r'}\frac{\partial v^{(1)}}{\partial \theta} + \frac{v^{(0)}u^{(1)}}{r'} - \kappa'\left(w^{(0)}\right)^2\sin\phi &= -\frac{1}{r'}\frac{\partial p^{(1)}}{\partial \theta} \\ \frac{\partial}{\partial r'}\left(r'u^{(1)}\right) + \frac{\partial v^{(1)}}{\partial \theta} + \kappa' v^{(0)}\sin\phi &= 0. \end{aligned} \tag{A.4.3}$$

Now we look for solutions for the flow field in the following form:

$$\begin{aligned} w^{(1)} &= w_0^{(1)} + w_{c_1}^{(1)}\cos\phi + w_{s_1}^{(1)}\sin\phi \\ u^{(1)} &= u_0^{(1)} + u_{c_1}^{(1)}\cos\phi + u_{s_1}^{(1)}\sin\phi \\ v^{(1)} &= v_0^{(1)} + v_{c_1}^{(1)}\cos\phi + v_{s_1}^{(1)}\sin\phi \\ p^{(1)} &= p_0^{(1)} + p_{c_1}^{(1)}\cos\phi + p_{s_1}^{(1)}\sin\phi \end{aligned} \tag{A.4.4}$$

A careful consideration of higher order terms in the Fourier expansion shows that the corresponding coefficients are identically zero. We also note that $u_0^{(1)} = 0$ from

(A.4.2). Substituting (A.4.4) into the reduced axial–momentum equation yields an equation whose Fourier coefficients are

$$\begin{aligned} u_0^{(1)}\frac{\partial w^{(0)}}{\partial r'} &= 0 \\ u_{c_1}^{(1)}\frac{\partial w^{(0)}}{\partial r'} + \frac{v^{(0)}w_{s_1}^{(1)}}{r'} &= 0 \\ u_{s_1}^{(1)}\frac{\partial w^{(0)}}{\partial r'} - \frac{v^{(0)}w_{c_1}^{(1)}}{r'} + \kappa' v^{(0)}w^{(0)} &= 0. \end{aligned} \tag{A.4.5}$$

Repeating this procedure for the radial–momentum equation yields

$$\begin{aligned} -2\frac{v^{(0)}v_0^{(1)}}{r'} &= -\frac{\partial p_0^{(1)}}{\partial r'} \\ \frac{v^{(0)}u_{s_1}^{(1)}}{r'} - 2\frac{v^{(0)}v_{c_1}^{(1)}}{r'} + \kappa'\left(w^{(0)}\right)^2 &= -\frac{\partial p_{c_1}^{(1)}}{\partial r'} \\ -\frac{v^{(0)}u_{c_1}^{(1)}}{r'} - 2\frac{v^{(0)}v_{s_1}^{(1)}}{r'} &= -\frac{\partial p_{s_1}^{(1)}}{\partial r'}. \end{aligned} \tag{A.4.6}$$

Again for the azimuthal–momentum equation

$$\begin{aligned} u_0^{(1)}\frac{\partial v^{(0)}}{\partial r'} + \frac{u_0^{(1)}v^{(0)}}{r'} &= 0 \\ u_{c_1}^{(1)}\frac{\partial v^{(0)}}{\partial r'} + \frac{v^{(0)}}{r'}\left(v_{s_1}^{(1)} + u_{c_1}^{(1)}\right) &= -\frac{p_{s_1}^{(1)}}{r'} \\ u_{s_1}^{(1)}\frac{\partial v^{(0)}}{\partial r'} + \frac{v^{(0)}}{r'}\left(-v_{c_1}^{(1)} + u_{s_1}^{(1)}\right) - \kappa'\left(w^{(0)}\right)^2 &= \frac{p_{c_1}^{(1)}}{r'}. \end{aligned} \tag{A.4.7}$$

Finally, from the reduced first order continuity equation we get

$$\begin{aligned} \frac{\partial}{\partial r'}\left(r'u_0^{(1)}\right) &= 0 \\ \frac{\partial}{\partial r'}\left(r'u_{c_1}^{(1)}\right) + v_{s_1}^{(1)} &= 0 \\ \frac{\partial}{\partial r'}\left(r'u_{s_1}^{(1)}\right) - v_{c_1}^{(1)} + \kappa' r' v^{(0)} &= 0. \end{aligned} \tag{A.4.8}$$

We recognize that the first equations from (A.4.5), (A.4.6) and (A.4.8) vanish identically because $u_0^{(1)} = 0$. The remaining equations from (A.4.5), the axial momentum equation, conveniently give $w_{c_1}^{(1)}$ and $w_{s_1}^{(1)}$ in terms of $u_{s_1}^{(1)}$ and $u_{c_1}^{(1)}$ and the leading order velocities as

$$\begin{aligned} w_{s_1}^{(1)} &= -\frac{r'u_{c_1}^{(1)}}{v^{(0)}}\frac{\partial w^{(0)}}{\partial r'} \\ w_{c_1}^{(1)} &= \kappa' r' w^{(0)} + \frac{r'u_{s_1}^{(1)}}{v^{(0)}}\frac{\partial w^{(0)}}{\partial r'} \end{aligned} \tag{A.4.9}$$

The remaining equations from (A.4.8) give the velocity components $v_{c_1}^{(1)}$ and $v_{s_1}^{(1)}$ in terms of $u_{s_1}^{(1)}$ and $u_{c_1}^{(1)}$ and the leading order velocities as

$$\begin{aligned} v_{s_1}^{(1)} &= -\frac{\partial}{\partial r'}\left(r' u_{c_1}^{(1)}\right) \\ v_{c_1}^{(1)} &= \kappa' r' v^{(0)} + \frac{\partial}{\partial r'}\left(r' u_{s_1}^{(1)}\right) \end{aligned} \qquad (A.4.10)$$

Now we eliminate $p_{s_1}^{(1)}$ using (A.4.6) and (A.4.7) and find through the subsequent elimination of $v_{s_1}^{(1)}$, using (A.4.10), that $u_{c_1}^{(1)}$ satisfies

$$r' v^{(0)} \frac{\partial^2 u_{c_1}^{(1)}}{\partial r'^2} + 3v^{(0)} \frac{\partial u_{c_1}^{(1)}}{\partial r'} - \left(r' \frac{\partial^2 v^{(0)}}{\partial r'^2} + \frac{\partial v^{(0)}}{\partial r'} - \frac{v^{(0)}}{r'} \right) u_{c_1}^{(1)} = 0. \quad (A.4.11)$$

Repeating this procedure for the pressure term $p_{c_1}^{(1)}$ leads to an expression for $u_{s_1}^{(1)}$ which is

$$\begin{aligned} r' v^{(0)} \frac{\partial^2 u_{s_1}^{(1)}}{\partial r'^2} + 3v^{(0)} \frac{\partial u_{s_1}^{(1)}}{\partial r'} - \left(r' \frac{\partial^2 v^{(0)}}{\partial r'^2} + \frac{\partial v^{(0)}}{\partial r'} - \frac{v^{(0)}}{r'} \right) u_{s_1}^{(1)} \\ = -3\kappa' \left(v^{(0)}\right)^2 - 2\kappa' r' v^{(0)} \frac{\partial v^{(0)}}{\partial r'} - 2\kappa' r' w^{(0)} \frac{\partial w^{(0)}}{\partial r'}. \end{aligned} \qquad (A.4.12)$$

We can solve (A.4.11) and (A.4.12) by noticing that the left–hand side of both equations is obtained by employing the same differential operator. Moreover, a homogeneous solution for the operator (i.e., a solution of (A.4.11)) is $v^{(0)}/r'$. Consequently, we look for a solution of the form $v^{(0)}\chi(r')/r'$ and find

$$\begin{aligned} u_{c_1}^{(1)} &= \alpha_{c_1}^{(1)} \frac{v^{(0)}(r')}{r'} \int_0^{r'} \frac{d\xi}{\xi \left(v^{(0)}(\xi)\right)^2} + \beta_{c_1}^{(1)} \frac{v^{(0)}(r')}{r'} \\ u_{s_1}^{(1)} &= \alpha_{s_1}^{(1)} \frac{v^{(0)}(r')}{r'} \int_0^{r'} \frac{d\xi}{\xi \left(v^{(0)}(\xi)\right)^2} + \beta_{s_1}^{(1)} \frac{v^{(0)}(r')}{r'} \\ &\quad - \kappa' \frac{v^{(0)}(r')}{r'} \int_0^{r'} \left(\xi + \xi \left(\frac{w^{(0)}(\xi)}{v^{(0)}(\xi)} \right)^2 \right) d\xi \\ &\quad - \kappa' \frac{v^{(0)}(r')}{r'} \int_0^{r'} \int_0^{\xi} \frac{\eta \left(\left(v^{(0)}(\eta)\right)^2 - 2\left(w^{(0)}(\eta)\right)^2 \right)}{\xi \left(v^{(0)}(\xi)\right)^2} d\eta d\xi. \end{aligned} \qquad (A.4.13)$$

By requiring the components $u_{c_1}^{(1)}$ and $u_{s_1}^{(1)}$ to vanish as $r' \to 0$, we find that the constants $\alpha_{c_1}^{(1)}$, $\alpha_{s_1}^{(1)}$, $\beta_{c_1}^{(1)}$ and $\beta_{s_1}^{(1)}$ must be chosen to be zero. Consequently, we find

$$\begin{aligned} u_{c_1}^{(1)} &= 0 \\ u_{s_1}^{(1)} &= -\frac{1}{2}\kappa' r' v^{(0)}(r') - \kappa' \frac{v^{(0)}(r')}{r'} \int_0^{r'} \xi \left(\frac{w^{(0)}(\xi)}{v^{(0)}(\xi)} \right)^2 d\xi \\ &\quad - \kappa' \frac{v^{(0)}(r')}{r'} \int_0^{r'} \int_0^{\xi} \frac{\eta \left(\left(v^{(0)}(\eta) \right)^2 - 2 \left(w^{(0)}(\eta) \right)^2 \right)}{\xi \left(v^{(0)}(\xi) \right)^2} d\eta d\xi. \end{aligned} \tag{A.4.14}$$

Now we employ (A.4.9) to find

$$\begin{aligned} w_{s_1}^{(1)} &= 0 \\ w_{c_1}^{(1)} &= \kappa' r' w^{(0)}(r') - \frac{1}{2}\kappa' r'^2 \frac{\partial w^{(0)}}{\partial r'} - \kappa' \frac{\partial w^{(0)}}{\partial r'} \int_0^{r'} \xi \left(\frac{w^{(0)}(\xi)}{v^{(0)}(\xi)} \right)^2 d\xi \\ &\quad - \kappa' \frac{\partial w^{(0)}}{\partial r'} \int_0^{r'} \int_0^{\xi} \frac{\eta \left(\left(v^{(0)}(\eta) \right)^2 - 2 \left(w^{(0)}(\eta) \right)^2 \right)}{\xi \left(v^{(0)}(\xi) \right)^2} d\eta d\xi. \end{aligned} \tag{A.4.15}$$

Similarly, using (A.4.10) we find

$$\begin{aligned} v_{s_1}^{(1)} &= 0 \\ v_{c_1}^{(1)} &= \kappa' r' v^{(0)}(r') + u_{s_1}^{(1)} + r' \frac{\partial u_{s_1}^{(1)}}{\partial r'}. \end{aligned} \tag{A.4.16}$$

The pressure terms follow from (A.4.7). Finally, we see that the first equation of (A.4.6) relates the pressure term $p_0^{(1)}$ to the azimuthal velocity term $v_0^{(1)}$. The axial velocity term $w_0^{(1)}$ does not appear in the equations at this order.

To find the asymptotic form of the velocity field as $r \to \infty$, we use the fact that $v^{(0)} \sim 1/r'$ and $w^{(0)} \sim O(1/r'^n)$ for any integer n. Now the only term that presents difficulty is the double integral that appears in (A.4.14–16). This integral we write as

$$\begin{aligned} &\int_0^{r'} \frac{d\xi}{\xi \left(v^{(0)}(\xi) \right)^2} \int_0^{\xi} \eta \left(\left(v^{(0)}(\eta) \right)^2 - 2 \left(w^{(0)}(\eta) \right)^2 \right) d\eta \\ &= \int_0^{r'} \frac{\xi d\xi}{\left(\xi v^{(0)}(\xi) \right)^2} \left(\int_0^{\xi} \left(\left(\eta v^{(0)}(\eta) \right)^2 - 2 \left(\eta w^{(0)}(\eta) \right)^2 \right) \frac{d\eta}{\eta} - \ln \xi \right) \end{aligned}$$

$$+\int_0^{r'}\frac{\xi d\xi}{\left(\xi v^{(0)}(\xi)\right)^2}\ln\xi$$

$$=\int_0^{r'}\left(\frac{\xi}{\left(\xi v^{(0)}(\xi)\right)^2}-\xi\right)\left(\int_0^{\xi}\left(\left(\eta v^{(0)}(\eta)\right)^2-2\left(\eta w^{(0)}(\eta)\right)^2\right)\frac{d\eta}{\eta}-\ln\xi\right)d\xi$$

$$+\int_0^{r'}\xi\left(\int_0^{\xi}\left(\left(\eta v^{(0)}(\eta)\right)^2-2\left(\eta w^{(0)}(\eta)\right)^2\right)\frac{d\eta}{\eta}-\ln\xi\right)d\xi$$

$$+\int_0^{r'}\left(\frac{\xi}{\left(\xi v^{(0)}(\xi)\right)^2}-\xi\right)\ln\xi\,d\xi+\int_0^{r'}\xi\ln\xi\,d\xi. \qquad (A.4.17)$$

The fourth integral in (A.4.17) clearly integrates yielding

$$\int_0^{r'}\xi\ln\xi\,d\xi=\frac{r'^2}{2}\ln r'-\frac{r'^2}{2}. \qquad (A.4.18)$$

If we examine the first integral, we see that the integrand at worst behaves like a constant, and so we can write

$$\int_0^{r'}\left(\frac{\xi}{\left(\xi v^{(0)}(\xi)\right)^2}-\xi\right)\left(\int_0^{\xi}\left(\left(\eta v^{(0)}(\eta)\right)^2-2\left(\eta w^{(0)}(\eta)\right)^2\right)\frac{d\eta}{\eta}-\ln\xi\right)d\xi$$
$$=O(r'). \qquad (A.4.19)$$

The second integral we write as

$$\int_0^{r'}\xi\left(\int_0^{\xi}\left(\left(\eta v^{(0)}(\eta)\right)^2-2\left(\eta w^{(0)}(\eta)\right)^2\right)\frac{d\eta}{\eta}-\ln\xi\right)d\xi$$

$$=\frac{r'^2}{2}\left(\int_0^{r'}\left(\left(\xi v^{(0)}(\xi)\right)^2-2\left(\xi w^{(0)}(\xi)\right)^2\right)\frac{d\xi}{\xi}-\ln r'\right)$$

$$-\frac{1}{2}\int_0^{r'}\xi^2\left(\frac{\left(\xi v^{(0)}(\xi)\right)^2-2\left(\xi w^{(0)}(\xi)\right)^2}{\xi}-\frac{1}{\xi}\right)d\xi$$

$$=\frac{r'^2}{2}\left(\int_0^{r'}\left(\left(\xi v^{(0)}(\xi)\right)^2-2\left(\xi w^{(0)}(\xi)\right)^2\right)\frac{d\xi}{\xi}-\ln r'\right)+O(r'). \qquad (A.4.20)$$

For the third integral in (A.4.17), we have that the integrand behaves like $\ln\xi$, and so we write

$$\int_0^{r'}\left(\frac{\xi}{\left(\xi v^{(0)}(\xi)\right)^2}-\xi\right)\ln\xi\,d\xi=O(r'\ln r'). \qquad (A.4.21)$$

Using (A.4.18–21) we find that the nonzero components for the order ϵ corrections to the flow field have the following asymptotic forms

$$u_{s_1}^{(1)} \sim -\frac{\kappa'}{2}\left(\lim_{r'\to\infty}\left(\int_0^{r'}\eta\left(v^{(0)}(\eta)\right)^2 d\eta - \ln r'\right) - 2\int_0^{\infty}\eta\left(w^{(0)}(\eta)\right)^2 d\eta\right) - \frac{\kappa'}{2}\ln r' - \frac{\kappa'}{4} \tag{A.4.22}$$

$$v_{c_1}^{(1)} \sim -\frac{\kappa'}{2}\left(\lim_{r'\to\infty}\left(\int_0^{r'}\eta\left(v^{(0)}(\eta)\right)^2 d\eta - \ln r'\right) - 2\int_0^{\infty}\eta\left(w^{(0)}(\eta)\right)^2 d\eta\right) - \frac{\kappa'}{2}\ln r' + \frac{\kappa'}{4} \tag{A.4.23}$$

$$w_{c_1}^{(1)} \sim 0. \tag{A.4.24}$$

A.5 Solution of the order ϵ^2 equations

For the solution of the order ϵ^2 equations, we look for a Fourier decomposition of the flow field in the form

$$\begin{aligned} w^{(2)} &= w_0^{(2)} + w_{c_1}^{(2)}\cos\phi + w_{s_1}^{(2)}\sin\phi + w_{c_2}^{(2)}\cos 2\phi + w_{s_2}^{(2)}\sin 2\phi \\ u^{(2)} &= u_0^{(2)} + u_{c_1}^{(2)}\cos\phi + u_{s_1}^{(2)}\sin\phi + u_{c_2}^{(2)}\cos 2\phi + u_{s_2}^{(2)}\sin 2\phi \\ v^{(2)} &= v_0^{(2)} + v_{c_1}^{(2)}\cos\phi + v_{s_1}^{(2)}\sin\phi + v_{c_2}^{(2)}\cos 2\phi + v_{s_2}^{(2)}\sin 2\phi \\ p^{(2)} &= p_0^{(2)} + p_{c_1}^{(2)}\cos\phi + p_{s_1}^{(2)}\sin\phi + p_{c_2}^{(2)}\cos 2\phi + p_{s_2}^{(2)}\sin 2\phi. \end{aligned} \tag{A.5.1}$$

The axial-momentum equation admits the following Fourier decomposition:

$$\begin{aligned} w^{(0)}\frac{\partial}{\partial s'}\left(\left(\frac{\partial \mathbf{X}'}{\partial t'}\right)^{(0)}\right)\cdot\mathbf{s} + \frac{\partial w^{(0)}}{\partial t'} + u_0^{(2)}\frac{\partial w^{(0)}}{\partial r'} + w^{(0)}\frac{\partial w_0^{(1)}}{\partial s'} &= -\frac{\partial p_0^{(1)}}{\partial s'} \\ -v^{(0)}\frac{\partial \mathbf{s}}{\partial t'}\cdot\mathbf{b} + u_{c_1}^{(2)}\frac{\partial w^{(0)}}{\partial r'} + \frac{v^{(0)}w_{s_1}^{(2)}}{r'} + \frac{v_0^{(1)}w_{s_1}^{(1)}}{r'} + w^{(0)}\frac{\partial w_{c_1}^{(1)}}{\partial s'} &= -\frac{\partial p_{c_1}^{(1)}}{\partial s'} \\ v^{(0)}\frac{\partial \mathbf{s}}{\partial t'}\cdot\mathbf{n} + u_{s_1}^{(1)}\frac{\partial w_0^{(1)}}{\partial r'} + u_{s_1}^{(2)}\frac{\partial w^{(0)}}{\partial r'} - \frac{v^{(0)}}{r'}w_{c_1}^{(2)} - \frac{v_0^{(1)}}{r'}w_{c_1}^{(1)} + \tau w^{(0)}w_{c_1}^{(1)} & \\ + \kappa' v^{(0)}w_0^{(1)} &= -\tau p_{c_1}^{(1)} \\ u_{c_2}^{(2)}\frac{\partial w^{(0)}}{\partial r'} + 2\frac{v^{(0)}}{r'}w_{s_2}^{(2)} &= 0 \\ u_{s_1}^{(1)}\frac{\partial w_{c_1}^{(1)}}{\partial r'} + 2u_{s_2}^{(2)}\frac{\partial w^{(0)}}{\partial r'} - 4\frac{v^{(0)}}{r'}w_{c_2}^{(2)} - \frac{v_{c_1}^{(1)}}{r'}w_{c_1}^{(1)} + \kappa' v_{c_1}^{(1)}w^{(0)} & \\ - \kappa' u_{s_1}^{(1)}w^{(0)} + \kappa' v^{(0)}w_{c_1}^{(1)} + \kappa'^2 r' v^{(0)}w^{(0)} &= 0 \end{aligned} \tag{A.5.2}$$

The terms containing τ come about from taking the derivative of the angle ϕ with respect to s', which equals $-\tau$ according to (A.1.8). As before, we will solve for the radial components of the velocity, and so it follows that we can write the latter four equations of (A.5.2) as equations for the axial components $w_{c_1}^{(2)}$, $w_{s_1}^{(2)}$, $w_{c_2}^{(2)}$ and $w_{s_2}^{(2)}$. Similarly, the radial–momentum equation admits the Fourier decomposition

$$
\begin{aligned}
u_{s_1}^{(1)}\frac{\partial u_{s_1}^{(1)}}{\partial r'} + \frac{u_{s_1}^{(1)}v_{c_1}^{(1)}}{r'} - \frac{\left(v_{c_1}^{(1)}\right)^2}{r'} - \frac{\left(v_0^{(1)}\right)^2}{r'} - 4\frac{v^{(0)}v_0^{(2)}}{r'} + \kappa'^2 r'\left(w^{(0)}\right)^2 \\
+ 2\kappa' w^{(0)} w_{c_1}^{(1)} = \frac{\partial p_0^{(2)}}{\partial r'} \\
2w^{(0)}\frac{\partial}{\partial s'}\left(\left(\frac{\partial \mathbf{X}'}{\partial t'}\right)^{(0)}\right)\cdot\mathbf{n} + \frac{u_{s_1}^{(2)}v^{(0)}}{r'} + \frac{u_{s_1}^{(1)}v_0^{(1)}}{r'} - 2\frac{v_{c_1}^{(1)}v_0^{(1)}}{r'} \\
-2\frac{v_{c_1}^{(2)}v^{(0)}}{r'} + 2\kappa' w^{(0)} w_0^{(1)} - \tau w^{(0)} u_{s_1}^{(1)} = -\frac{\partial p_{c_1}^{(2)}}{\partial r'} \\
2w^{(0)}\frac{\partial}{\partial s'}\left(\left(\frac{\partial \mathbf{X}'}{\partial t'}\right)^{(0)}\right)\cdot\mathbf{b} - \frac{u_{c_1}^{(2)}v^{(0)}}{r'} - 2\frac{v_{s_1}^{(2)}v^{(0)}}{r'} \qquad (A.5.3) \\
+ w^{(0)}\frac{\partial u_{s_1}^{(1)}}{\partial s'} = -\frac{\partial p_{s_1}^{(2)}}{\partial r'} \\
-u_{s_1}^{(1)}\frac{\partial u_{s_1}^{(1)}}{\partial r'} + 4\frac{u_{s_2}^{(2)}v^{(0)}}{r'} + \frac{u_{s_1}^{(1)}v_{c_1}^{(1)}}{r'} - \frac{\left(v_{c_1}^{(1)}\right)^2}{r'} - 4\frac{v^{(0)}v_{c_2}^{(2)}}{r'} \\
+\kappa'^2 r'\left(w^{(0)}\right)^2 + 2\kappa' w^{(0)} w_{c_1}^{(1)} = -2\frac{\partial p_{c_2}^{(2)}}{\partial r'} \\
-2\frac{u_{c_2}^{(2)}v^{(0)}}{r'} - 2\frac{v^{(0)}v_{s_2}^{(2)}}{r'} = -\frac{\partial p_{s_2}^{(2)}}{\partial r'}.
\end{aligned}
$$

The Fourier decomposition of the azimuthal–momentum equation yields

$$
\begin{aligned}
&\frac{\partial v^{(0)}}{\partial t'} + u_0^{(2)}\frac{\partial v^{(0)}}{\partial r'} + \frac{u_0^{(2)}v^{(0)}}{r'} + w^{(0)}\frac{\partial v_0^{(1)}}{\partial s'} = 0 \\
&2w^{(0)}\frac{\partial}{\partial s'}\left(\left(\frac{\partial \mathbf{X}'}{\partial t'}\right)^{(0)}\right)\cdot\mathbf{b} + u_{c_1}^{(2)}\frac{\partial v^{(0)}}{\partial r'} + \frac{v^{(0)}v_{s_1}^{(2)}}{r'} + \frac{v^{(0)}u_{c_1}^{(2)}}{r'} \\
&\qquad + w^{(0)}\frac{\partial v_{c_1}^{(1)}}{\partial s'} = -\frac{p_{s_1}^{(2)}}{r'} \\
&-2w^{(0)}\frac{\partial}{\partial s'}\left(\left(\frac{\partial \mathbf{X}'}{\partial t'}\right)^{(0)}\right)\cdot\mathbf{n} + u_{s_1}^{(1)}\frac{\partial v_0^{(1)}}{\partial r'} + u_{s_1}^{(2)}\frac{\partial v^{(0)}}{\partial r'} - \frac{v^{(0)}v_{c_1}^{(2)}}{r'} \\
&+\frac{v^{(0)}u_{s_1}^{(2)}}{r'} - \frac{v_0^{(1)}v_{c_1}^{(1)}}{r'} + \frac{v_0^{(1)}u_{s_1}^{(1)}}{r'} - 2\kappa' w^{(0)}w_0^{(1)} + \tau w^{(0)}v_{c_1}^{(1)} = \frac{p_{c_1}^{(2)}}{r'} \\
&\qquad u_{c_2}^{(2)}\frac{\partial v^{(0)}}{\partial r'} + 2\frac{v^{(0)}v_{s_2}^{(2)}}{r'} + \frac{v^{(0)}u_{c_2}^{(2)}}{r'} = -2\frac{p_{s_2}^{(2)}}{r'} \\
&u_{s_1}^{(1)}\frac{\partial v_{c_1}^{(1)}}{\partial r'} + 2u_{s_2}^{(2)}\frac{\partial v^{(0)}}{\partial r'} - 4\frac{v^{(0)}v_{c_2}^{(2)}}{r'} + 2\frac{v^{(0)}u_{s_2}^{(2)}}{r'} - \frac{\left(v_{c_1}^{(1)}\right)^2}{r'} \\
&\qquad + \frac{u_{s_1}^{(1)}v_{c_1}^{(1)}}{r'} - 2\kappa' w^{(0)}w_{c_1}^{(1)} - \kappa'^2 r'\left(w^{(0)}\right)^2 = 4\frac{p_{c_2}^{(2)}}{r'}.
\end{aligned}
\tag{A.5.4}
$$

Finally, the Fourier decomposition of the continuity equation yields

$$
\begin{aligned}
&\frac{\partial}{\partial r'}\left(r'u_0^{(2)}\right) + r'\frac{\partial w_0^{(1)}}{\partial s'} + r'\frac{\partial}{\partial s'}\left(\left(\frac{\partial \mathbf{X}'}{\partial t'}\right)^{(0)}\right)\cdot\mathbf{s} = 0 \\
&\qquad \frac{\partial}{\partial r'}\left(r'u_{c_1}^{(2)}\right) + v_{s_1}^{(2)} + r'\frac{\partial w_{c_1}^{(1)}}{\partial s'} = 0 \\
&\qquad \frac{\partial}{\partial r'}\left(r'u_{s_1}^{(2)}\right) - v_{c_1}^{(2)} + \tau r' w_{c_1}^{(1)} = 0 \\
&\qquad \frac{\partial}{\partial r'}\left(r'u_{c_2}^{(2)}\right) + 2v_{s_2}^{(2)} = 0 \\
&2\frac{\partial}{\partial r'}\left(r'u_{s_2}^{(2)}\right) - \kappa'\frac{\partial}{\partial}\left(r'^2 u_{s_1}^{(1)}\right) - 4v_{c_2}^{(2)} + \kappa' r' v_{c_1}^{(1)} = 0.
\end{aligned}
\tag{A.5.5}
$$

For convenience, we adopt the following the shorthand expressions:

$$
S = \frac{\partial}{\partial s'}\left(\left(\frac{\partial \mathbf{X}'}{\partial t'}\right)^{(0)}\right)\cdot\mathbf{s} \tag{A.5.6}
$$

$$
N = \frac{\partial}{\partial s'}\left(\left(\frac{\partial \mathbf{X}'}{\partial t'}\right)^{(0)}\right)\cdot\mathbf{n} \tag{A.5.7}
$$

$$
B = \frac{\partial}{\partial s'}\left(\left(\frac{\partial \mathbf{X}'}{\partial t'}\right)^{(0)}\right)\cdot\mathbf{b} \tag{A.5.8}
$$

where S, N and B depend only on s'. Solving for the radial components $u_{c_1}^{(2)}$ and $u_{s_1}^{(2)}$, in the same way that we solved for their first order counterparts, yields the complicated expressions

$$\begin{aligned} u_{c_1}^{(2)} = & 2B\frac{v^{(0)}}{r'}\int_0^{r'}\frac{d\xi}{\xi\left(v^{(0)}(\xi)\right)^2}\int_0^{\xi}\eta^2\frac{\partial w^{(0)}}{\partial\eta}d\eta \\ & - 2\frac{v^{(0)}}{r'}\frac{\partial\kappa'}{\partial s'}\int_0^{r'}\frac{d\xi}{\xi\left(v^{(0)}(\xi)\right)^2}\int_0^{\xi}\eta^2 v^{(0)}w^{(0)}d\eta \\ & - \frac{v^{(0)}}{r'}\int_0^{r'}\frac{d\xi}{\xi\left(v^{(0)}(\xi)\right)^2}\int_0^{\xi}\frac{\partial}{\partial\eta}\left(\eta^3\frac{\partial w^{(0)}}{\partial\eta}\right)\frac{\partial u_{s_1}^{(1)}}{\partial s'}d\eta \\ & + \frac{v^{(0)}}{r'}\int_0^{r'}\frac{d\xi}{\xi\left(v^{(0)}(\xi)\right)^2}\int_0^{\xi}w^{(0)}\frac{\partial}{\partial\eta}\left(\eta^3\frac{\partial}{\partial\eta}\left(\frac{\partial u_{s_1}^{(1)}}{\partial s'}\right)\right)d\eta \end{aligned} \quad (A.5.9)$$

and

$$\begin{aligned} u_{s_1}^{(2)} = & -2N\frac{v^{(0)}}{r'}\int_0^{r'}\frac{d\xi}{\xi\left(v^{(0)}(\xi)\right)^2}\int_0^{\xi}\eta^2\frac{\partial w^{(0)}}{\partial\eta}d\eta \\ & - 2\kappa'\tau'\frac{v^{(0)}}{r'}\int_0^{r'}\frac{d\xi}{\xi\left(v^{(0)}(\xi)\right)^2}\int_0^{\xi}\eta^2 v^{(0)}w^{(0)}d\eta \\ & - 2\kappa'\frac{v^{(0)}}{r'}\int_0^{r'}\frac{d\xi}{\xi\left(v^{(0)}(\xi)\right)^2}\int_0^{\xi}\eta^2\frac{\partial}{\partial\eta}\left(w^{(0)}w_0^{(1)}\right)d\eta \\ & - \tau'\frac{v^{(0)}}{r'}\int_0^{r'}\frac{d\xi}{\xi\left(v^{(0)}(\xi)\right)^2}\int_0^{\xi}\frac{\partial}{\partial\eta}\left(\eta^3\frac{\partial w^{(0)}}{\partial\eta}\right)\frac{\partial u_{s_1}^{(1)}}{\partial s'}d\eta \\ & + \tau'\frac{v^{(0)}}{r'}\int_0^{r'}\frac{d\xi}{\xi\left(v^{(0)}(\xi)\right)^2}\int_0^{\xi}w^{(0)}\frac{\partial}{\partial\eta}\left(\eta^3\frac{\partial}{\partial\eta}\left(\frac{\partial u_{s_1}^{(1)}}{\partial s'}\right)\right)d\eta. \end{aligned} \quad (A.5.10)$$

The corresponding terms for $v_{c_1}^{(1)}$, $v_{s_1}^{(1)}$, etc., follow from the equations.

Repeating the procedure for the terms $u_{c_2}^{(2)}$ and $u_{s_2}^{(2)}$ yields the following pair of differential equations:

$$r'v^{(0)}\frac{\partial^2 u_{c_2}^{(2)}}{\partial r'^2} + 3v^{(0)}\frac{\partial u_{c_2}^{(2)}}{\partial r'} - \left(r'\frac{\partial^2 v^{(0)}}{\partial r'^2} + \frac{\partial v^{(0)}}{\partial r'} + \frac{2v^{(0)}}{r'}\right)u_{c_2}^{(2)} = 0 \quad (A.5.11)$$

$$\begin{aligned} & r'v^{(0)}\frac{\partial^2 u_{s_2}^{(2)}}{\partial r'^2} + 3v^{(0)}\frac{\partial u_{s_2}^{(2)}}{\partial r'} - \left(r'\frac{\partial^2 v^{(0)}}{\partial r'^2} + \frac{\partial v^{(0)}}{\partial r'} + \frac{2v^{(0)}}{r'}\right)u_{s_2}^{(2)} \\ & \qquad = F\left[v^{(0)}(r'), w^{(0)}(r')\right] \end{aligned} \quad (A.5.12)$$

where the right–hand side of (A.5.12) is a complicated nonlinear functional of the leading order core velocities given by

$$
\begin{aligned}
F\left[v^{(0)}(r'),w^{(0)}(r')\right] = & \\
& \frac{2u_{s_1}^{(1)}}{r'v^{(0)}}\left(\frac{3}{2}\kappa' v^{(0)}+\frac{\kappa' r'}{2}\frac{\partial v^{(0)}}{\partial r'}+\frac{r'}{4}\left(\frac{\partial^2 v_{c_1}^{(1)}}{\partial r'^2}+\frac{2}{r'}\frac{\partial v_{c_1}^{(1)}}{\partial r'}+\frac{2v_{c_1}^{(1)}}{r'^2}\right)\right) \\
& +\frac{2}{v^{(0)}}\frac{\partial u_{s_1}^{(1)}}{\partial r'}\left(\frac{3}{2}\kappa' v^{(0)}+\frac{\kappa' r'}{4}\frac{\partial v^{(0)}}{\partial r'}+\frac{1}{4}\left(\frac{\partial v_{c_1}^{(1)}}{\partial r'}+\frac{v_{c_1}^{(1)}}{r'}\right)\right) \\
& -\frac{2v_{c_1}^{(1)}}{r'v^{(0)}}\left(\frac{3}{2}\kappa' v^{(0)}+\frac{\kappa' r'}{2}\frac{\partial v^{(0)}}{\partial r'}+\frac{1}{2}\left(\frac{\partial v_{c_1}^{(1)}}{\partial r'}+\frac{v_{c_1}^{(1)}}{r'}\right)\right) \\
& -\frac{u_{s_1}^{(1)}}{r'v^{(0)}}\frac{\partial u_{s_1}^{(1)}}{\partial r'}-\kappa'\frac{\partial v_{c_1}^{(1)}}{\partial r'}+\frac{\kappa' r'}{2}\frac{\partial^2 u_{s_1}^{(1)}}{\partial r'^2} \\
& -\frac{\kappa' w_{c_1}^{(1)}}{v^{(0)}}\frac{\partial w^{(0)}}{\partial r'}-\frac{\kappa' w^{(0)}}{v^{(0)}}\frac{\partial w_{c_1}^{(1)}}{\partial r'}-\frac{\kappa'^2 r' w^{(0)}}{v^{(0)}}\frac{\partial w^{(0)}}{\partial r'}+\frac{\kappa' w^{(0)}w_{c_1}^{(1)}}{r'v^{(0)}}. \qquad (A.5.13)
\end{aligned}
$$

Unfortunately, the differential operator appearing on the left–hand side of (A.5.11–12) has no simple homogeneous solutions. (Recall that the differential operator appearing on the left–hand side of (A.4.11–12) had $v^{(0)}/r'$ as an homogeneous solution, from which we were able to construct a general solution.) If we examine the operator, we find that it has regular singular points at the origin and at infinity, all remaining points are ordinary points. Furthermore, for the point at the origin there is a regular solution, $u_0^r(r')$, which vanishes at the origin and a singular solution $u_0^i(r')$. For the point at infinity, there is a regular solution $u_\infty^r(r') \sim 1/r'^3$ and a singular solution $u_\infty^i(r') \sim r'$. If we look for a solution proportional to $u_\infty^r(r')$, then we obtain solutions of the form

$$
u_{c_2}^{(2)} = \alpha_{c_2}^{(2)} u_\infty^r(r') \int_0^{r'} \frac{d\xi}{\xi^3 \left(u_\infty^r(\xi)\right)^2} + \beta_{c_2}^{(2)} u_\infty^r(r') \qquad (A.5.14)
$$

$$
\begin{aligned}
u_{s_2}^{(2)} = & \alpha_{s_2}^{(2)} u_\infty^r(r') \int_0^{r'} \frac{d\xi}{\xi^3 \left(u_\infty^r(\xi)\right)^2} + \beta_{s_2}^{(2)} u_\infty^r(r') \\
& + u_\infty^r(r') \int_0^{r'} \frac{d\xi}{\xi^3 \left(u_\infty^r(\xi)\right)^2} \int_0^{\xi} \eta^3 u_\infty^r(\eta) F\left[v^{(0)}(\eta),w^{(0)}(\eta)\right] d\eta. \qquad (A.5.15)
\end{aligned}
$$

Alternatively, we could use the fact that these components of the velocity must vanish as $r' \to 0$ to write the solutions as

$$
u_{c_2}^{(2)} = \gamma_{c_2}^{(2)} u_0^r(r') \qquad (A.5.16)
$$

$$u^{(2)}_{s_2} = \gamma^{(2)}_{s_2} u^r_0(r') + u^r_\infty(r') \int_0^{r'} \frac{d\xi}{\xi^3 \left(u^r_\infty(\xi)\right)^2} \int_0^{\xi} \eta^3 u^r_\infty(\eta) F\left[v^{(0)}(\eta), w^{(0)}(\eta)\right] d\eta \quad (A.5.17)$$

where $\gamma^{(2)}_{c_2}$ and $\gamma^{(2)}_{s_2}$ are arbitrary. For a pair of constants b and c, not both zero, we must have

$$u^r_0(r') = b u^i_\infty(r') + c u^r_\infty(r'). \quad (A.5.18)$$

The constants b and c depend on the form of the leading order core velocity $v^{(0)}$, since it is this velocity that determines the type of homogeneous solutions admitted by the differential operator on the left–hand side of (A.5.11–12).

Using (A.5.2–5) we can deduce the solutions for $v^{(2)}_{c_2}$, $v^{(2)}_{s_2}$, etc., but since we will not explicitly use these terms, we will not carry out this step. However, we do require the asymptotic forms of the components $u^{(2)}_{c_2}$ and $u^{(2)}_{s_2}$. To obtain these expressions we require the asymptotic form of the nonlinear functional, which is

$$F\left[v^{(0)}(r'), w^{(0)}(r')\right] \sim -\frac{3}{2}\frac{\kappa'^2}{r'} \quad (A.5.19)$$

as $r' \to \infty$. Using this fact we deduce that the asymptotic forms of (A.5.16–17) are

$$u^{(2)}_{c_2} \sim \gamma^{(2)}_{c_2} b r' \quad (A.5.20)$$

$$u^{(2)}_{s_2} \sim \gamma^{(2)}_{s_2} b r' - \frac{3\kappa'^2}{8} r' \ln r' + \left(\mathcal{A} + \frac{3\kappa'^2}{8}\right)\frac{r'}{4} \quad (A.5.21)$$

where

$$\mathcal{A} = \lim_{\zeta \to \infty} \left\{ \int_0^{\zeta} \eta^3 u^r_\infty(\eta) F\left[v^{(0)}(\eta), w^{(0)}(\eta)\right] d\eta - \frac{3}{2}\ln(\zeta) \right\}. \quad (A.5.22)$$

The dependence of the solutions on $u^r_\infty(r')$ has dropped out of (A.5.20–21) since in the asymptotic limit $u^r_\infty(r')$ will be dominated by the first order terms in the asymptotic expansion of $u^i_\infty(r')$. For reference we include the asymptotic forms of $u^{(2)}_{c_1}$ and $u^{(2)}_{s_1}$; these are by

$$u^{(2)}_{c_1} \sim -2B \int_0^{\infty} \eta w^{(0)} d\eta$$

$$
\begin{aligned}
&- \frac{\partial \kappa'}{\partial s'} \int_0^\infty \eta^2 v^{(0)} w^{(0)} d\eta \\
&- \frac{1}{2} \int_0^\infty \frac{\partial}{\partial \eta} \left(\eta^3 \frac{\partial w^{(0)}}{\partial \eta} \right) \frac{\partial u_{s_1}^{(1)}}{\partial s'} d\eta \\
&+ \frac{1}{2} \int_0^\infty w^{(0)} \frac{\partial}{\partial \eta} \left(\eta^3 \frac{\partial}{\partial \eta} \left(\frac{\partial u_{s_1}^{(1)}}{\partial s'} \right) \right) d\eta
\end{aligned} \tag{A.5.23}
$$

and

$$
\begin{aligned}
u_{s_1}^{(2)} \sim\ & 2N \int_0^\infty \eta w^{(0)} d\eta \\
&- \kappa' \tau' \int_0^\infty \eta^2 v^{(0)} w^{(0)} d\eta \\
&+ 2\kappa' \int_0^\infty \eta w^{(0)} w_0^{(1)} d\eta \\
&- \frac{1}{2} \tau' \int_0^\infty \frac{\partial}{\partial \eta} \left(\eta^3 \frac{\partial w^{(0)}}{\partial \eta} \right) \frac{\partial u_{s_1}^{(1)}}{\partial s'} d\eta \\
&+ \frac{1}{2} \tau' \int_0^\infty w^{(0)} \frac{\partial}{\partial \eta} \left(\eta^3 \frac{\partial}{\partial \eta} \left(\frac{\partial u_{s_1}^{(1)}}{\partial s'} \right) \right) d\eta.
\end{aligned} \tag{A.5.24}
$$

APPENDIX B

FLOW DESCRIPTION IN THE OUTER REGION

Dominant terms in the expansion of the Biot–Savart integral

In this appendix we determine the behavior of the Biot–Savart integral, for the external velocity field,

$$\mathbf{u}(\mathbf{x},t) = \frac{\Gamma}{4\pi}\oint \mathbf{s}' \times \frac{(\mathbf{x}-\mathbf{X}(s',t))}{|\mathbf{x}-\mathbf{X}(s',t)|^3} ds', \qquad (B.1)$$

in the limit where $|\mathbf{x}-\mathbf{X}(s,t)| \to 0$. It is assumed that the point $\mathbf{x}$ is close enough to the filament that there is a unique closest point $\mathbf{X}(s,t)$. We adopt the curvilinear polar coordinate system introduced in appendix A.1 and write

$$\mathbf{x}(s,r,\theta) = \mathbf{X}(s,t) + r\mathbf{e}_r(s,\theta). \qquad (B.2)$$

In (B.2), $\mathbf{X}$ is explicitly shown to be a function of time. The coordinates s, r and θ also are functions of time, but this dependence has been suppressed for convenience. To find the limiting behavior of (B.1) as $r \to 0$, we consider a Taylor series expansion of $\mathbf{X}(s',t)$ about the point $s' = s$. The first few terms in this expansion are

$$\mathbf{X}(s',t) = \mathbf{X}(s,t) + (s'-s)\,\mathbf{s} + \frac{1}{2}(s'-s)^2\,\kappa\mathbf{n} + \frac{1}{6}(s'-s)^3\left(-\kappa^2\mathbf{s} + \kappa_s\mathbf{n} + \kappa\tau\mathbf{b}\right) + O\left((s'-s)^4\right) \qquad (B.3)$$

where $\kappa_s = \partial\kappa/\partial s$. Accordingly, we have

$$\mathbf{x}-\mathbf{X}(s',t) = r\cos\phi\mathbf{n} + r\sin\phi\mathbf{b} - (s'-s)\,\mathbf{s} - \frac{1}{2}(s'-s)^2\,\kappa\mathbf{n} - \frac{1}{6}(s'-s)^3\left(-\kappa^2\mathbf{s} + \kappa_s\mathbf{n} + \kappa\tau\mathbf{b}\right) + O\left((s'-s)^4\right) \qquad (B.4)$$

where we have used (A.1.2). We also have

$$\mathbf{s}' = \mathbf{s} + (s'-s)\,\kappa\mathbf{n} + \frac{1}{2}(s'-s)^2\left(-\kappa^2\mathbf{s} + \kappa_s\mathbf{n} + \kappa\tau\mathbf{b}\right) + O\left((s'-s)^3\right). \qquad (B.5)$$

The remaining part of the integrand is the denominator; this is obtained by taking the inner product of (B.4) with itself, yielding

$$|\mathbf{x}-\mathbf{X}(s',t)|^{-3} = \Big(r^2+(s'-s)^2-\frac{\kappa^2}{12}(s'-s)^4 - 2r\cos\phi\left(\frac{\kappa}{2}(s'-s)^2+\frac{\kappa_s}{6}(s'-s)^3\right) - 2r\sin\phi\left(\frac{\kappa\tau}{6}(s'-s)^3\right)+O\left((s'-s)^5\right)\Big)^{-3/2}. \quad (B.6)$$

If we set

$$\mathcal{D}^2 = \rho^2+(s'-s)^2 \quad (B.7)$$

then (B.6) can be expanded to yield

$$|\mathbf{x}-\mathbf{X}(s',t)|^{-3} = \mathcal{D}^{-3}+\frac{1}{8}\kappa^2(s'-s)^4\mathcal{D}^{-5}+\frac{3}{2}r\kappa\cos\phi\,(s'-s)^2\mathcal{D}^{-5} + \frac{1}{2}r\kappa_s\cos\phi\,(s'-s)^3\mathcal{D}^{-5}+\frac{1}{2}r\kappa\tau\sin\phi\,(s'-s)^3\mathcal{D}^{-5} + \frac{15}{8}r^2\kappa^2\cos^2\phi\,(s'-s)^4\mathcal{D}^{-7}+O\left((s'-s)^5\mathcal{D}^{-5}\right). \quad (B.8)$$

Assembling the integrand we obtain as a first step the cross–product

$$\mathbf{s}'\times(\mathbf{x}-\mathbf{X}(s',t)) = r\mathbf{e}_\theta+r\kappa\sin\phi\,(s'-s)\,\mathbf{s} + \frac{1}{2}\kappa(s'-s)^2\,\mathbf{b}-\frac{1}{2}r\kappa^2(s'-s)^2\,\mathbf{e}_\theta - \frac{1}{2}(r\kappa\tau\cos\phi-r\kappa_s\sin\phi)(s'-s)^2\,\mathbf{s} + O\left((s'-s)^2\right). \quad (B.9)$$

The effect of the denominator can be taken into account by multiplying by the right–hand side of (B.8). This leads to the approximation of the Biot–Savart integrand, using the Taylor series for the filament curve,

$$\left[\mathbf{s}'\times\frac{(\mathbf{x}-\mathbf{X}(s',t))}{|\mathbf{x}-\mathbf{X}(s',t)|^3}\right]_{TS} = \Big(r\mathbf{e}_\theta+r\kappa\sin\phi\,(s'-s)\,\mathbf{s} + \frac{1}{2}\kappa(s'-s)^2\,\mathbf{b}-\frac{1}{2}r\kappa^2(s'-s)^2\,\mathbf{e}_\theta$$

$$
\begin{aligned}
&- \frac{1}{2}\left(r\kappa\tau\cos\phi - r\kappa_s\sin\phi\right)\left(s'-s\right)^2\mathbf{s}\Big) \\
&\cdot\Big(\mathcal{D}^{-3} + \frac{1}{8}\kappa^2\left(s'-s\right)^4\mathcal{D}^{-5} + \frac{3}{2}r\kappa\cos\phi\left(s'-s\right)^2\mathcal{D}^{-5} \\
&+ \frac{1}{2}r\kappa_s\cos\phi\left(s'-s\right)^3\mathcal{D}^{-5} + \frac{1}{2}r\kappa\tau\sin\phi\left(s'-s\right)^3\mathcal{D}^{-5} \\
&+ \frac{15}{8}r^2\kappa^2\cos^2\phi\left(s'-s\right)^4\mathcal{D}^{-7}\Big). \qquad (B.10)
\end{aligned}
$$

We integrate (B.10) with respect to s' from $s-L$ to $s+L$, where L is a length characteristic of the axial dimensions of the filament, i.e., if ρ is the radius of curvature of the filament, then $L = O(\rho)$. In the limit where $r/L \to 0$, we find

$$
\begin{aligned}
&\int_{s-L}^{s+L}\left[\mathbf{s}'\times\frac{(\mathbf{x}-\mathbf{X}(s',t))}{|\mathbf{x}-\mathbf{X}(s',t)|^3}\right]_{TS}ds' \sim \\
&\quad\frac{2}{r}\mathbf{e}_\theta + \frac{1}{\rho}\left\{\left[\ln\left(\frac{2L}{r}\right)-1\right]\sin(\phi)\mathbf{e}_r + \left[\ln\left(\frac{2L}{r}\right)\right]\cos(\phi)\mathbf{e}_\theta\right\} \\
&\quad+\frac{3r}{2\rho^2}\left\{\left[\ln\left(\frac{2L}{r}\right)-\frac{4}{3}\right]\sin(2\phi)\mathbf{e}_r + \left[\ln\left(\frac{2L}{r}\right)-\frac{5}{6}\right]\cos(2\phi)\mathbf{e}_\theta + \frac{1}{18}\mathbf{e}_\theta\right\}. \qquad (B.11)
\end{aligned}
$$

Consequently, the Biot–Savart integral can be written as

$$
\begin{aligned}
&\frac{\Gamma}{4\pi}\oint\mathbf{s}'\times\frac{(\mathbf{x}-\mathbf{X}(s',t))}{|\mathbf{x}-\mathbf{X}(s',t)|^3}ds' \sim \\
&\quad\frac{\Gamma}{2\pi r}\mathbf{e}_\theta + \frac{\Gamma}{4\pi\rho}\left\{\left[\ln\left(\frac{2L}{r}\right)-1\right]\sin(\phi)\mathbf{e}_r + \left[\ln\left(\frac{2L}{r}\right)\right]\cos(\phi)\mathbf{e}_\theta\right\} \\
&\quad+\frac{3\Gamma r}{8\pi\rho^2}\left\{\left[\ln\left(\frac{2L}{r}\right)-\frac{4}{3}\right]\sin(2\phi)\mathbf{e}_r + \left[\ln\left(\frac{2L}{r}\right)-\frac{5}{6}\right]\cos(2\phi)\mathbf{e}_\theta + \frac{1}{18}\mathbf{e}_\theta\right\} \\
&\quad+\mathbf{Q} \qquad (B.12)
\end{aligned}
$$

where $\mathbf{Q}$ is

$$
\mathbf{Q} = \frac{\Gamma}{4\pi}\oint\left(\mathbf{s}'\times\frac{(\mathbf{x}-\mathbf{X}(s',t))}{|\mathbf{x}-\mathbf{X}(s',t)|^3} - \left[\mathbf{s}'\times\frac{(\mathbf{x}-\mathbf{X}(s',t))}{|\mathbf{x}-\mathbf{X}(s',t)|^3}\right]_{TS}\mathcal{H}\left(1-\frac{|s'-s|}{L}\right)\right)ds' \qquad (B.13)
$$

where $\mathcal{H}$ is the Heaviside step function. Equations (B.12–13) provide a convenient representation for the Biot–Savart integral since the singular terms have effectively

been removed from the integrand. However, we should note that the (B.12) is really independent of L (as long as it scales like the radius of curvature) since the terms explicitly containing L, in (B.12), are exactly balanced by equal and opposite terms in $\mathbf{Q}$.

APPENDIX C

ULTRA–THIN TRAILING VORTICES

Estimation of the core radius for an ultra–thin trailing vortex

In chapter 2 we claimed that a vortex filament belonging to the Klein and Majda regime was necessarily an ultra–thin filament. This claim was based on the fact that filaments belonging to the Klein and Majda regime satisfied equation (2.1.5), which forces the core radius of the filament to be exponentially small. In terms of the dimensional quantities, introduced in (2.1.12), equation (2.1.5) can be written as

$$\epsilon^2 \left[\ln\left(\frac{2\Lambda}{a}\right) + C \right] = 1, \qquad (C.1)$$

where Λ is the wavelength of the perturbation to the filament, a is the core radius and C contains information about the core structure (see equation (2.1.6) or its dimensional counterpart (2.1.15)). The parameter C is an $O(1)$ quantity and for the sake of convenience we will take $C = -1/4$, which corresponds to the value for a filament with uniform vorticity in the core and having no axial velocity in the core. Inverting (C.1) we obtain the following expression for the core radius

$$a = 2\Lambda \exp\left(-\frac{1}{\epsilon^2} - \frac{1}{4}\right), \qquad (C.2)$$

which gives the exponential behavior of a in terms of Λ and ϵ.

Any waves present on a trailing vortex are most likely to be the unstable waves predicted by Crow (1970). Crow's results suggest that such waves have wavelengths on the order of $8.6b$, where b is the seperation of the vortices and is on the order of the wingspan of the aircraft. If we take $b = 100m$, it follows that for $\epsilon \leq 0.2$ we must have $a \leq 1.86 \times 10^{-8} m$. Since the mean free path in air is $6.5 \times 10^{-8} m$ (at standard atmospheric conditions), it consequently follows that an ultra–thin filament has a core radius less than the mean free path in air at standard atmospheric conditions.

APPENDIX D

THE ROTATION RATE OF A HELICAL FILAMENT OF LARGE PITCH

High order computation of the rotation rate of a helical filament of large pitch using the Moore–Saffman equations

In this appendix we consider the application of the Moore–Saffman equations to compute the motion of a helical filament of large pitch. We assume that in the core of the filament there is no axial flow and the vorticity is uniform. For such a filament with centerline $\mathbf{X}$, core radius a and circulation Γ, the Moore–Saffman equation (1.2.2) reduces to

$$\frac{\partial \mathbf{X}}{\partial t} = \mathbf{Q}_{MS} + \frac{\Gamma}{4\pi\rho}\left[\ln(\frac{8\rho}{a}) - \frac{1}{4}\right]\hat{\mathbf{b}}. \qquad (D.1)$$

In (D.1), $\mathbf{Q}_{MS}$ is the desingularized Biot–Savart integral

$$\mathbf{Q}_{MS} = \frac{\Gamma}{4\pi}\left\{\int \frac{\hat{\mathbf{s}}' \times (\mathbf{X} - \mathbf{X}')}{|\mathbf{X} - \mathbf{X}'|^3} ds' - \int \frac{\hat{\mathbf{s}}_o \times (\mathbf{X} - \mathbf{X}_o)}{|\mathbf{X} - \mathbf{X}_o|^3} ds_o\right\}, \qquad (D.2)$$

where the first integral refers to the filament itself and the second, to a ring type filament coinciding with the osculating circle to the curve $\mathbf{X}$ at the current position. Of the remaining quantities in (D.1–2), $\hat{\mathbf{b}}$ is the unit binormal, $\hat{\mathbf{s}}$ is the unit tangent and ρ is the radius of curvature, all of which are geometrical quantities associated with $\mathbf{X}$. The quantities with subscript o refer to the osculating circle which has radius ρ. We note that the absence of axial flow in the core means that the Moore–Saffman equations are the same as the cut–off equation. In fact, it would be a little less involved to compute the rotation rate using the cut–off equation, but since we extend the result derived in Moore and Saffman's paper, we will use the same equations as they use. The centerline of the filament we take to be given by

$$\mathbf{X} = D\left(\mathbf{i}\cos\theta + \mathbf{j}\sin\theta - \mathbf{k}(\theta - \Omega t)/\gamma\right), \qquad (D.3)$$

where θ is an angular variable ranging from $-\infty$ to ∞. The pitch of this helix is $1/\gamma$, so for large pitch we require $\gamma \ll 1$. Using (D.3) in the Frenet–Serret formulae yields the orthonormal triad of vectors $\hat{\mathbf{s}}$, $\hat{\mathbf{n}}$ and $\hat{\mathbf{b}}$ which we now compute

$$\begin{aligned}\hat{\mathbf{s}} &= \frac{\partial \mathbf{X}}{\partial \theta} \Big/ \left|\frac{\partial \mathbf{X}}{\partial \theta}\right| \\ &= \frac{\gamma}{\sqrt{1+\gamma^2}} \left(-\mathbf{i}\sin\theta + \mathbf{j}\cos\theta - \mathbf{k}\frac{1}{\gamma}\right), \end{aligned} \tag{D.4}$$

with

$$\begin{aligned}\frac{ds}{d\theta} &= \left|\frac{\partial \mathbf{X}}{\partial \theta}\right| \\ &= \frac{D}{\gamma}\sqrt{1+\gamma^2}. \end{aligned} \tag{D.5}$$

It follows that

$$\begin{aligned}\frac{1}{\rho}\hat{\mathbf{n}} &= \frac{\partial \hat{\mathbf{s}}}{\partial s} \\ &= -\frac{\gamma^2}{D\left(1+\gamma^2\right)}\left(\mathbf{i}\cos\theta + \mathbf{j}\sin\theta\right), \end{aligned} \tag{D.6}$$

$$\begin{aligned}\hat{\mathbf{b}} &= \hat{\mathbf{s}} \times \hat{\mathbf{n}} \\ &= \frac{1}{\sqrt{1+\gamma^2}}\left(-\mathbf{i}\sin\theta + \mathbf{j}\cos\theta + \mathbf{k}\gamma\right). \end{aligned} \tag{D.7}$$

Without loss of generality we may evaluate the induced velocity at the point corresponding to $\theta = 0$ and time $t = 0$. At this point the osculating circle lies in the plane normal to the binormal, which according to (D.7) reduces to

$$\hat{\mathbf{b}} = \frac{1}{\sqrt{1+\gamma^2}}\left(\mathbf{j} + \mathbf{k}\gamma\right). \tag{D.8}$$

The radius of the circle equals the radius of curvature at the point corresponding to $\theta = 0$. This is easily read off from (D.6)

$$\rho = \frac{D\left(1+\gamma^2\right)}{\gamma^2}. \tag{D.9}$$

Consequently, the equation for the osculating circle is

$$\mathbf{X}_\circ = \mathbf{i}(1-\rho) + \rho\left(\mathbf{i}\cos\phi + \left(\hat{\mathbf{b}} \times \mathbf{i}\right)\sin\phi\right), \tag{D.10}$$

where ϕ is an angular variable ranging from $-\pi$ to π. To evaluate the desingularized velocity $\mathbf{Q}_{MS}$, we employ a limiting process whereby an interval about the point $\theta = 0$ is removed from the range of integration, and then finally the length of the interval is allowed to go to zero. For small values $\theta = \theta_0$ and $\phi = \phi_0$, we find the following inter–relationship (by considering how the arc–length is related to the angular variables for both curves)

$$\phi_0 \approx \theta_0 \left(\frac{\gamma}{\sqrt{1+\gamma^2}} \right). \tag{D.11}$$

Using this limiting process we write the induced velocity at $\theta = 0$ as

$$\mathbf{Q}_{MS} = \frac{\Gamma}{4\pi} \lim_{\theta_0, \phi_0 \to 0} \left[\left(\int_{-\infty}^{-\theta_0} + \int_{\theta_0}^{\infty} \right) \frac{\hat{\mathbf{s}}' \times (\mathbf{X} - \mathbf{X}')}{|\mathbf{X} - \mathbf{X}'|^3} ds' - \left(\int_{-\pi}^{-\phi_0} + \int_{\phi_0}^{\pi} \right) \frac{\hat{\mathbf{s}}_\circ \times (\mathbf{X} - \mathbf{X}_\circ)}{|\mathbf{X} - \mathbf{X}_\circ|^3} ds_\circ \right]. \tag{D.12}$$

Using the fact that γ is small allows us to write

$$\left(\int_{-\infty}^{-\theta_0} + \int_{\theta_0}^{\infty} \right) \frac{\hat{\mathbf{s}}' \times (\mathbf{X} - \mathbf{X}')}{|\mathbf{X} - \mathbf{X}'|^3} ds' = \frac{2\gamma^2}{D} \int_{\theta_0}^{\infty} \left[\mathbf{j} \left(J_0(\theta) - 3\gamma^2 J_1(\theta) \right) + \mathbf{k}\gamma \left(K_0(\theta) - 3\gamma^2 K_1(\theta) \right) + O(\gamma^4) \right] d\theta, \tag{D.13}$$

where

$$J_0(\theta) = \frac{\theta \sin\theta - 1 + \cos\theta}{\theta^3}, \tag{D.14}$$

$$J_1(\theta) = \left(\frac{1 - \cos\theta}{\theta^2} \right) J_0(\theta), \tag{D.15}$$

$$K_0(\theta) = \frac{1 - \cos\theta}{\theta^3}, \tag{D.16}$$

$$K_1(\theta) = \left(\frac{1 - \cos\theta}{\theta^2} \right) K_0(\theta). \tag{D.17}$$

Making use of the cosine integral $\mathrm{Ci}(z) = -\int_z^\infty (\cos x / x) dx$, we find the following:

$$\int_{\theta_0}^{\infty} J_0(\theta) d\theta = \frac{1}{2\theta_0^2} \left(\cos\theta_0 + \theta_0 \sin\theta_0 - 1 - \theta_0^2 \mathrm{Ci}(\theta_0) \right), \tag{D.18}$$

$$\int_{\theta_0}^{\infty} J_1(\theta) d\theta = \frac{1}{24\theta_0^4} \Big((12 + 2\theta_0^2) \cos\theta_0 - (3 + 2\theta_0^2) \cos 2\theta_0$$

$$+(4\theta_0-2\theta_0^3)\sin\theta_0-(2\theta_0-4\theta_0^3)\sin 2\theta_0$$

$$-9+2\theta_0^4\mathrm{Ci}(\theta_0)-8\theta_0^4\mathrm{Ci}(2\theta_0)\Big), \qquad (D.19)$$

$$\int_{\theta_0}^{\infty} K_0(\theta)d\theta=\frac{1}{2\theta_0^2}\left(1-\cos\theta_0+\theta_0\sin\theta_0-\theta_0^2\mathrm{Ci}(\theta_0)\right), \qquad (D.20)$$

$$\int_{\theta_0}^{\infty} K_1(\theta)d\theta=\frac{1}{24\theta_0^4}\Big(-(12-2\theta_0^2)\cos\theta_0+(3-2\theta_0^2)\cos 2\theta_0$$

$$+(4\theta_0-2\theta_0^3)\sin\theta_0-(2\theta_0-4\theta_0^3)\sin 2\theta_0$$

$$+9+2\theta_0^4\mathrm{Ci}(\theta_0)-8\theta_0^4\mathrm{Ci}(2\theta_0)\Big). \qquad (D.21)$$

For small z we have $\mathrm{Ci}(z)=E+\ln(z)+O(z^2)$. Consequently, if we use the fact that θ_0 is small, the integrals (D.18–21) reduce to

$$\int_{\theta_0}^{\infty} J_0(\theta)d\theta=\frac{1}{4}-\frac{1}{2}E-\frac{1}{2}\ln(\theta_0)+O(\theta_0^2), \qquad (D.22)$$

$$\int_{\theta_0}^{\infty} J_1(\theta)d\theta=\frac{19}{48}-\frac{1}{4}E-\frac{1}{4}\ln(\theta_0)-\frac{1}{3}\ln 2+O(\theta_0^2), \qquad (D.23)$$

$$\int_{\theta_0}^{\infty} K_0(\theta)d\theta=\frac{3}{4}-\frac{1}{2}E-\frac{1}{2}\ln(\theta_0)+O(\theta_0^2), \qquad (D.24)$$

$$\int_{\theta_0}^{\infty} K_1(\theta)d\theta=\frac{25}{48}-\frac{1}{4}E-\frac{1}{4}\ln(\theta_0)-\frac{1}{3}\ln 2+O(\theta_0^2). \qquad (D.25)$$

(D.22–25) provide the expansion for (D.13) to $O(\theta_0^2)$. Next we consider the second group of integral terms in (D.12)

$$\left(\int_{-\pi}^{-\phi_0}+\int_{\phi_0}^{\pi}\right)\frac{\hat{\mathbf{s}}_\circ\times(\mathbf{X}-\mathbf{X}_\circ)}{|\mathbf{X}-\mathbf{X}_\circ|^3}ds_\circ$$

$$=\frac{\hat{\mathbf{b}}}{\rho}\int_{\phi_0/2}^{\pi/2}\frac{d\psi}{\sin\psi}$$

$$=\frac{\gamma^2}{D}\left(1-\frac{3}{2}\gamma^2+O(\gamma^4)\right)\left(\ln\phi_0-2\ln 2+O(\phi_0^2)\right)(\mathbf{j}+\mathbf{k}\gamma). \qquad (D.26)$$

Recalling (D.11) which relates ϕ_0 to θ_0 and using (D.22–26) in (D.12) leads to the following expression for the induced velocity

$$\mathbf{Q}_{MS}=\frac{\Gamma\gamma^2}{4\pi D}\left[\mathbf{j}\left(\ln\gamma-2\ln 2+\frac{1}{2}-E-\frac{3}{2}\gamma^2\left(\ln\gamma-\frac{10}{3}\ln 2+\frac{23}{12}-E\right)\right)\right.$$

$$\left.+\gamma\mathbf{k}\left(\ln\gamma-2\ln 2+\frac{3}{2}-E-\frac{3}{2}\gamma^2\left(\ln\gamma-\frac{10}{3}\ln 2+\frac{29}{12}-E\right)\right)\right]. \qquad (D.27)$$

At this point we note that we can in principle determine $\mathbf{Q}_{MS}$ to arbitrary order in γ. If we denote the velocity of the filament at $\theta = 0$ by $\mathbf{u}$, then according to (D.1) and (D.27) we have

$$\mathbf{u} = \frac{\Gamma\gamma^2}{4\pi D}\left[\mathbf{j}\left(\ln\left(\frac{2D}{a\gamma}\right) + \frac{1}{4} - E - \frac{3}{2}\gamma^2\left(\ln\left(\frac{2D}{a\gamma}\right) - \frac{4}{3}\ln 2 + 1 - E\right)\right)\right.$$
$$\left. +\gamma\mathbf{k}\left(\ln\left(\frac{2D}{a\gamma}\right) + \frac{5}{4} - E - \frac{3}{2}\gamma^2\left(\ln\left(\frac{2D}{a\gamma}\right) - \frac{4}{3}\ln 2 + \frac{3}{2} - E\right)\right)\right]. \quad (D.28)$$

Now returning to (D.3) we find that the velocity at $\theta = 0$ is given by

$$\frac{\partial \mathbf{X}}{\partial t} = \frac{D\Omega}{\gamma}\mathbf{k}. \quad (D.29)$$

Since the filament velocity is arbitrary up to a slipping velocity (i.e., some unknown component parallel to the curve), we must have

$$\frac{D\Omega}{\gamma}\mathbf{k} - \mathbf{u} = \alpha\left(\gamma\mathbf{j} - \mathbf{k}\right), \quad (D.30)$$

where α is some unknown scalar quantity and $\gamma\mathbf{j} - \mathbf{k}$ is parallel to the helix at $\theta = 0$ (see Saffman (1992)). Solving for Ω yields

$$\Omega = \gamma\left(\mathbf{u}\cdot\mathbf{k}\right) + \left(\mathbf{u}\cdot\mathbf{j}\right)$$
$$= \frac{\Gamma\gamma^2}{4\pi D^2}\left(\ln\left(\frac{2D}{a\gamma}\right) + \frac{1}{4} - E - \frac{1}{2}\gamma^2\left(\ln\left(\frac{2D}{a\gamma}\right) - 4\ln 2 - \frac{1}{2} + E\right)\right) \quad (D.31)$$

which is what we required.

APPENDIX E

THE GROWTH RATE OF A TILTING VORTEX RING

Estimation of the growth rate of a tilting ring using the experimental results of Weidman and Riley

In chapter 3 we reported that the experimental work of Weidman and Riley (1993) seems to provide some evidence that a vortex ring in a pipe may be subject to a tilt–mode type instability. Briefly, their experimental work sought to examine the motion of a concentric and coplanar vortex ring pair that moves inside a concentric pipe. To generate the vortex ring pair, fluid is forced through an annular orifice in a flat plate. The vortex rings form by roll up of the boundary layer at the sharp edges of the orifice. For a full description of the experimental results one should examine the original paper, but from the perspective of the stability of the vortex pair we can state that their results indicated that the outer ring was usually subject to a Krutsch type instability (i.e., the growth of waves on the centerline of the core, whose wavelength is on the order of the core radius) while the inner ring usually suffered from an *irrepressible mode–one tilt*! They attributed the tilt to an elastic distortion of the inner disc, whose edge makes up the inner part of annular orifice, during the formation process. It seems likely that any such distortion would provide a seed for the tilt–mode type instability. In the remainder of this appendix we attempt to estimate the growth rate of a tilting mode associated with the inner ring of experimental run #13.

Suppose a vortex ring is subject to a tilt–mode type instability, then the axial position of a point on the core centerline (as measured with respect to the unperturbed ring) is proportional to $\exp(\sigma t)$, where σ is the growth rate. If $\psi(t)$ is the tilt angle then $\tan\psi$ equals the ratio of the maximum axial perturbation to the ring radius

$$\tan\psi = \frac{z_{max}}{R}. \qquad (E.1)$$

Consequently, for small tilt angles we can write

$$\psi(t) = \psi_0 \exp(\sigma t), \tag{E.2}$$

for some angle ψ_0. It follows that the growth rate is given by

$$\sigma = \frac{\ln(\psi(t_2)) - ln(\psi(t_1))}{t_2 - t_1}, \tag{E.3}$$

where t_1 and t_2 are two instants in time. Unfortunatly, we do not have a complete data set which allows us to determine the tilt angle and the corresponding time, but the data set does allow us to determine the tilt angle and the axial position at each instant in time. If $z(t)$ is the axial position of the ring at time t, then assuming a constant ring speed between U, between t_1 and t_2, we find

$$t_2 - t_1 = \frac{z(t_2) - z(t_1)}{U}. \tag{E.4}$$

If we eliminate $t_2 - t_1$ from (E.3), using (E.4), we find

$$\frac{\sigma}{U} = \frac{\ln(\psi(t_2)) - ln(\psi(t_1))}{z(t_2) - z(t_1)}. \tag{E.5}$$

The only difficulty with using (E.5) is that it assumes that the ring speed remains constant between t_1 and t_2. Most of the realisations have trajectories which indicate that the core radius changes as the vortex ring moves down the tube, with a concommitant change in the ring speed. However, the inner ring at position numbers 3 and 4 of trajectory #13 have approximately equal diameters and so we can obtain a reasonable estimate for the growth rate from the data at these positions. In table E.1 we present some of the data for the first five positions in run #13. (I am indebted to Patrick Weidman for providing me with a copy of the original data for a number of runs which exhibited a tilting inner ring. The data in table E.1 is based on measurements taken from this data.) Using the data from position 3 and 4 in equation (E.5) yields the value $\sigma/U \approx 9.54$. To compare with the theoretical results from chapter 3 we need a value of λ. In this case we will take the outer vortex ring to be at the position of an image ring so that the effective pipe radius D is given by the formula

$$R_{\text{outer}} = \frac{D^2}{R_{\text{inner}}} \tag{E.6}$$

which yields a value of λ given by

$$\lambda = \sqrt{\frac{R_{\text{inner}}}{R_{\text{outer}}}}. \qquad (E.7)$$

The outer ring has a radius of approximately 10.02cm so that the appropriate value of λ is 0.73. In table E.2 we present the theoretical predicted values of the speed, the growth rate and their ratio for a range of different values of core radius (actually the parameter that we vary is $\delta_* = a\delta/R$). The important entries in the table are the values of $\hat{\sigma}/\hat{U} = R\sigma/U$. The corresponding value from the experimental data is $R\sigma/U = 50.94$ (i.e., 9.54×5.34), which is a bit larger than the theoretical values in table E.2. The larger value may be on account of the pipe wall, which should also induce the tilting mode insability.

Position	R (cm)	Z (cm)	ψ
1	5.30	1.05	0.0000
2	5.39	1.40	0.0019
3	5.34	1.66	0.0169
4	5.34	1.80	0.0215
5	5.43	2.01	0.0313

Table E.1 The values of the inner ring radius, R, axial position, Z, and tilt angle, ψ, for the first five positions in experimental run #13 of Weidman and Riley's experiments.

δ_*	$\hat{U}$	$\hat{\sigma}^2$	$\hat{\sigma}/\hat{U}$
0.01	2.90	122.55	3.82
0.02	2.21	104.65	4.63
0.03	1.80	94.18	5.39
0.04	1.51	86.75	6.17
0.05	1.29	80.98	6.98
0.06	1.11	76.27	7.87
0.07	0.95	72.29	8.95
0.08	0.82	68.84	10.12
0.09	0.70	65.80	11.59
0.10	0.60	63.08	13.24

Table E.2 Values of the scaled speed, $\hat{U} = 4\pi RU/\Gamma$, the scaled growth rate, $\hat{\sigma} = 4\pi R^2\sigma/\Gamma$, for ranges of the parameter δ_*. Their ratio $\hat{\sigma}/\hat{U} = R\sigma/U$.

BIBLIOGRAPHY

Adebiyi, A., On the existance of steady helical vortex tubes of small cross–section, Q. J. Mech. Appl. Math. **XXXIV** pp 153–177 (1981)

Batchelor, G.K., *An introduction to fluid dynamics*, Cambridge University Press (1967)

Callegari, A.J., Ting, L., Motion of a curved vortex filament with decaying vortical core and axial velocity, SIAM J. Appl. Math. **35** pp 148–175 (1978)

Canuto, C., Hussaini, M.Y., Quarteroni, A., Zang, T.A., *Spectral Methods in Fluid Mechanics*, Springer Verlag (1986)

Chorin, A.J., The evolution of a turbulent vortex, Comm. Math. Phys. **83** pp 517–535 (1982)

Crow, S.C., Stability theory for a pair of trailing vortices, AIAA J. **8** pp 2172–2179 (1970)

Dhanak, M.R., Interaction between a vortex filament and an approaching rigid sphere, J. Fluid Mech. **110** pp 129–147 (1981)

Dhanak, M.R., de Bernardinis, B., The evolution of an elliptic vortex ring, J. Fluid Mech. **109** pp 189–216 (1981)

Dyson, F.W., Potential of an anchor ring, part II, Phil. Trans. Roy. Soc. pp 1041–1106 (1893)

Fraenkel, L.E., On steady vortex ring of small cross–section in and ideal fluid, Proc. Roy. Soc. London **A316** (1970)

Fukumoto, Y., Miyazaki, T., Three–dimensional distortions of a vortex filament with axial velocity, J. Fluid Mech. **222** pp 369–416 (1991)

Hasimoto, H., A soliton on a vortex filament, J. Fluid Mech. **51** pp 477–485 (1972)

Helmholtz, H., Über Integrale der Hydrodynamischen Gleichungen welche den Wirbelbewegungen entsprehen Crelles J. **55** p 25 (1858)

Hicks, W.M., Researches on the theory of vortex rings — part II, Phil. Trans. Roy. Soc. **A176** pp 725–780 (1885)

Kelvin, Lord, The translatory velocity of a circular vortex ring, Phil. Mag. **33** pp 511–512 (1867)

Kelvin, Lord, Vibrations of a columnar vortex, Phil. Mag. **10** pp 152–165 (1880)

Klein, R., Majda, A.J., Self stretching of a perturbed vortex filament I: The asymptotic equation for deviations from a straight line, Physica D **49** pp 323–352 (1991a)

Klein, R., Majda, A.J., Self stretching of perturbed vortex filaments II: Structure of solutions, Physica D **53** pp 267–294 (1991b)

Leonard, A., Vortex Methods for Flow Simulation J. Comp. Phys. **37** pp 289–335 (1980)

Moore, D.W., Finite amplitude waves on aircraft trailing vortices, Aeronaut. Quart. **23** pp 307–314 (1972)

Moore, D.W., Saffman, P.G., The motion of a vortex filament with axial flow, Phil. Trans. Roy. Soc. London **A 272** pp 403–429 (1972)

Moore, D.W., Saffman, P.G., A note on the stability of a vortex ring of small cross–section, Proc. R. Soc. London **A 338** pp 535–537 (1974)

Raja Gopal, E.S., Motion and stability of vortices in a finite channel: application to liquid Helium II, Ann. Phys. **55** pp 196–220 (1963)

Rosenhead, L., The spread of vorticity in the wake behind a cylinder, Proc. Roy. Soc. **A 127** pp 590–612 (1930)

Saffman, P.G., The velocity of viscous vortex rings, Stud. Appl. Math. **49** pp 371–380 (1970)

Saffman, P.G., *Vortex Dynamics*, Cambridge University Press (1992)

Siggia, E.D., Collapse and amplification of a vortex filament Phys. Fluids **28** pp 794–805 (1985)

Tait, P.G., Translation of the Helmholtz paper "On integrals of the hydrodynamical equations which express vortex motion." Phil. Mag. **33** pp 485–512 (1867)

Thomson, J.J., *A treatise on the motion of vortex rings*, Macmillan (1883)

Weidman, P.D., Riley, N., Vortex ring pairs: numerical simulation and experiment, J. Fluid Mech. **257** pp 311–337 (1993)

Whitham, G.B., *Linear and Nonlinear Waves*, Wiley Interscience Series. (1974)

Widnall, S.E., The stability of a helical vortex filament, J. Fluid Mech. **54** pp 641–663 (1972)

Widnall, S.E., Bliss, D.B., Slender body analysis of the motion and stability of a vortex filament containing axial flow, J. Fluid Mech. **50** pp 335–353 (1971)

Widnall, S.E., Bliss, D.B., Tsai, C.Y., The instability of short waves on a vortex ring, J. Fluid Mech. **66** pp 35–47 (1974)

Widnall, S.E., Sullivan, J., On the stability of vortex rings, Proc. Roy. Soc. London **A332** pp 335–353 (1973)

Widnall, S.E., Tsai, C.Y., The instability of the thin vortex ring of constant vorticity, Phil. Trans. Roy. Soc. London **A287** pp 273–305 (1977)